Title

Euphausiid spatial displacements and habitat shifts in the southern California Current System in response to El Niño variability

Authors

Lilly, Laura E

Ohman, Mark D

Publication Date

2021-04-01

DOI

10.1016/j.pocean.2021.102544

Peer reviewed

Progress in Oceanography 193 (2021) 102544

Contents lists available at ScienceDirect

Progress in Oceanography

journal homepage: www.elsevier.com/locate/pocean

Euphausiid spatial displacements and habitat shifts in the southern California Current System in response to El Niño variability

Laura E. Lilly *, Mark D. Ohman

Integrative Oceanography Division (IOD) and California Current Ecosystem Long-Term Ecological Research Program (CCE-LTER), Scripps Institution of Oceanography, UC San Diego, La Jolla, CA 92093, United States

ARTICLE INFO

Regional Index Terms:
Southern California Current System
USA, California, Point Conception
USA, California, San Diego
Mexico, Baja California
Mexico, Baja California Sur

Keywords:
El Niño variability
2014–15 Warm Anomaly
Habitat shifts
Population advection
Euphausiids
CalCOFI

ABSTRACT

We analyzed spatial distributions of 10 euphausiid species in the southern California Current System across seven El Niño events (1951–2018) and the 2014–15 Warm Anomaly to determine variations in habitat utilization and reproduction during Eastern Pacific (EP) and Central Pacific (CP) Niños. Our goal was to characterize the main forcing mechanisms by which El Niño events influence these dominant species. Our findings suggest cool-water euphausiids respond predominantly to changing *in situ* habitat conditions during El Niño, while subtropical species require initial advection to increase in the southern CCS. Cool-water coastally-associated species (*Euphausia pacifica, Thysanoessa spinifera*) compress shoreward and retract poleward to upwelling waters during EP Niños, likely in response to offshore warming. A subtropical coastal species (*Nyctiphanes simplex*) extends poleward nearshore during EP Niños, suggesting anomalous advection, but increases only moderately and variably off southern California during CP Niños. A Tropical Pacific-Baja California species (*Euphausia eximia*) only appears off southern California in spring during El Niño years (EP, some CP), suggesting direct advection and low tolerance for cooler, fresher conditions. Subtropical offshore species (*Euphausia gibboides, Euphausia recurva, Stylocheiron affine, Euphausia hemigibba*) expand shoreward during most Niños (strongest during 2014–15 Warm Anomaly) and show moderate *in situ* post-event persistence, suggesting combined influence of advection and temporarily favorable habitat nearshore. Regionwide temperate species (*Nematoscelis difficilis, Thysanoessa gregaria*) contract only moderately shoreward during some Niños. Predictions of Year 2100 distributions using generalized additive models suggest future non-Niño conditions and CP Niños will produce regionwide *in situ* increases in subtropical species and moderate poleward and onshore expansions, while EP Niños will produce continued nearshore habitat compression and reduced abundance of coastal species. Understanding zooplankton spatial responses to El Niño can help predict community compositional shifts under other ocean changes (e.g., long-term trends, basin-wide warm anomalies).

1. Introduction

Euphausiids (krill) are shrimp-like crustacean zooplankton that comprise one of the dominant mesozooplankton taxa in the California Current System (CCS) and form an important link in energy transfer from primary production to higher trophic levels (Croll et al., 2005; Dorman et al., 2011; Tanasichuk, 1998). Euphausiids show high species diversity in the southern CCS, to 39 species, 24 of which have been observed consistently since the California Cooperative Oceanic Fisheries Investigations program (CalCOFI) began zooplankton sampling in 1949 (Brinton, 1962; Brinton et al., 2000). Brinton (1962, 1967, 1981) characterized biogeographic affinities of common CCS euphausiid species into four regions: 1) Northern CCS/North Pacific Drift (*Euphausia pacifica, Nematoscelis difficilis*), 2) Intermediate/Subtropical Offshore (*E. gibboides, E. recurva, Thysanoessa gregaria*), 3) Baja California/Subtropical (*E. eximia, E. hemigibba, Stylocheiron affine*), and 4) Coastal: northern CCS (*T. spinifera*) and Baja California (*Nyctiphanes simplex*). Departures from these affinities, particularly increases of subtropical species in the southern and central CCS, have been used as indicators of Eastern North Pacific anomalous ocean conditions such as El Niño events and Pacific Decadal Oscillation phase changes (Brinton, 1960, 1979, 1981; Brinton & Townsend, 2003; Di Lorenzo & Ohman, 2013; Lavaniegos et al., 2019; Lavaniegos et al., 2002; Lilly & Ohman, 2018; Marinovic et al., 2002; Pares-Escobar et al., 2018).

* Corresponding author.
E-mail address: l1lilly@ucsd.edu (L.E. Lilly).

https://doi.org/10.1016/j.pocean.2021.102544
Received 27 June 2020; Received in revised form 31 January 2021; Accepted 1 March 2021
Available online 6 March 2021

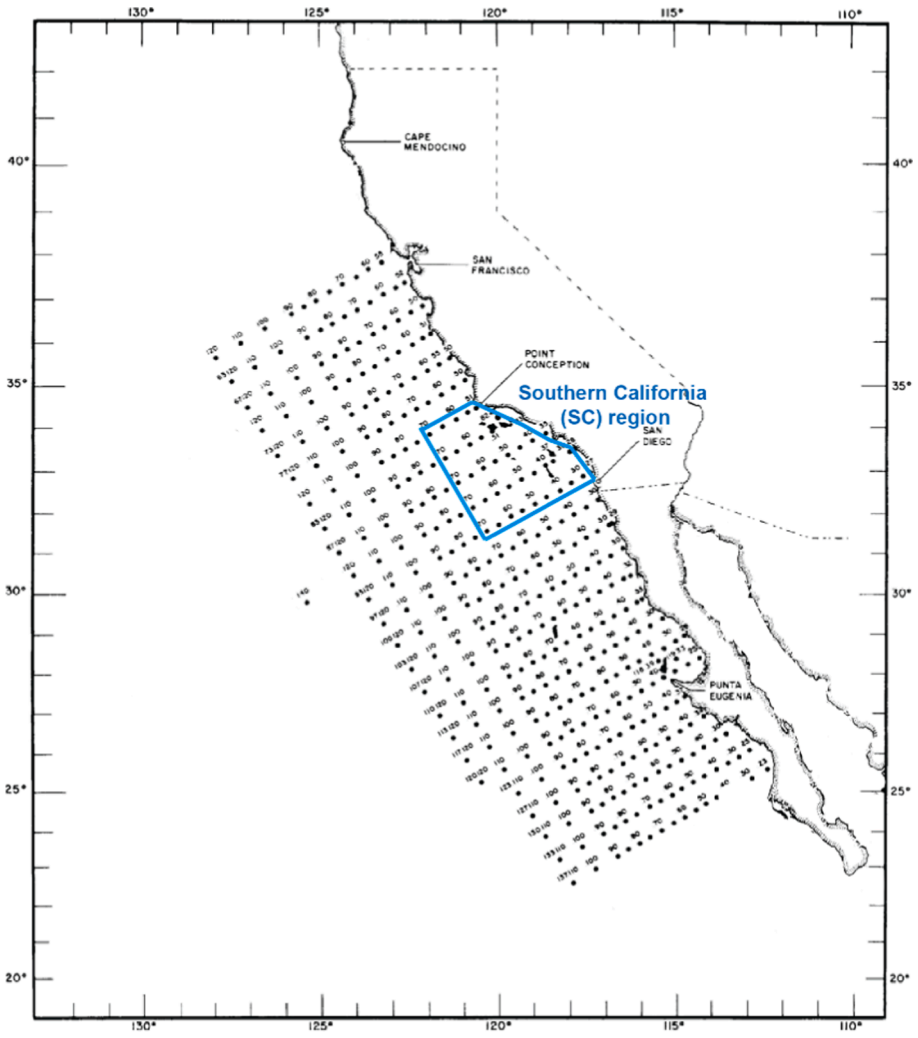

Fig. 1. Locations of all California Cooperative Oceanic Fisheries Investigations (CalCOFI) sampling stations used in this study. The region shown here is a subset of the fullest sampling extent; see https://calcofi.org/. The sampling pattern within this region varies by year. See Fig. S10 for year-specific coverages. Blue box depicts Southern California ('SC') region. See Methods for more information. (For interpretation of the references to colour in this figure legend, the reader is referred to the web version of this article.)

The dominant physical perturbation in the Pacific Ocean is the El Niño-Southern Oscillation (ENSO) cycle, which originates in the equatorial region. El Niño, the ENSO warm phase, develops every 3–8 years due to weakening equatorial trade winds (Cane, 1986; McPhaden, 1999; Wyrtki, 1975). El Niño events can vary substantially in physical expression and biological impacts in the equatorial Pacific and in extratropical latitudes such as the CCS (Ashok et al., 2007; Capotondi et al., 2015; Kao & Yu, 2009; Larkin & Harrison, 2005). Whether this variability in El Niño characteristics has a clear typology is an ongoing debate (Karnauskas, 2013), but one proposed categorization is into Eastern Pacific (EP) and Central Pacific (CP) events (Capotondi et al., 2015; Kao & Yu, 2009; Ren & Jin, 2011; Timmermann et al., 2019; Yeh et al., 2009). Eastern Pacific El Niños are initiated, in part, by significant Kelvin wave propagation eastward along the Equator and characterized by anomalously warm temperatures and a deep thermocline off South America, with heat discharge to the extra-tropics via oceanic propagation (principally coastally trapped waves, CTWs; Capotondi et al., 2015; Kao & Yu, 2009; Kug et al., 2009). Central Pacific El Niños generally have more moderate temperature anomalies that are expressed most strongly near the International Dateline; are usually forced by local winds and zonal advective feedback, although they can sometimes induce Kelvin waves; and rarely show off-Equator heat discharge (Ashok et al., 2007; Ashok & Yamagata, 2009; Capotondi, 2013; Kao & Yu, 2009; Kim et al., 2011).

El Niño signals can travel to extra-tropical latitudes such as the CCS via combinations of oceanic and atmospheric pathways (Jacox et al., 2015): 1) CTWs can strengthen poleward advection and transport subtropical waters from Baja California (Lynn & Bograd, 2002; Ramp et al., 1997; Schwing et al., 2002; Strub & James, 2002); 2) atmospheric teleconnections from the equatorial Pacific can alter the Aleutian Low pressure system, affecting local wind-driven circulation (Alexander et al., 2002; Simpson, 1984); and 3) warm, salty waters of southern offshore origin can be advected into the CCS due to altered atmospheric circulation (Bograd & Lynn, 2001; Jacox et al., 2016; Simpson, 1984). El Niño propagation mechanisms and CCS expressions can vary substantially, even for events of similar equatorial forms (see Supplemental Information to this manuscript for detailed physical characteristics and propagation mechanisms of each El Niño event analyzed in this study).

Maximum lifespans of CCS euphausiids range from approximately 8 months for *N. simplex* (Lavaniegos, 1992) to 1–1.5 years for *E. pacifica* (Brinton, 1976; Smiles & Pearcy, 1971) and possibly 1.5 years for *E. eximia* (Gomez, 1995), although lifespans for most species have not been well quantified. However, lifespans on the order of one year make euphausiids optimal organisms to track interannual perturbations such as El Niño (Brinton, 1960) and lower-frequency variations such as the Pacific Decadal Oscillation (Di Lorenzo & Ohman, 2013). Southern CCS total euphausiid biomass has generally decreased, and subtropical species presence increased, during and immediately following most El Niño events of the past seventy years (Brinton, 1981; Brinton & Townsend, 2003; Lavaniegos et al., 2019; Lavaniegos et al., 2002; Lavaniegos & Ohman, 2007; Lilly & Ohman, 2018; Mackas et al., 2006; Pares-Escobar et al., 2018). Baja California species (*N. simplex, E. eximia)* have been

collected as far north as Oregon (Keister et al., 2005), Washington (Brodeur, 1986), and Vancouver Island, British Columbia (Mackas & Galbraith, 2002), during past El Niños, indicating significant short-term range extensions of subtropical species (Brinton, 1960; Marinovic et al., 2002). In contrast, dominant cool-water CCS species (*E. pacifica, T. spinifera*) have decreased and shown evidence for northward retraction (Brinton, 1960; Brinton & Townsend, 2003). Such species-specific responses highlight that aggregated euphausiid bulk biomass, whether assessed by direct sampling or bioacoustics, is unlikely to be a sensitive indicator of either the true impact of El Niño or the underlying causal mechanisms.

Past studies have often attributed El Niño-related zooplankton shifts to advection of organisms into or out of a region, with only secondary consideration of *in situ* effects (Brinton, 1979, 1981; Wickett, 1967). However, the specific impacts of an El Niño event on a given euphausiid species depend upon the physical characteristics of the event; the biogeographic origin and inherent habitat tolerances of the species (i.e., mortality, growth, reproduction thresholds); and El Niño-induced alterations in *in situ* prey, predator, and physical-chemical characteristics of the ambient environment (Lavaniegos & Ambriz-Arreola, 2012; Ohman et al., 2017; Pares-Escobar et al., 2018). Analyzing species- and life history-specific spatial changes can provide insight beyond aggregated biomass metrics into the relative contributions of direct advection and *in situ* population growth or mortality during El Niño events. Clarifying these contributions will improve our understanding of the underlying mechanisms that influence community variability under anomalous ocean conditions, thus enabling better predictions of zooplankton responses to future El Niño events and longer-term ocean changes. Improving our understanding of euphausiid population spatial changes can also improve predictions of habitat use by higher trophic levels, particularly whales, seabirds, and mobulids that selectively forage on certain euphausiid species (Lee et al., 2007; Nickels et al., 2018; Notarbartolo-di-Sciara, 1988; Stewart et al., 2017; Sydeman et al., 2006; Szesciorka et al., 2020).

Previously we presented temporal changes in regionally-aggregated total zooplankton community composition during CCS El Niños (Lilly & Ohman, 2018). Here we analyze variability in spatial distributions, habitat conditions, and population stage structure of ten euphausiid species across seven decades of EP and CP Niño events to address the following questions:

1) Do spatial distributions of euphausiid species change in a consistent manner during El Niño events relative to non-Niño years?
2) Do spatial distributional changes differ between Eastern Pacific and Central Pacific El Niños?
3) Do species occupy different ranges of habitat conditions (temperature, salinity, O_2, Chl-*a*) during El Niño and non-Niño years?
4) Does the population structure (i.e., developmental stage composition) of any species change during El Niño, suggesting altered rates of population growth?
5) How will euphausiid spatial distributions likely change during future El Niño events?

Our overarching goals are to i) characterize 'typical' EP and CP Niño responses to assess whether distributional shifts provide insight into the relative impacts of physical (advection) and biological (*in situ* growth and mortality) forcing mechanisms in altering species abundances and distributions, and ii) to use the above mechanistic insights to inform predictions of euphausiid changes during future El Niño events.

2. Methods

2.1. Study region

All data are from the California Cooperative Oceanic Fisheries Investigations sampling program (CalCOFI, Bograd et al., 2003). The full CalCOFI sampling region extends from the northern border of California (Line 40: 42°N, 125°W at coast to 39°N, 131°W offshore) to the southern tip of Baja California (Line 157: 23.5°N, 109°W to 20°N, 114.5°W). However, not every station was sampled or enumerated for zooplankton every year in the timeseries. We thus show in Fig. 1 the maximum region that was available for our analyses, which includes stations from Lines 60 (north)-130 (south) and from the coast out to Station 120 (Station 140 on Line 90), from 1951 to 2018. Even within this region, the sampling pattern for each year has varied, so our objective maps (see Section 2.4) include different coverage for each year (see Fig. S10). We refer here to the 'full CalCOFI region', which includes all available samples and variable coverage between years (Fig. 1, full grid), and the 'Southern California (SC) region', which is only the region consistently sampled across all years (Fig. 1, blue box). The SC region is defined as CalCOFI Lines 80–93.3, from the coast out to Station 70 (ranging from 180 km to 350 km offshore, due to the coastline curve) and excluding stations in < 200 m water depth (see https://calcofi.org/ for additional sampling information). Zooplankton samples are collected four times per year but only enumerated consistently for spring cruises, which occur between 15 Feb-31 May (exact dates vary by year). Where available, winter data are presented in supplemental material. Euphausiid data are not available for 1967, 1968, 1971, or 1973 due to a temporary switch to triannual sampling. CalCOFI stations have occasionally been sampled multiple times within one spring period. If a station has multiple samples from one spring, we averaged replicate samples to a single value per station per year to maintain equal contribution of all stations (see Appendix A).

2.2. Euphausiid samples

CalCOFI zooplankton sampling procedures have changed during the timeseries. In all instances, at each station a net is lowered obliquely from the surface to depth, towed for 30 seconds, and recovered obliquely. Net types and depths are as follows: from 1951 to 1968, a 1-m ring net with 550 μm mesh was towed from 0 to 140 m; from 1969 to 1977, a 1-m ring net with 505 μm mesh was towed from 0 to 210 m; and from 1978-present a 0.71-m twin-opening bongo net with 505 μm mesh has been towed from 0 to 210 m (Ohman & Smith, 1995). These sampling changes have been discussed elsewhere (Brinton & Townsend, 1981; Ohman & Lavaniegos, 2002) and do not affect the results presented here. Following net recovery, each zooplankton sample is preserved in sodium tetraborate-buffered formaldehyde and archived in the Pelagic Invertebrate Collection at Scripps Institution of Oceanography (Lavaniegos & Ohman, 2007; Lilly & Ohman, 2018). For euphausiids, an aliquot from each station on spring cruises is sorted and enumerated by species and length. Body lengths are converted to carbon biomass using known species length-carbon relationships (Lavaniegos & Ohman, 2007; Ross, 1982). We include only nighttime samples in this study to remove variance from day/night double-sampling, diel vertical migration, and daytime net avoidance. Data are available at https://oceaninformatics.ucsd.edu/euphausiid/. Twenty-four euphausiid species have been consistently observed and enumerated for the SC region since 1951. Here we examined ten euphausiid species: seven (*Euphausia pacifica, Nyctiphanes simplex, E. eximia, E. gibboides, E. recurva, E. hemigibba, Stylocheiron affine*) that we previously identified as having consistent regionwide biomass changes associated with El Niño (Lilly & Ohman, 2018), and three (*Nematoscelis difficilis, Thysanoessa gregaria, T. spinifera*) that did not show consistent El Niño changes but are numerically dominant in the southern CCS (Brinton & Townsend, 2003).

2.3. El Niño delineations

We defined El Niño events based on previous delineation of 'California Current System El Niños' (Lilly & Ohman, 2018). A 'CCS El Niño' refers to an El Niño event that reaches ≥ 1 standard deviation above the corresponding 1951–2016 mean for at least one Equatorial Pacific Niño

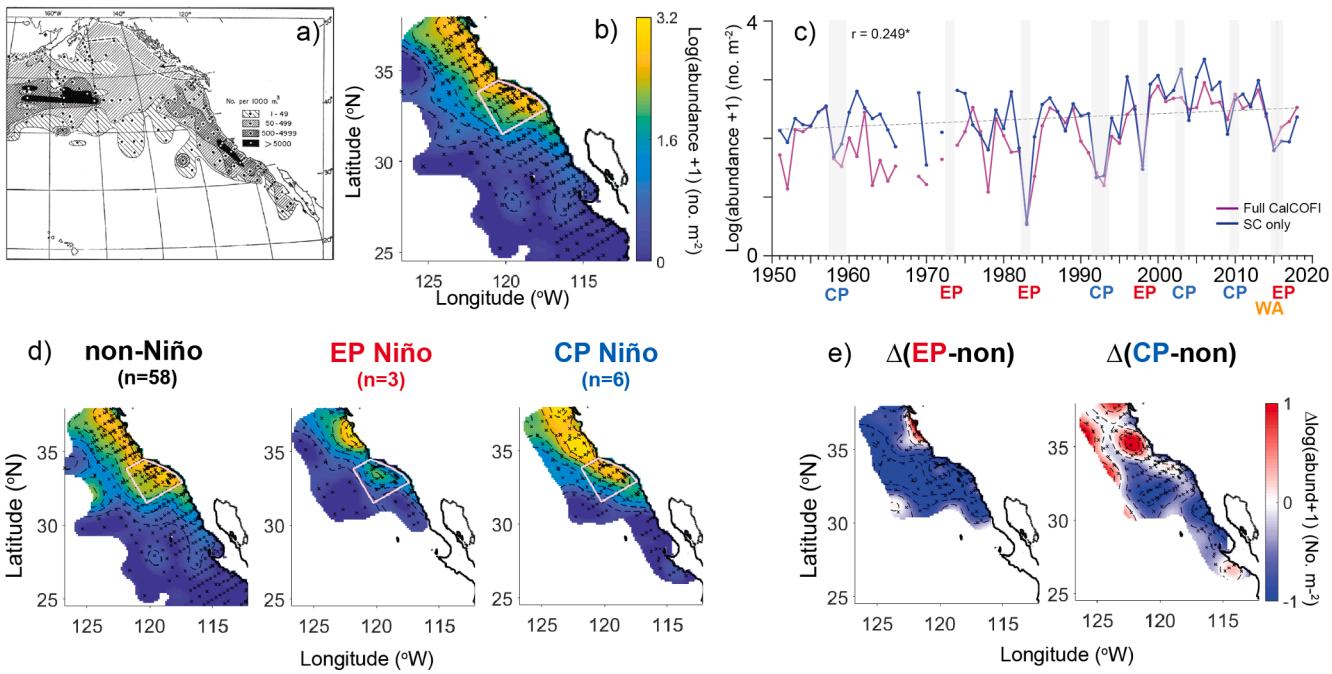

Fig. 2. *Euphausia pacifica* (a) biogeographic affinity from Brinton (1962), (b) average spring distribution across full CalCOFI region, (c) timeseries of region-averaged spring abundance for full CalCOFI (pink) and SC region only (blue), (d) average spring abundance distributions for non-Niño years, EP Niños, and CP Niños, and (e) differences between EP or CP and non-Niño averages. 'n' indicates number of years in average. The sampling pattern varies by year, so average maps are calculated from different numbers of stations in different regions (see Fig. S10 for individual year samples and Fig. B1 for total number of samples by station). Grey dashed linear fit in 'c' indicates significant long-term SC region trend; Spearman rank significance is shown at top (*$p < 0.05$). Vertical grey bars denote El Niño years (EP – Eastern Pacific; CP – Central Pacific). 1973 was an EP Niño, but zooplankton were not sampled. Black crosses on maps show actual CalCOFI stations sampled. Light pink boxes denote SC region. Maps are objectively mapped representations of CalCOFI data (see Methods and Appendix A). (For interpretation of the references to colour in this figure legend, the reader is referred to the web version of this article.)

index (Niño3.4 or Niño1 + 2: Nov-Dec-Jan average) and one CCS Niño index (San Diego Harbor detrended sea level anomaly (SDSLA) or depth of the 26.0 kg/m^3 density isopycnal averaged along CalCOFI Line 90, Stations 26.7–37 ($z_{26.0}$): Dec-Jan-Feb averages). We refer to El Niño 'springs' as the spring CalCOFI cruise following the determinate winter physical average (e.g., spring 1983 for the 1982–83 El Niño). Since all our CCS El Niño events reached ≥ 1 S.D. in the Niño3.4 index, EP Niño events were defined using the additional criterion of also reaching ≥ 1 S.D. in the Niño1 + 2 region. CP Niño events met the Niño3.4 but not Niño1 + 2 criterion. We examined nine El Niño springs (EP: 1983, 1998, 2016; CP: 1958, 1959, 1992, 1993, 2003, 2010) and the 2014–15 Warm Anomaly (spring 2015), which was not significant in equatorial El Niño indices but produced unprecedented positive temperature anomalies in the CCS. Spring 1973 was categorized as an EP Niño, but we do not have zooplankton samples for that year. For analyses involving comparisons of non-Niño, EP Niño, and CP Niño years, we did not include spring 2015 in any group because it was characterized by different physical forcing mechanisms than El Niño events but was also significantly different from non-Niño years (Di Lorenzo & Mantua, 2016; Jacox et al., 2016; Lilly et al., 2019).

2.4. Objective maps

We used objective mapping to project euphausiid abundances measured at individual CalCOFI stations onto a uniform x/y grid and interpolate between points to produce regionwide spatial estimates. Objective mapping produces a minimum mean-square error estimate of a continuous function across a region based on discrete sampling points (i.e., CalCOFI stations; see Bretherton et al., 1976; Davis, 1985). We applied a rotation angle of −60° (negative indicates clockwise rotation) to the CalCOFI grid to align the cross-shore and alongshore grid axes with x and y, respectively. Our mapping grid has evenly spaced resolutions of 14 km and 15 km in the x and y directions, respectively. We selected decorrelation length-scales of 160 km in the x and 190 km in the y directions for all species based on optimal fits of Gaussian curves to autocovariance matrices, with the goal of smoothing small-scale variability resulting from discrete sampling of patchily distributed organisms, in order to depict the regionwide distribution of each species. We assumed an uncorrelated observation error variance of 0.1 of the signal variance (see Appendix B and Fig. B1 for objective mapping process). We set a mean-square error threshold of 0.3 across all years to standardize all maps to a uniform interpolation error limit (Fig. B2).

We used $\log_{10}$(abundance + 1) euphausiid abundances for map calculations to avoid dominance by extreme untransformed abundance spikes. For mean interannual distribution maps, we averaged all yearly values for each station and objectively mapped the averaged grid using the same mapping parameters as for individual years. As noted in Section 2.1, sampling spatial coverage varies by year, so average maps (all years, e.g., Fig. 2b; or non, EP, and CP Niño categories; e.g., Fig. 2d) include different numbers of years for each station average within a map (see Fig. B1 for total number of samples at each station and Fig. S10 for sampling coverage by year). We used the ETOPO1 global relief model (available from NOAA National Centers for Environmental Information, Amante & Eakins, 2009), subsetted for the CCS region and interpolated to our x/y mapping grid, to mask land projections. Coastline was compiled from shapefiles available through the UC Berkeley GeoData Library (https://geodata.lib.berkeley.edu/catalog). To quantitatively examine interannual species variability, we calculated yearly mean regionwide abundances for each species (e.g., Fig. 2c) and centers of gravity (COG) in the cross-shore (x) and alongshore (y) directions for both the SC and full CalCOFI regions (see Fig. S1 and Appendix C). We calculated least squares linear regressions of abundance timeseries to evaluate significance of long-term trends (Fig. 2c).

2.5. Habitat conditions

2.5.1. Habitat range distributions

To determine the habitat range of each euphausiid species, we analyzed spring and winter (separate) abundance distributions in relation to four variables: temperature (50 m depth), salinity (50 m), oxygen (100 m), and chlorophyll-*a* (10 m). We include data from 1951 to 2017 (Chl-*a* available only from 1984 to 2017). Habitat data are from CalCOFI hydrocasts conducted concurrently by station with zooplankton sampling. Post-collection processing is described on the CalCOFI website (https://calcofi.org/field-work/bottle-sampling.html). We chose habitat variable depths that best represent upper water column conditions that impact the species we examined, several of which vertically migrate to the upper 50–100 m at night (Brinton, 1960; Matthews et al., 2020), and because El Niño events tend to have strongest influence in the upper 150 m (Ramp et al., 1997). Our initial temperature-abundance comparisons showed strongest El Niño responses above 100 m. Similarly, salinity is most strongly influenced by the California Current, which is freshest at 50–100 m (Rudnick et al., 2017). We therefore selected temperature and salinity at 50 m to represent upper ocean habitat conditions. We evaluated oxygen at 100 m because we expect these somewhat deeper waters to more closely approach oxygen undersaturation and hypoxia that may have detrimental effects on euphausiids. We included Chl-*a* at 10 m to represent both potential feeding and predator encounter; we expect near-surface Chl-*a* to reflect spatial variability in the subsurface Chl-*a* maximum layer while also correlating strongly with light attenuation, which can determine visual risk of predation on zooplankton (Aksnes & Ohman, 2009; Ohman & Romagnan, 2016). We applied a natural log transformation to chlorophyll-*a* data to reduce skewness. We calculated separate euphausiid range distributions for non-Niño, EP Niño, and CP Niño categories of years, and calculated a weighted mean for each category using station-by-station product vectors: [value of habitat variable]*[euphausiid abundance at variable value]. The weighted mean accounts for varying abundances at different values of a habitat variable by multiplying each habitat value by its corresponding abundance before calculating the mean. We compared distributions of the three Niño conditions using a Kruskal-Wallis test ('kruskalwallis') and the 'multcompare' function in Matlab for post-hoc pairwise comparisons (Matlab 2018b; see Tables S1 and S2 for spring and S3-S4 for winter mean values and inter-Niño differences, respectively). We did not include spring 2015 in any Niño group (see Section 2.3).

2.5.2. Euphausiid-water mass associations

To assess euphausiid species associations with specific water masses, we analyzed species distributions across previously calculated spring proportions of three dominant water masses that comprise the southern CCS (defined and calculated by Bograd et al., 2019). Pacific Subarctic Upper Water (PSUW) flows southward from the North Pacific Current via the core California Current, and is characterized as relatively cool, fresh, and high-O_2; Pacific Equatorial Water (PEW) flows northward coastally from the North Equatorial Countercurrent along Mexico, and is warm, salty, high-nutrient, and subsurface, representing the California Undercurrent; Eastern North Pacific Central Gyre Water (ENPCW) occurs offshore of the California Current and is warm, moderately salty, low-nutrient, and near-surface. Each water mass was defined from a 'source' box upstream of the SC region and characterized by measurements of temperature, salinity, oxygen, phosphate, nitrate, and silicic acid from the World Ocean Database (Bograd et al., 2019). Each water mass was first characterized by upper and lower temperature and salinity limits based on its T-S diagram; optimum multiparameter analysis was then applied to the six upper and lower characterizations and the above six physical and nutrient variables to calculate the proportion of each water mass at each CalCOFI station in the SC region. Water mass proportions were only calculated from 1985 to 2017 due to prior lack of nutrient data (see Bograd et al., 2019 for methods and maps). We considered each water mass at the depth of its strongest interannual expression in the CCS: PSUW at 150 m, PEW at 200 m, and ENPCW at 100 m. We calculated species' mean abundances using weighted means (Tables S5 and S6; see Section 2.5.1). We also calculated the regionwide timeseries mean proportion of each water mass for each Niño group (i.e., the average proportion of PSUW across the SC region and 1985–2017; see arrows below x-axes in Fig. 11).

2.6. Adult and calyptopis abundance proportions

We quantified the relative proportions of adult and calyptopis abundances of each euphausiid species, averaged across the SC region, during each El Niño year and the three years before and after. Proportions are the abundance of each phase divided by the sum of the two phases (e.g., [adult]/[calyptopis + adult]). We calculated proportions individually for each station in the SC region and then averaged the proportions from all stations to obtain a region-averaged value. Years of no abundances of either adults or calyptopes (indicated by a missing bar in Figures 12, S6) may still have species presence as furcilia and juvenile phases.

2.7. Generalized additive models

We developed spring species niche models based on generalized additive models (GAMs, Hastie & Tibshirani, 1987) to estimate individual and combined effects of habitat conditions on species abundances. We developed models from only SC region spring data, 1984–2017, because this region was consistently sampled across all years. Models were constructed from optimal combinations of individual and interactive terms: Temperature, O_2, ln(Chl-*a*), Lat, Lon, (Lat,Lon), (Temp,O_2), (Temp,lnChla), and (O_2,lnChla). Early model runs determined that salinity was non-significant for all species, so we removed it from further analyses. We applied default spline basis smoothers ('s') to individual terms and tensor-product smooth functions ('te') to interactive terms, and initialized each model with 5 knots per term, a Gaussian distribution, and method = 'REML'. We used log-transformed species abundances ($\log_{10}$(abund + 1)) to reduce skew. We included 'Year' as a categorical variable to account for interannual variability in species abundances. We selected the top 3 models for each species from all term combinations, based on Akaike Information Criterion (AIC) and percent (%) deviance explained, and further adjusted k-values of those models to find the optimal model. We selected the optimal model for each species using a combination of lowest AIC, highest %deviance explained, and significance of all model terms ($p < 0.05$; see Figs. 13 and S8 for equations and Table S9 for values). We calculated and plotted GAMs using the 'mgcv' (v1.8–31) and 'mgcViz' (v0.1.6) packages in R (Fasiolo et al., 2019; Wood et al., 2017). We further tested the efficacy of each optimal model by cross-validation, i.e., omitting one year and using all other years to predict its abundances.

We next used each species' optimal GAM to predict potential spatial distributions during the three Niño categories (non, EP, CP) in Year 2100, given forecasted *in situ* conditions. We first calculated baseline (1951–2017) average habitat conditions for each Niño type by averaging each input habitat variable station-by-station across all years in that Niño group. We then added expected habitat changes to each average to produce 'Year 2100 conditions': +1°C temperature, −0.63 ml/L oxygen, and +0.10 μg/L chlorophyll-*a* (untransformed scale), based on current trends and estimated projections for the SC region (Bograd et al., 2008; Hazen et al., 2013; Rykaczewski & Dunne, 2010). Although we calculated baseline conditions from the full (1951–2017) datasets for temperature and O_2, the Year 2100 distributions only include coverage based on the distributions from 1984-present because Chl-*a* data were not sampled prior to 1984. No CalCOFI samples exist south of San Diego for the EP and CP Niño years from 1984-present, so the EP and CP Niño predictions do not extend to Baja California (some non-Niño years from 1984-present did include sampling off Baja

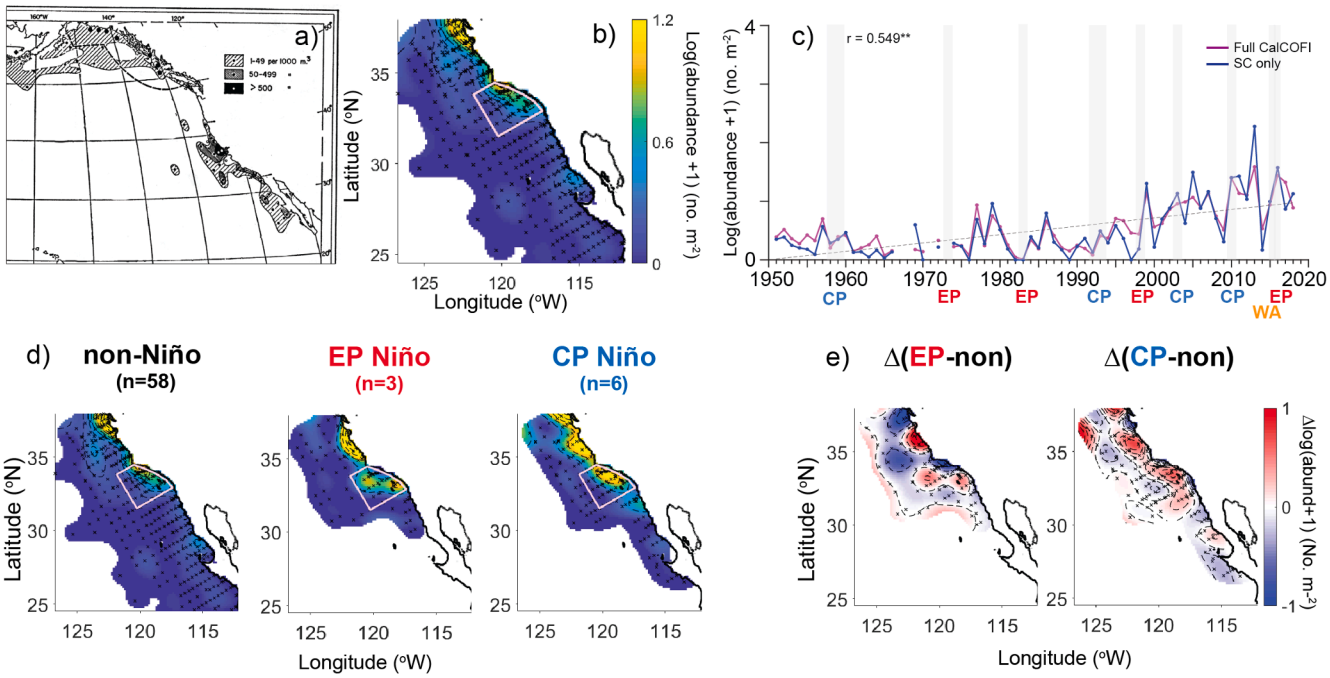

Fig. 3. As in Fig. 2, but for *Thysanoessa spinifera*. Grey dashed linear fit indicates significant long-term trend; Spearman rank significance shown (**p < 0.001).

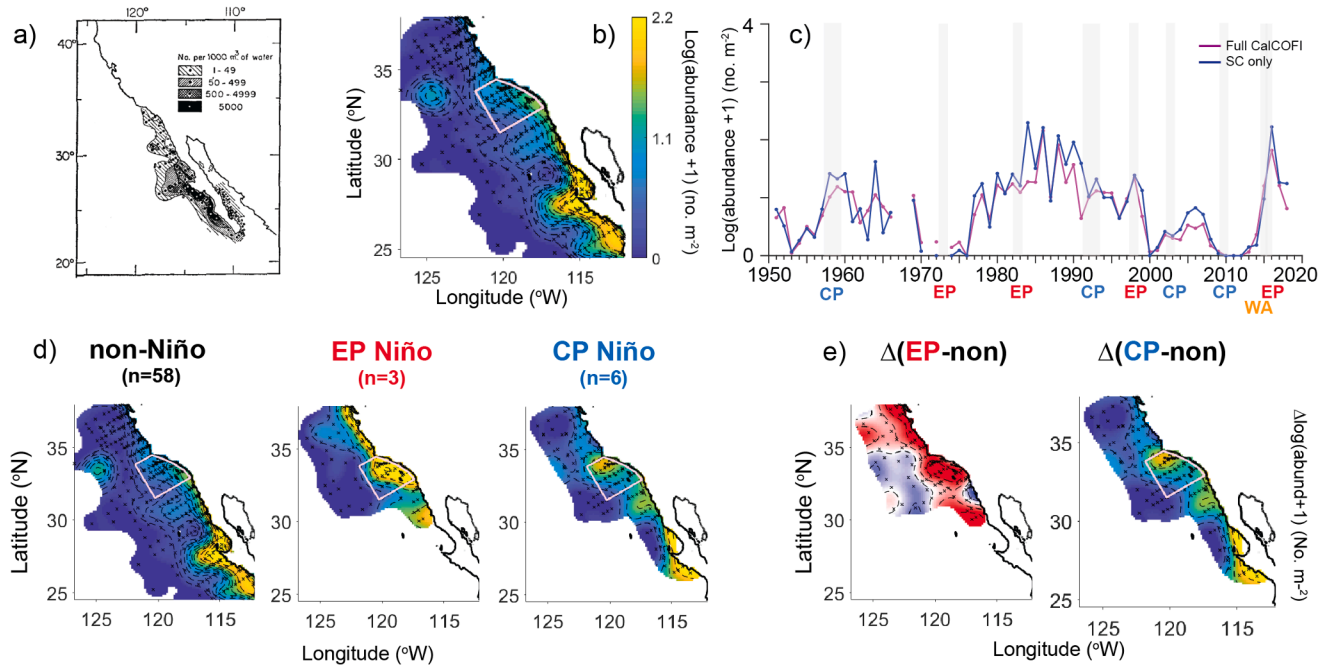

Fig. 4. As in Fig. 2, but for *Nyctiphanes simplex*. Lack of linear trendline in 'c' indicates no significant long-term trend (p > 0.05).

California).

To avoid negative abundance predictions arising from inclusion of station coordinates south and west of the SC region for which the GAMs were developed, we removed Lat/Lon terms from each GAM and only used habitat terms for Year 2100 predictions. To assess GAM accuracy without geographic terms, we evaluated the original GAM fits (SC region, 1984–2017) with and without Lat/Lon terms for four species. Non-Lat/Lon model fits and remaining term significance were similar to the original models for all terms (see Table S9 for comparisons for first four species). For calculations of total positive or negative distributional area in the difference maps (e.g., Fig. 2e: [average EP or CP]-[average non-Niño]; Fig. 14: [2100 prediction]-[current average]), we counted the total number of stations with a positive (or negative) difference and multiplied that count by the average 'station area of influence' (2100 km^2, see Appendix C).

3. Results

3.1. Spatial variability during El Niño events

We categorize five groups of southern CCS euphausiid species responses to El Niño: 1) Cool-Water Coastally-Associated (*Euphausia*

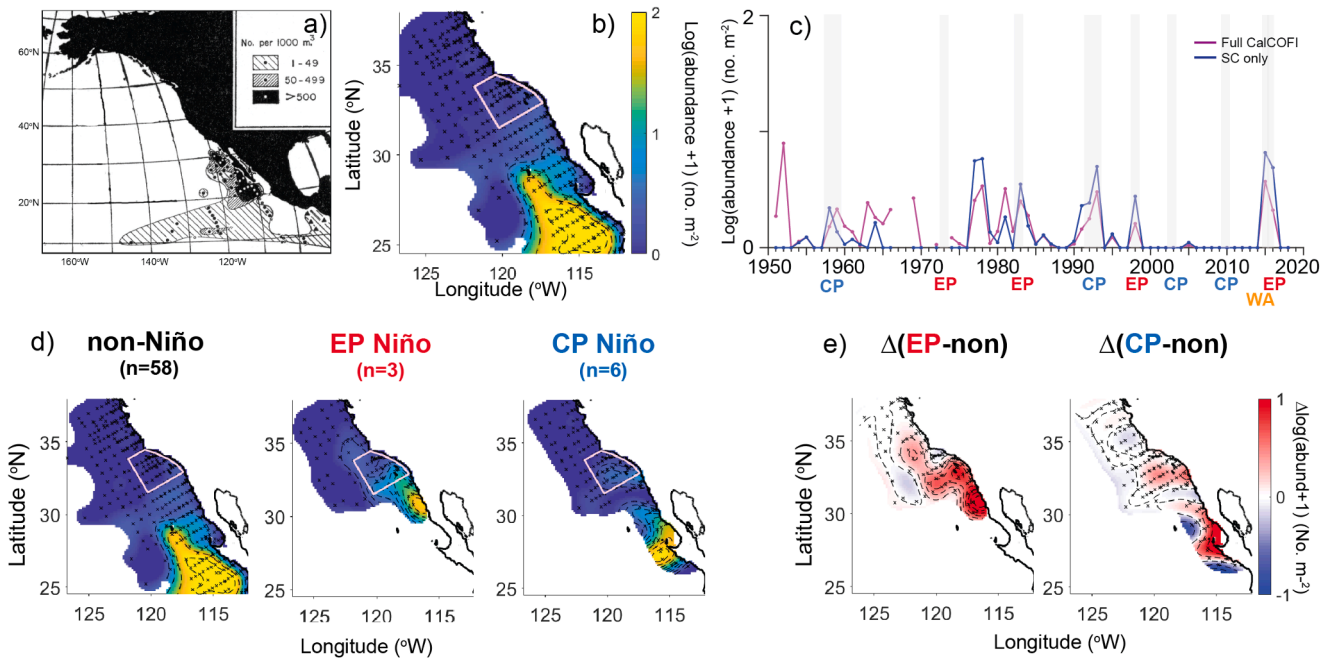

Fig. 5. As in Fig. 2, but for *Euphausia eximia*. Lack of linear trendline in 'c' indicates no significant long-term trend ($p > 0.05$).

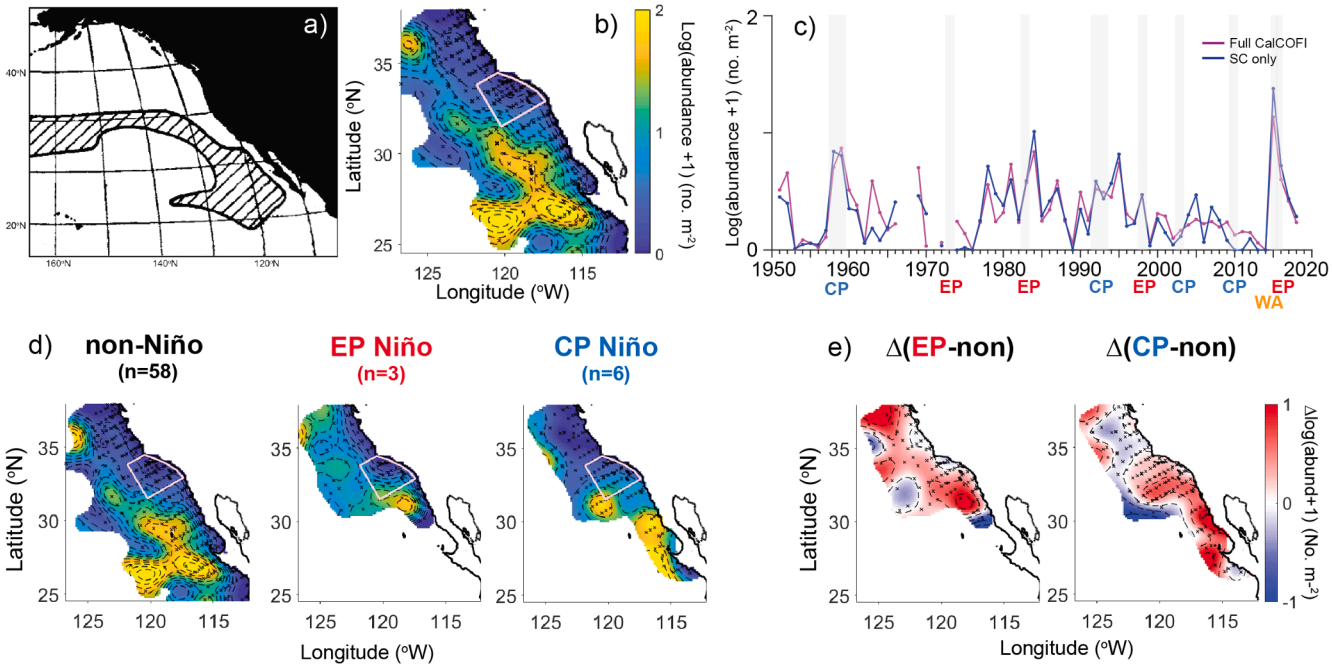

Fig. 6. As in Fig. 2, but for *Euphausia gibboides*. Lack of linear trendline in 'c' indicates no significant long-term trend ($p > 0.05$).

pacifica, Thysanoessa spinifera), 2) Subtropical Coastal *(Nyctiphanes simplex*), 3) Tropical Pacific-Baja California (*Euphausia eximia*), 4) Subtropical Offshore (*Euphausia gibboides, Euphausia recurva, Stylocheiron affine, Euphausia hemigibba*), and 5) Regionwide Temperate (*Nematoscelis difficilis, Thysanoessa gregaria*). While these groupings partially align with the biogeographic affinities of Brinton (1962, 1981), they are a new set of categorizations based specifically on euphausiid responses to El Niño events. Our multiple groupings indicate that coastal or offshore origins are important considerations beyond 'warm' and 'cool' designations. To assess patterns of distributional change within each El Niño category, we calculated average non-Niño, Eastern Pacific (EP) Niño, and Central Pacific (CP) Niño distributions for each species from the entire 1951–2018 timeseries, although we note that these averages include variable sampling coverage by year (Figs. 2d–9d, S2d-S3d). We also present the individual El Niño events and their preceding and following years (Figs. S10 and S19).

3.1.1. *Cool-water, coastally-associated species*

Euphausia pacifica is the dominant euphausiid species in the central and southern CCS and associates with cool waters (<15 °C) extending from the Subarctic Pacific to northern Baja California (Fig. 2a; see Brinton, 1962). The 1951–2018 CalCOFI mean spring distribution of *E. pacifica* indicates consistent presence from Monterey, CA, to the U.S.-Mexico border and out to 300 km offshore, with low abundance off

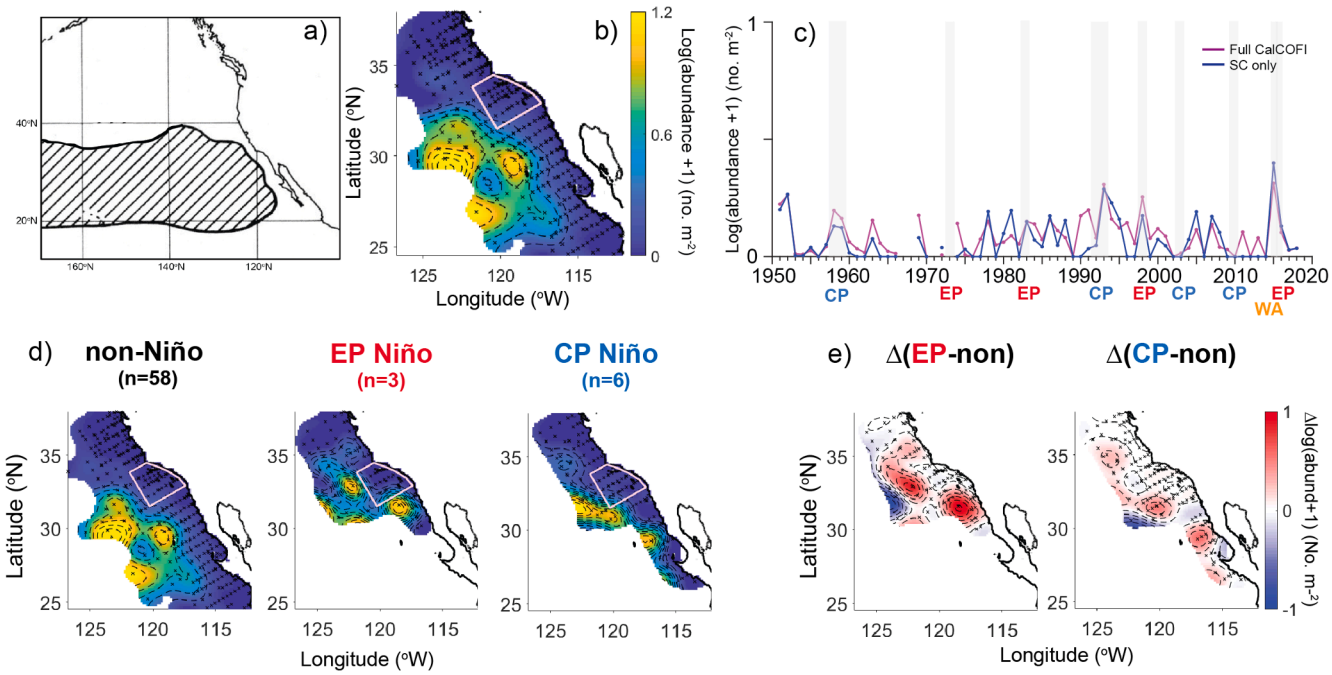

Fig. 7. As in Fig. 2, but for *Euphausia hemigibba*. Lack of linear trendline in 'c' indicates no significant long-term trend ($p > 0.05$).

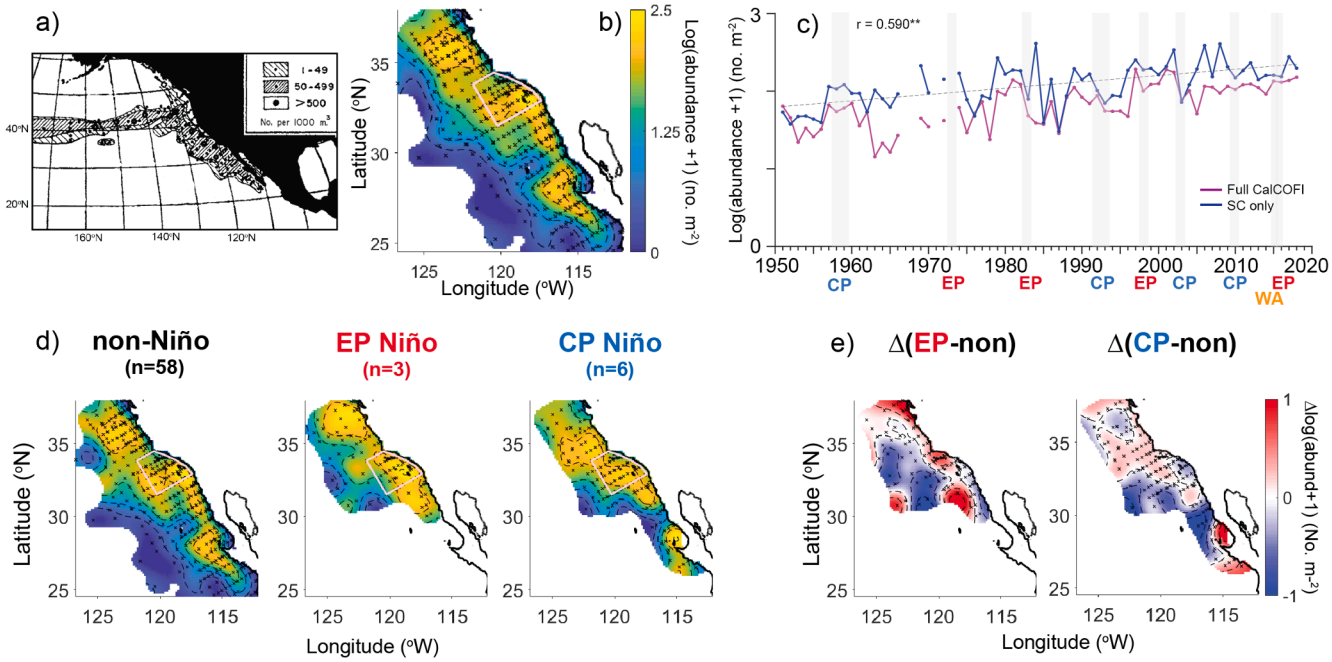

Fig. 8. As in Fig. 2, but for *Nematoscelis difficilis*. Grey dashed linear fit indicates significant long-term trend; Spearman rank significance shown (**$p < 0.001$).

northern Baja California (Fig. 2b). Total abundance of *E. pacifica* in both the Southern California (SC; light pink box on maps, blue line in Fig. 2c) and full CalCOFI (pink line in Fig. 2c) regions decreased during every El Niño event except 2002–03 and 2009–10 (Figs. 2c and S10). The average EP Niño distribution of *E. pacifica* shows clear shoreward compression, poleward retraction, and regionwide population decreases relative to non-Niño years (Fig. 2d-e). The 1982–83 EP Niño induced the most significant reduction in regionwide abundance of *E. pacifica* of the entire timeseries, as well as nearshore compression and poleward retraction to well north of Point Conception, CA (Figs. 2c and S10). Center of gravity metrics reflect substantial shoreward compression and poleward retraction in 1983 (Fig. S1a). The 1997–98 EP Niño also caused substantial shoreward compression and decreased overall abundance of *E. pacifica*, although less severe than in 1983 (Figs. 2c and S1a, S10). In contrast, the 2015–16 EP Niño produced only moderate shoreward compression. High abundance in coastal regions suggests only moderate physical impacts and persistent nearshore upwelling during the event.

The average *E. pacifica* distribution during CP Niños shows only moderate poleward retraction compared to the non-Niño average (Fig. 2d-e). These changes are reflected in population decreases in the southern half of the distribution but localized nearshore increases in the northern third (Fig. 2d-e). However, *E. pacifica* distributional shifts vary substantially across individual CP Niños: 1957–59 (springs 1958, 1959)

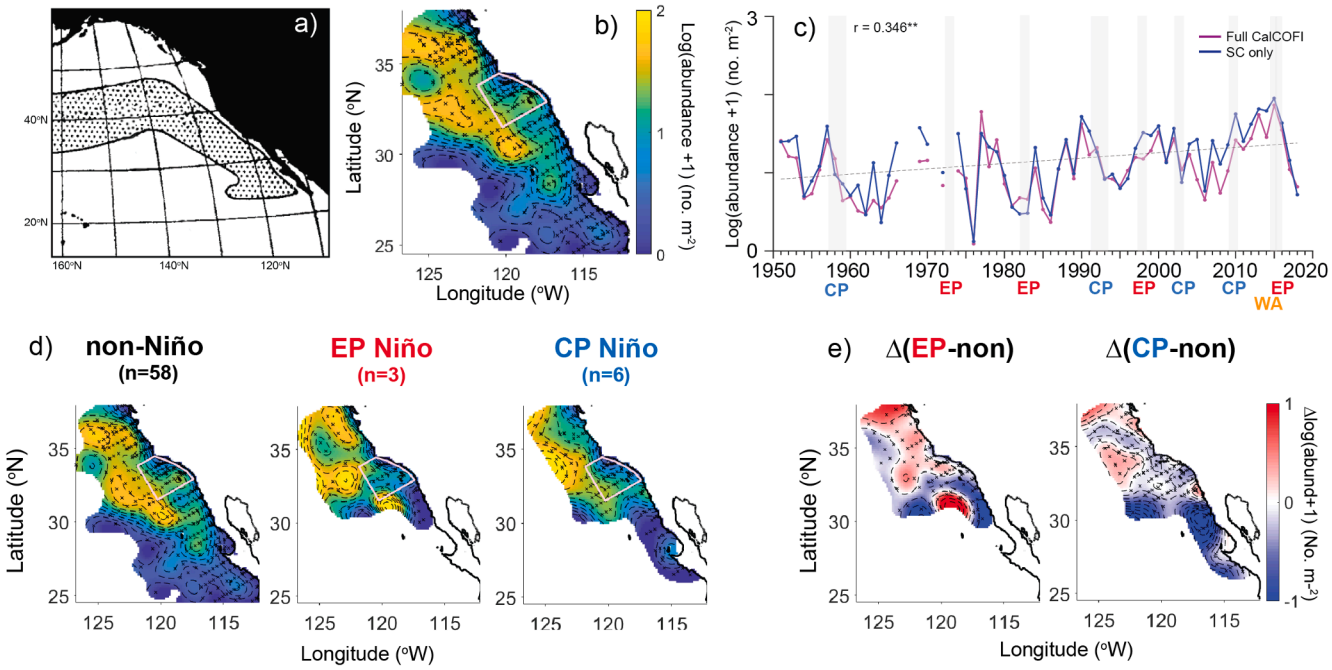

Fig. 9. As in Fig. 2, but for *Thysanoessa gregaria.* Grey dashed linear fit indicates significant long-term trend; Spearman rank significance shown (**p < 0.01).

produced only moderately decreased abundance and poleward retraction, while 1991–93 (springs 1992, 1993) reduced abundance on par with EP Niños (Figs. S1a and S10). The 2002–03 and 2009–10 CP Niños, characterized as anomalously cool (spring 2003; Bograd & Lynn, 2003) or without enhanced poleward advection (spring 2010; Todd et al., 2011), showed average or elevated *E. pacifica* abundances and were part of a high-abundance period throughout the 2000s. The 2014–15 Warm Anomaly (spring 2015) produced greater poleward retraction and coastal compression than the 2015–16 El Niño (Fig. S10), likely due to the Warm Anomaly's more expansive and persistently warm, low-productivity conditions.

Thysanoessa spinifera is another dominant cool-water species of the central CCS, although it inhabits only neritic upwelling waters with limited offshore extent (Fig. 3a-b; see Brinton, 1962). Previous analyses of *T. spinifera* did not detect consistent El Niño variability in regionwide total abundance (Lilly & Ohman, 2018), but the species shows El Niño-related spatial change (Fig. 3d). Both the EP and CP average Niño distributions show slight offshore expansion relative to the non-Niño average, and the '[CP]-[non-Niño]' difference plot shows a slight nearshore increase (Fig. 3e), although these patterns are likely dominated by single Niño extreme population increases (EP: 2016, CP: 2010; Fig. S11). *Thysanoessa spinifera* was present only at very low abundances in nearshore northern regions in springs 1958–59, 1992–93, and 1998, and completely absent from the CalCOFI region in spring 1983 (Fig. S11), likely due to significant reductions in upwelling habitat. These findings are corroborated by shoreward (1993, 2015, 2016) and poleward (1958–59, 1983, 1998) shifts in COG (Fig. S1b). As with *E. pacifica, T. spinifera* increased in abundance in springs 2003 and 2010 and was notably elevated off Point Conception in spring 2016, likely reflecting the return of upwelling at the end of the 2015–16 El Niño. Regionwide abundance of *T. spinifera* was also high in springs 1999 and 2017, suggesting rapid recovery following El Niño events. Both *E. pacifica* and *T. spinifera* show significant long-term increases in Southern California region average abundance across the 1951–2018 period ($p < 0.05$ and 0.001, respectively; Figs. 2c and 3c).

3.1.2. Subtropical coastal species

Nyctiphanes simplex inhabits coastal waters off southern and Baja California and has a similar, though more southerly-centered, distribution to *T. spinifera* (Fig. 4a-b; see Brinton, 1962). The mean CalCOFI distribution of *N. simplex* shows a narrow nearshore band of moderate abundance up to Point Conception, CA. Regionwide mean abundance undergoes decadal variability associated with the Pacific Decadal Oscillation (Brinton & Townsend, 2003; Di Lorenzo & Ohman, 2013) but also varies significantly with El Niño events (Fig. 4c; Lilly & Ohman, 2018). Average EP and CP Niño distributions of *N. simplex* show clear but different poleward extensions: EP Niños show high abundance in a narrow coastal band, while CP Niños show more spatially diffuse poleward extension and low presence north of Point Conception (Fig. 4d). Average distributions of both Niño categories show significant increases in the nearshore California region compared to the non-Niño average. All El Niño springs except 2003 and 2010, as well as the Warm Anomaly (spring 2015), showed regionwide increases in *N. simplex* abundance (Fig. S12). Spring 2016 had the highest *N. simplex* abundance of the timeseries aside from 1984, while the 1983 and 1998 EP Niño springs had the farthest poleward population extensions of any El Niño year, in narrow coastal bands (Figs. S1c and S12). Such extreme northward extension suggests that these El Niño events likely had a different dominant forcing mechanism (i.e., enhanced poleward advection) than other Niños. In contrast, the 2016 EP Niño spring produced significant offshore expansion in the SC region, similar to two-year CP Niños (springs 1958–59, 1992–93) and the Warm Anomaly (spring 2015) (Figs. S1c and S12). *Nyctiphanes simplex* was only present in spring 2003 in a low-abundance pocket off Monterey Bay, and completely absent in spring 2010.

3.1.3. Tropical Pacific-Baja California species

Euphausia eximia has a mean distribution centered farther south and offshore than *N. simplex*, extending to the margins of tropical equatorial Pacific waters and mostly absent off California in spring except during El Niño events and the late 1970s (Fig. 5; see Brinton, 1962, 1981). *Euphausia eximia* expands shoreward to coastal Baja California during both EP and CP Niños, although only EP events and the Warm Anomaly show spring poleward extension north to the SC region (Fig. 5d). Highest *E. eximia* abundance in the SC region occurred during the Warm Anomaly (spring 2015), characterized by COG shifts poleward and onshore, while the 2016 EP Niño distribution was centered farther south (Figs. S1d and S13). In contrast, *E. eximia* was scarcely or not at all

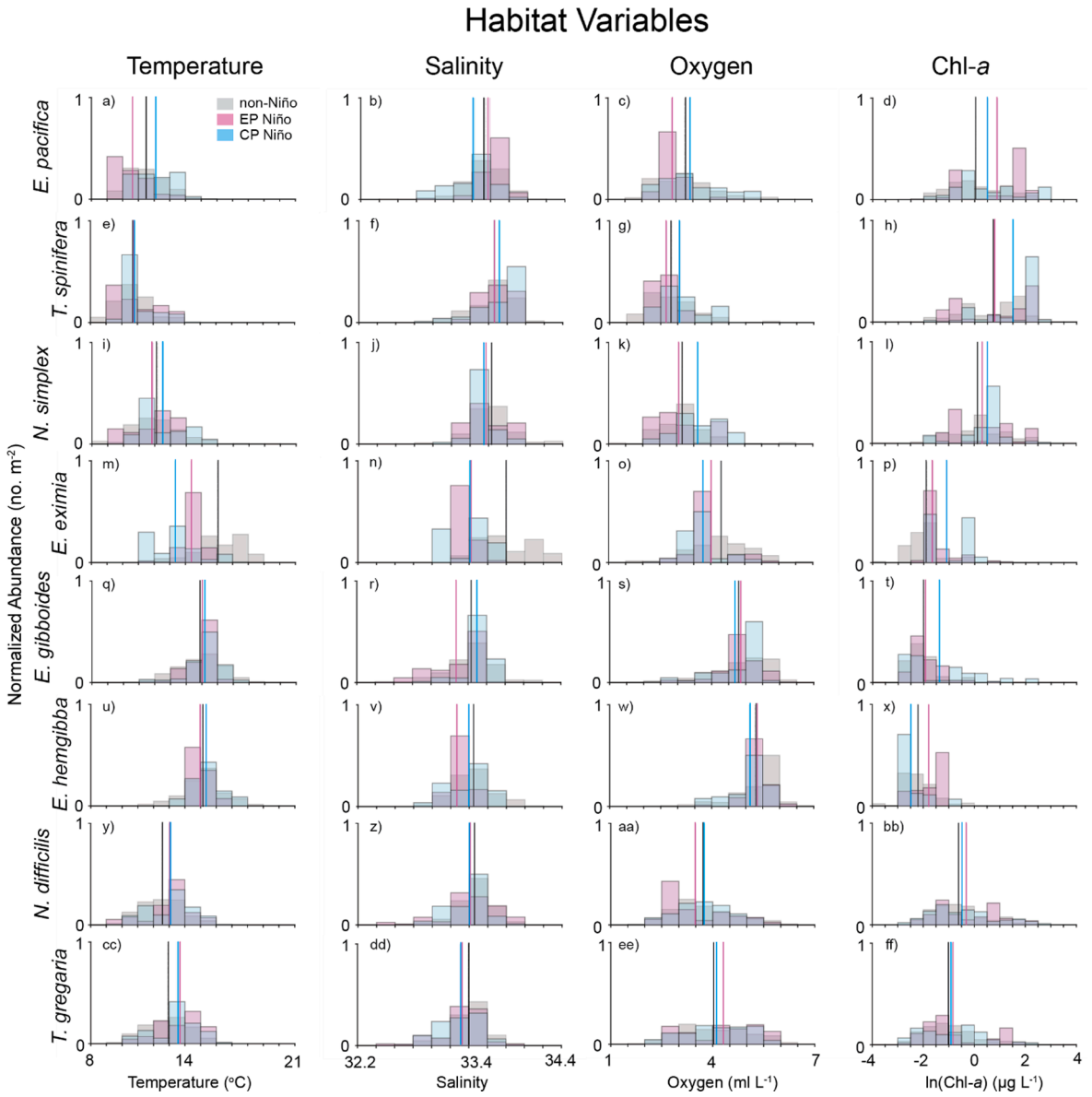

Fig. 10. Spring abundance-weighted species distributions across four habitat variables: temperature at 50 m depth, salinity at 50 m, oxygen at 100 m, ln(chlorophyll-a) at 10 m. Vertical bars indicate means for each Niño type (grey bars and black line – non-Niño; pink bars and line – EP Niño; blue bars and line – CP Niño). See Fig. S4 for the remaining two species. (For interpretation of the references to colour in this figure legend, the reader is referred to the web version of this article.)

present off California during CP Niño springs except 1992–93. As mentioned for *N. simplex*, EP Niños likely have physical characteristics that induce more onshore expansion and poleward extension of tropical species than do CP events, explaining the SC region presence of *E. eximia* predominantly during EP Niños.

3.1.4. Subtropical offshore species

Euphausia gibboides and *E. recurva* classify as subtropical offshore species that inhabit North Pacific Subtropical (Central) Gyre waters, extending eastward to within 100 km of Baja California. Brinton (1962) classified *Stylocheiron affine* as a Baja California/Subtropical species along with *E. eximia*. However, the CalCOFI distribution and El Niño responses of *S. affine* align more closely with those of *E. gibboides* and *E. recurva*, so we categorize it as a Subtropical Offshore response. The three species show very similar El Niño responses, so we focus here on *E. gibboides* (Figs. 6, S1e, S14; see Figs. S1f, S2, S15 for *E. recurva,* and S1g, S3, S16 for *S. affine*). On average, during EP Niños *E. gibboides* expands poleward and shoreward regionwide except for a narrow coastal band (Fig. 6d). In contrast, the average CP Niño distribution shows *E. gibboides* expansion all the way to shore off southern and Baja California, perhaps transported by stronger onshore flows, although it does not extend as far poleward as during EP events. The total area of increase (Fig. 6e, sum of all red patches) during EP Niños compared to the non-Niño average is three times greater than the area of no change or decrease (sum of white and blue patches; values not shown), while the area of increase during CP Niños is only moderately greater than the corresponding area of decrease or no change.

However, *E. gibboides* shows variability between El Niño events of a given category (Fig. S14): the 1958–59 CP, 1992–93 CP, and 1983 EP Niño springs showed substantial population expansions into the near-shore SC region, though at only moderate abundances, while the 1998 and 2016 EP Niño springs produced elevated abundances offshore. During the 2003 and 2010 CP Niño springs, *E. gibboides* extended poleward offshore. Highest SC abundance and farthest shoreward expansion of *E. gibboides* occurred during the 2015 Warm Anomaly (Figs. 6c and S1e). Lack of full shoreward expansion of *E. gibboides* during two EP Niños suggests that offshore species may be inhibited from onshore movement by the strongly anomalous coastal poleward

flows of those events. In contrast, anomalous onshore advection and a lack of anomalously strong alongshore flow during other events (e.g., 1983 EP Niño, Simpson (1984); 1992–93 CP Niño, Ramp et al. (1997); 2015 Warm Anomaly, Zaba and Rudnick (2016)) corresponded to farther shoreward population expansions. *Euphausia recurva* and *S. affine* show similar average distributions to *E. gibboides* across Niño categories, although both species extend farther north and *S. affine* extends farther south and has a patchier El Niño distribution (Figs. S2-S3, S15-S16).

Euphausia hemigibba has a subtropical–tropical offshore distribution that lies between *E. eximia* and *E. gibboides* (Fig. 7a-b; Brinton, 1962; Brinton & Townsend, 2003). Its El Niño responses likewise show characteristics of both *E. eximia* and *E. gibboides*: it has the lowest SC average abundance of all 10 species but a more consistent presence than *E. eximia* (Fig. 7c). However, *E. hemigibba* population centers do not extend nearly as far poleward or onshore as *E. gibboides* during either Niño category, remaining mostly off Baja and southernmost California. Total areas of increase of *E. hemigibba* during average EP and CP Niños are slightly greater than areas of decrease (Fig. 7e, total red patches [increase] or blue patches [decrease]). As with *E. gibboides*, *E. hemigibba* had highest SC abundance and positive (poleward) COGy shifts during the 2015 Warm Anomaly, elevated offshore abundance and poleward extension in springs 1993 and 1998, and moderate offshore elevated populations in 1958–59, 1983, and 2016 (Figs. S1h and S17).

3.1.5. Regionwide temperate species

Nematoscelis difficilis and *Thysanoessa gregaria* are temperate-to-cool species that extend from the North Pacific Current (~40°N) to southern Baja California and to 300 km offshore (Figs. 8a-b and 9a-b; see Brinton, 1962, 1981). *T. gregaria* is displaced slightly offshore from *N. difficilis* and was classified by Brinton (1981) as an Intermediate Subtropical species. *Nematoscelis difficilis* is the second most abundant species in the CCS after *E. pacifica* (Fig. 8c; see Brinton & Townsend, 2003). Regionwide abundance of *N. difficilis* is relatively consistent across Niño and non-Niño years, with dips in 1983, 1992–93, and 2003 (Fig. 8c). *Thysanoessa gregaria* shows similar, though greater and more prolonged, decreases in abundance during the same events and 1958–59 (Fig. 9c). Average EP and CP distributions for both species are similar to non-Niño years, although with minor increases in the northern coastal California region during EP Niños and substantial decreases in the southern region during both EP and CP Niños (Figs. 8d-e, 9d-e). Centers of gravity were generally insensitive to population shifts because both species have consistent regionwide distributions (Fig. S1i-j). As with other cool-water species, *N. difficilis* and *T. gregaria* show significant long-term abundance increases in the SC region ($p < 0.001$ and 0.01, respectively).

3.2. El Niño-related habitat variability

3.2.1. Spring habitat distributions and source water masses

To determine El Niño-related variability in euphausiid habitats, we analyzed species abundances in comparison to four habitat variables measured at each CalCOFI station (Figs. 10 and S4; see Tables S1 for mean distribution values and S2 for Kruskal-Wallis values of similarity comparisons across Niño types for a given variable). We focus on spring distributions but also analyzed habitat variables in winter (Section 3.2.2.: DJF, 1951–2002; Fig. S4, Tables S3 and S4). To determine species associations with certain water masses, we further analyzed euphausiid abundance distributions in relation to proportions of three dominant water masses that comprise the SC region (Figs. 11 and S5, Tables S5 and S6). Pacific Subarctic Upper Water (PSUW) is southward-flowing, cool, high-oxygen, and indicative of the core CA Current; Pacific Equatorial Water (PEW) is warm, salty, subsurface, nearshore poleward-flowing, and indicative of the CA Undercurrent; and Eastern North Pacific Central Gyre Water (ENPCW) is warm, moderately salty, near-surface, and of southwestern offshore origin (see Methods Section 2.5.2 and Bograd et al. (2019) Figs. 1 and 2 for complete information). We present species abundance distributions across proportions of each water mass, where proportion is the contribution of that water mass to the total regional water makeup (sum of all water masses). We also show the mean proportion of each water mass averaged across the SC region and all years within each Niño category (see arrows below x-axes in Figs. 11 and S5; colors correspond to Niño category).

3.2.1.1. Cool-water, coastally-associated species.

Consistent with their spatial distributions, *Euphausia pacifica* and *Thysanoessa spinifera* inhabit upwelling-characteristic waters (cool, salty, low O_2, higher Chl-*a*) (Fig. 10a-h). During EP Niños, the *E. pacifica* distribution shifts even farther into these conditions, reflecting spatial compression to only nearshore waters. In contrast, *T. spinifera* habitat remains consistent across non, EP, and CP Niños. Water mass associations indicate that during EP Niños, *E. pacifica* associates with higher proportions of PSUW and lower PEW than the mean regional proportions of each water mass, reflecting northward population compression into PSUW waters (Fig. 11a-b, Table S5; vertical arrows below x-axes indicate mean regionwide water mass proportions for each Niño category). Association of *E. pacifica* during CP Niños with lower PSUW and higher PEW reflects the species' elevated coastal presence in 2003 and 2010. *Thysanoessa spinifera* has similar water mass associations to *E. pacifica* across non-Niño and CP Niño types but much lower association with PSUW and higher associations with PEW and ENPCW during EP Niños (Fig. 11d-f). These differences likely reflect a combination of the more neritic distribution of *T. spinifera*, its stronger shoreward compression during EP Niños, and its population extension farther south into the SCB (ENPCW waters) in spring 2016 (Figs. 3d and S11).

3.2.1.2. Subtropical coastal species.

Nyctiphanes simplex shows habitat characteristics between cool-water coastal species and subtropical offshore-tropical species (Fig. 10i-l), reflecting its intermediate distribution as a subtropical but coastal species that regularly inhabits the nearshore Southern California Bight. Although *N. simplex* extends significantly poleward during EP Niños, it does not show dramatic habitat shifts, suggesting the population may initially be advected in conjunction with parent water masses. Elevated oxygen habitat during CP Niños could reflect outward population expansion toward the core California Current, while slightly warmer temperatures could reflect its center in more southerly and somewhat offshore waters off Baja California compared to its nearshore poleward transits during EP Niños (Fig. 10k). As with habitat characteristics, *N. simplex* shows similar water mass associations to *E. pacifica*, though lower PSUW and higher PEW during EP Niños and higher ENPCW across all years, reflecting its southerly and nearshore distribution (Fig. 11g-i).

3.2.1.3. Tropical Pacific-Baja California species.

Euphausia eximia inhabits a significantly different habitat during EP and CP Niños compared to non-Niño years (Fig. 10m-p). During non-Niño years, *E. eximia* inhabits the warmest, saltiest waters of all species examined here. During El Niños it shifts to cooler, fresher, lower-O_2, higher-Chl-*a* waters, with greatest shifts during CP Niños. These changes corroborate the hypothesis of El Niño advection of *E. eximia* into cooler, fresher waters off southern California from its normal southern warm, salty, tropical habitat. Highest *E. eximia* abundances occur at the mean proportions of PSUW and PEW across all Niño categories, again suggesting Niño-related population advection into the SC region with certain water masses (Fig. 11j-l). Low associations of *E. eximia* with ENPCW during EP and CP Niños suggest that it moves into the SC region via coastal PEW rather than offshore ENPCW.

3.2.1.4. Subtropical offshore species.

Euphausia gibboides inhabits a narrow temperature range with mean values similar to *E. eximia,* but lowest salinity and Chl-*a* and highest O_2 ranges of all species analyzed, reflecting offshore, subtropical, Central Gyre-associated habitat

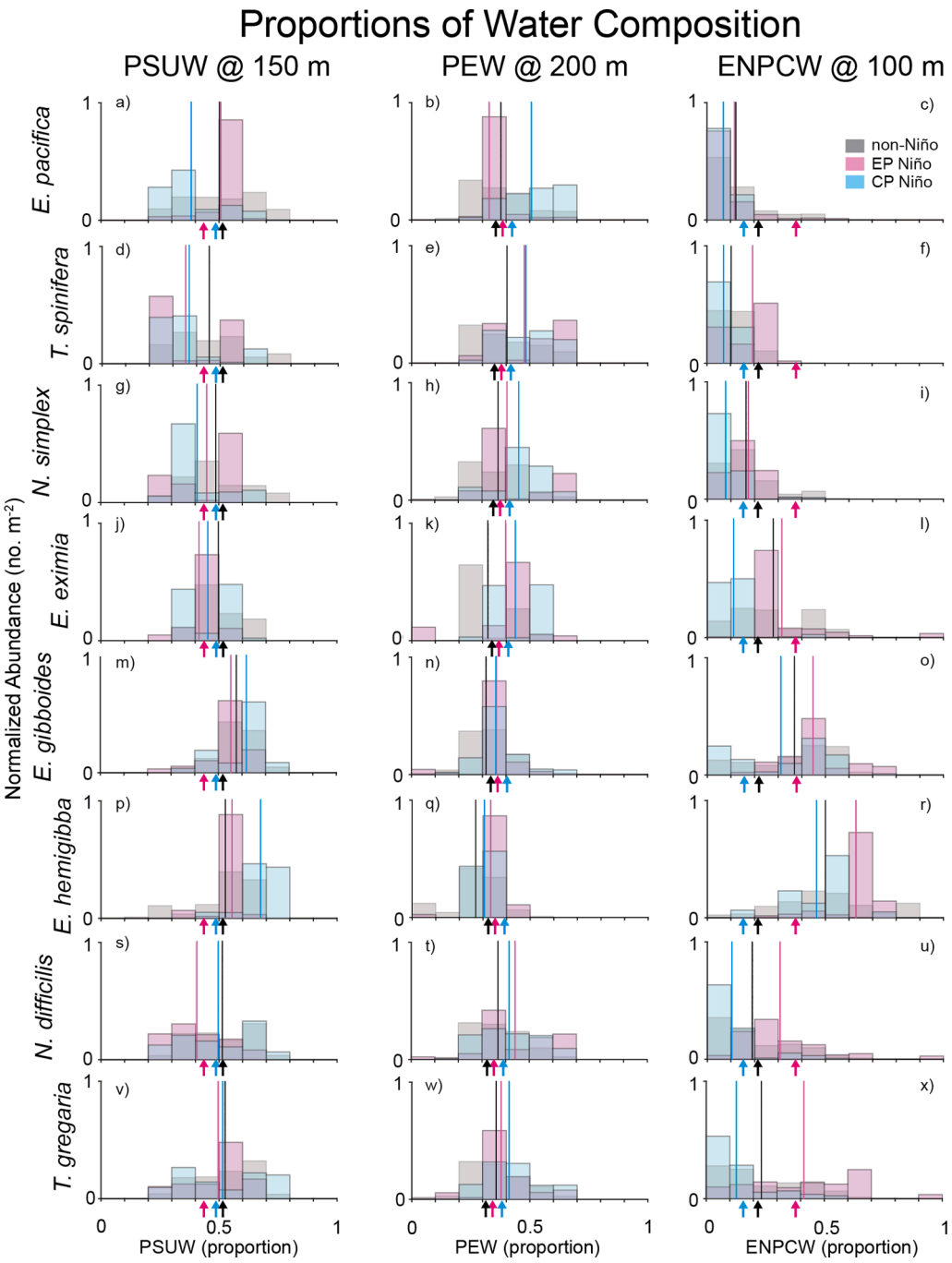

Fig. 11. Spring species abundance distributions for proportions of three water masses (Pacific Subarctic Upper Water, PSUW; Pacific Equatorial Water, PEW; Eastern North Pacific Central Gyre Water, ENPCW) at given depths. Data are from the SC region only, 1985–2017. Arrows below x-axes indicate mean water mass proportions across the entire SC region and time period.

(Fig. 10q-t). Consistent habitat distributions across Niño categories suggest advection with parent water masses (i.e., enhanced onshore flow during some Niños) rather than species movement into dramatically new environments. The low-salinity distribution may come from the portion of the *E. gibboides* population that overlaps the fresh core California Current, and appears to be strongest during EP Niños, perhaps due to shoreward expansion (Fig. 10r). *Euphausia recurva* and *S. affine* have similar habitat distributions to *E. gibboides,* although slightly lower oxygen (both species) and higher Chl-*a* (*S. affine*), reflecting farther shoreward intrusions (Fig. S4, rows f-g). *Euphausia hemigibba* has similar habitat ranges to *E. gibboides* but the highest O_2 and lowest Chl-*a* of the ten species (Fig. 10u-x).

Water mass associations indicate that *E. gibboides* inhabits high proportions of PSUW and ENPCW and low PEW across all Niño categories, reflecting its offshore distribution (Fig. 11m-o). Associations with decreased ENPCW and increased PSUW during CP Niños may reflect offshore northward population expansion, while opposite associations during EP Niños indicate onshore expansion into the southern SC region. Both *E. recurva* and *S. affine* have similar water mass associations to *E. gibboides,* although stronger PEW (*S. affine*) and ENPCW (both species) during EP Niños, likely due to shoreward population incursions into the SCB (Fig. S5). *Euphausia hemigibba* associates with all three water masses similarly to *E. gibboides* but with lower PSUW and PEW and the highest ENPCW association of any species, reflecting its

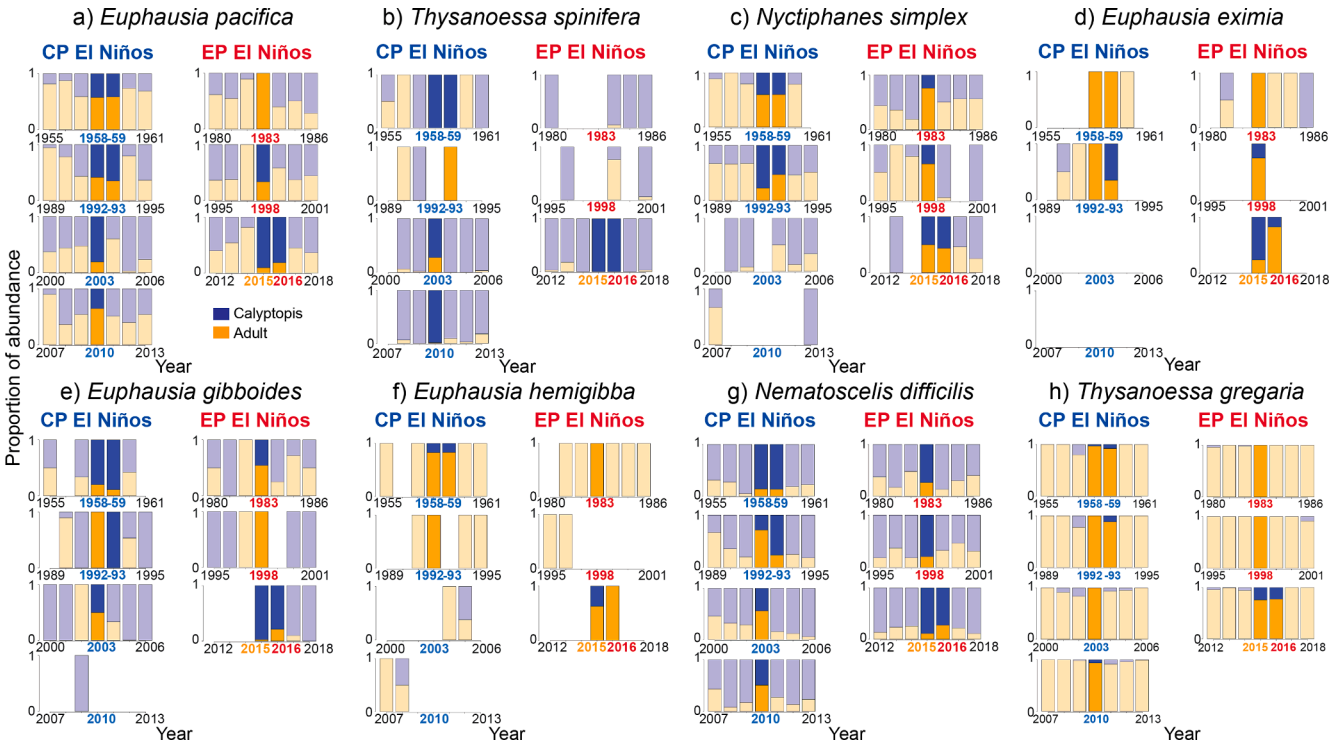

Fig. 12. Average proportions of adult (orange) and calyptopis (blue) SC region spring abundance during each El Niño year (bold colors) and the three prior and three following years (pale colors). Proportions are calculated out of the sum (adult + calyptopis). Lack of bars indicates a lack of both the adult and calyptopis phases, although furcilia or juvenile phases may be present. (For interpretation of the references to colour in this figure legend, the reader is referred to the web version of this article.)

presence predominantly in the southern offshore CCS (Fig. 11p-r).

3.2.1.5. Regionwide temperate species. *Nematoscelis difficilis* and *T. gregaria* have comparable habitat ranges and habitat consistency across Niño categories. The habitat ranges of *T. gregaria* are slightly higher-O_2 and lower-Chl-*a* than for *N. difficilis,* reflecting the *T. gregaria* center farther offshore (Fig. 10y-ff). Water mass associations of both species are comparable to *E. pacifica* for PSUW and PEW across most Niño categories, and align with the mean proportions of each water mass for the region (Fig. 11s-w). Both species are positively associated with ENPCW across all Niño categories, reflecting their elevated presence in the offshore SCB (Fig. 11u,x).

3.2.2. Winter-spring habitat shifts (all species)

Winter habitat conditions of cool and warm coastally-associated species (*E. pacifica, T. spinifera, N. simplex*) are warmer, fresher, higher-O_2, and lower-Chl-*a* than their corresponding spring distributions across all Niño categories, reflecting the usual winter-to-spring transition to upwelling conditions (Fig. S4, rows a-c; spring plots are reproduced from Fig. 10). Habitat distributions of coastal species during EP Niño winters show significantly higher temperatures and lower oxygen than during non-Niños, emphasizing winter onset of El Niño conditions. Winter initiation of extreme EP Niño conditions likely induces population die-off and reduced reproduction of cool-water coastal species that cannot tolerate such extremes, explaining spring shoreward compressions and poleward retractions (Figs. 2d and 3d).

In contrast, winter distributions of *E. eximia* are largely consistent across Niño categories, and generally align with the species' spring non-Niño distributions (Fig. S4, row d). Only during El Niño springs does *E. eximia* shift into significantly altered waters with characteristics of the core California Current, suggesting late winter-spring population poleward advection during EP events. In contrast, winter distributions of *E. gibboides* align with its spring habitat, further corroborating the idea of population movement with parent water masses; the exception is elevated winter temperatures during EP Niños, likely due to regionwide warming (Fig. S4, row e). This interpretation is corroborated by similar winter/spring distributions and EP Niño shifts of *E. recurva* and *S. affine*, since all three species inhabit the same waters (Fig. S4, rows f-g). *Euphausia hemigibba* has higher overall temperature and oxygen ranges than the above three species but also shows consistency between winter and spring distributions (Fig. S4, row h). As with cool-water coastal species, regionwide temperate species (*N. difficilis, T. gregaria*) inhabit significantly warmer waters during EP Niño winters relative to non-Niño years (Fig. S4, rows i-j), which may instigate subsequent spring population die-off and reduced growth in offshore waters. However, the overall temperature and salinity ranges of *N. difficilis* and *T. gregaria* during both EP and CP Niño groups are the same as for non-Niño years, perhaps reflecting the sub-thermocline ranges of these species and therefore their lower susceptibility to El Niño.

3.3. Population structure during El Niño

To determine whether euphausiid population stage structure, as an index of potential population growth, is impacted by El Niño, we first examined SC region-averaged spring proportions of adult and calyptopis stages for each species across each El Niño event and surrounding years (Figs. 12 and S6). We then examined spring habitat ranges for the calyptopis phase only, to determine whether reproduction occurs across a species' habitat range or only in a subset of conditions (Fig. S7, Tables S7 and S8).

3.3.1. Cool-water, coastally-associated species

Euphausia pacifica spring adult and calyptopis proportions did not change appreciably during CP Niños from surrounding years, while responses to EP Niños differed by event (Fig. 12a). The adult phase dominated *E. pacifica* during the 1983 event, suggesting reduced reproduction and calyptopis production or survival, while both 1998

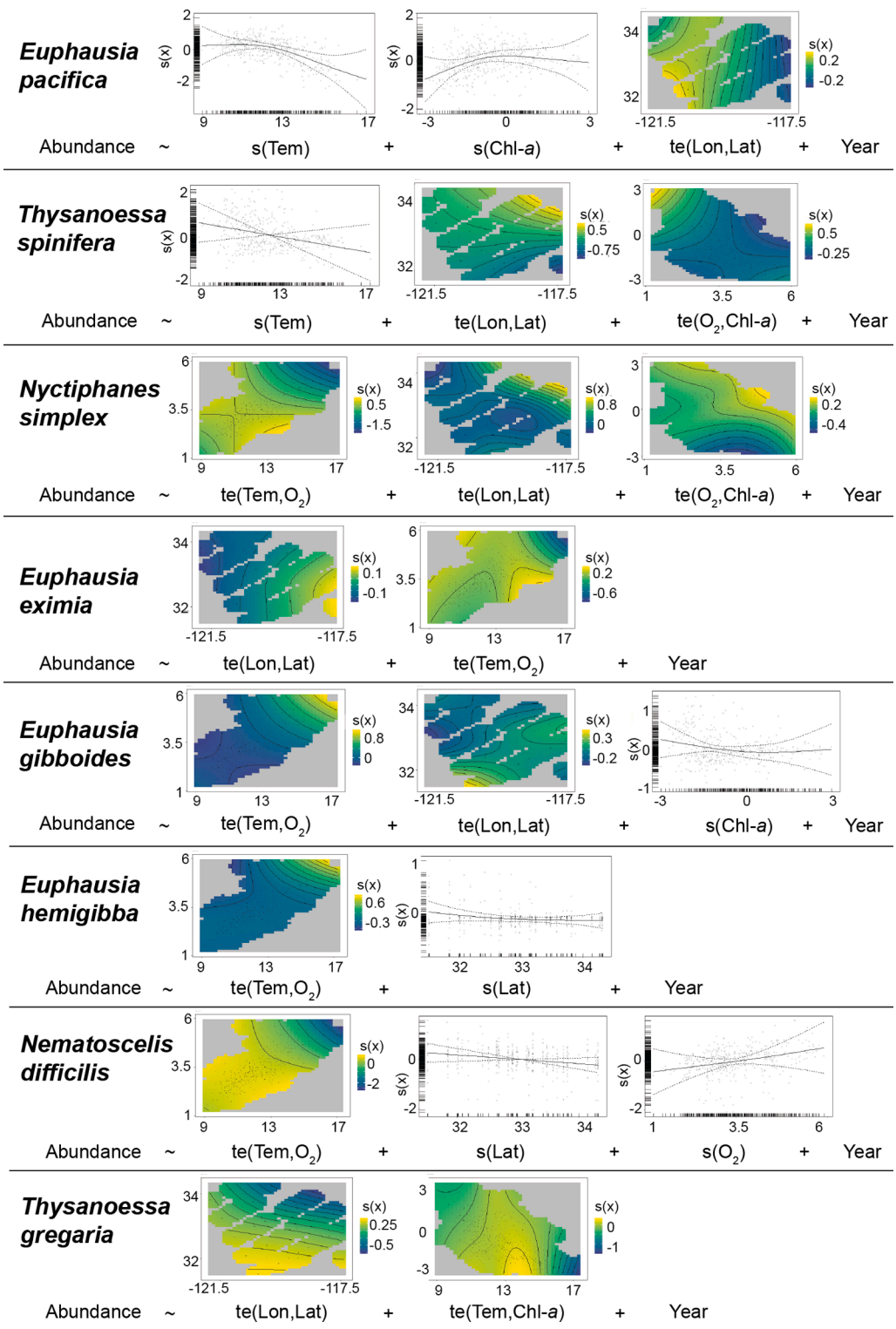

Fig. 13. Generalized additive model (GAM) optimal equations and outputs, where species spring abundance is modeled as a combination of habitat variables. Abundance is $\log_{10}$-transformed; Chl-*a* is natural log-transformed. Model terms and plots are ordered by decreasing significance (*left to right*). For two-variable terms, the first term listed in parentheses is the x-axis term, and the second is the y-axis term. Numbers of knots associated with each term are listed in Table S7. 's' = single-variable smoothers, 'te' = tensor smoothers for interactive terms. GAMs were modeled for the SC region only, 1984–2017.

and 2015–2016 had elevated calyptopis proportions, suggesting return of population reproduction in those El Niño/Warm Anomaly springs. Brinton (1962) noted relatively equal adult and larval calyptopis proportions of *E. pacifica* in the Eastern North Pacific, so short-term dominance by one phase likely reflects temporary increases or decreases in reproduction. In contrast, *T. spinifera* is the species most consistently dominated by the calyptopis phase in the SC region in spring (Fig. 12b; Brinton, 1962). However, in three post-Niño years (1960, 1993, 1999), notably after complete absences of both adult and calyptopis phases in 1992 and 1997–1998, *T. spinifera* was only present in adult forms. Calyptopis phases of both *E. pacifica* and *T. spinifera* had similar habitat ranges to their total populations, suggesting reproduction habitat-wide rather than only in a subset of conditions (Fig. S7a-h).

3.3.2. Subtropical coastal species

Nyctiphanes simplex had higher calyptopis proportions during the 1958–59 and 1992–93 CP Niños and the 2015–2016 Warm Anomaly-El Niño springs compared to surrounding years (Fig. 12c), suggesting

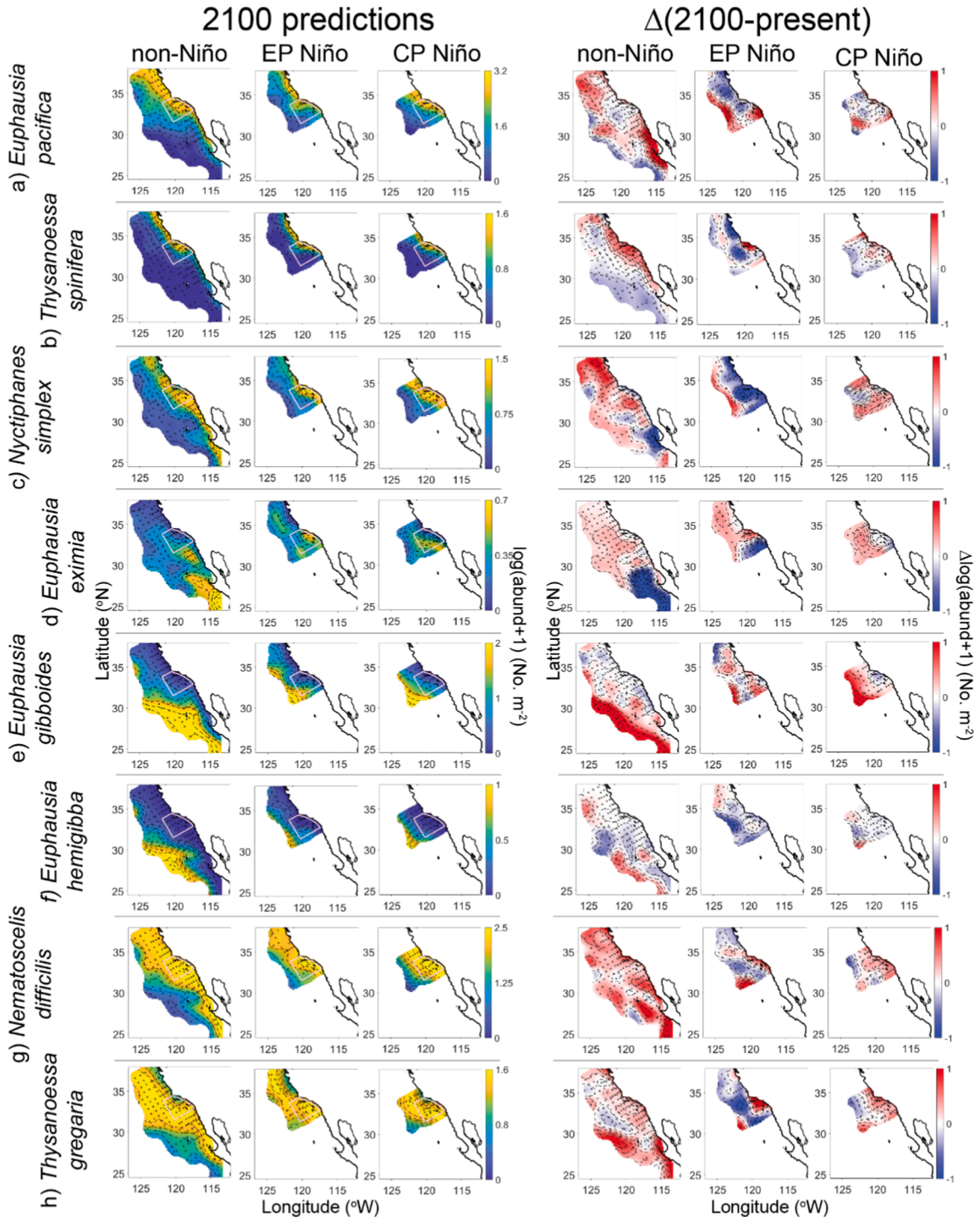

Fig. 14. (*left panel*) Predictions of euphausiid species spring distributions under average non-Niño, EP Niño, and CP Niño conditions in Year 2100, using GAMs from Fig. 13 and habitat variables adjusted to Year 2100 predicted values. (*right panel*) Differences between Year 2100 predictions and current average distributions. Spatial coverage during El Niño years is lower than in Figs. 2d–9d due to lack of input variables at certain stations. All units are log (abundance + 1), as (No. m^{-2}).

enhanced *in situ* reproduction under prolonged favorable conditions. In the 1983 and 1998 Niño springs, proportions of *N. simplex* calyptopes were relatively low (Fig. 12c), perhaps due to wintertime increases in abundance that grew to adult populations by spring. *N. simplex* calyptopes inhabit fresher, higher-oxygen, higher-Chl-*a* waters than the total population during non-Niño years, suggesting preferential reproduction in California Current waters rather than off Baja California (Fig. S7i-l). During El Niños, *N. simplex* calyptopis and total population habitats are similar, suggesting consistent advection across life history phases.

3.3.3. Tropical Pacific-Baja California species

Euphausia eximia has a consistently adult-dominated population stage structure across years in the SC region (Fig. 12d; see Brinton, 1962). Only springs 1993 and 2015 had significant calyptopis proportions, perhaps due to favorable reproductive habitat following entire years of sustained elevated temperatures. *Euphausia eximia* calyptopes inhabit similar waters to the total population in non-Niño years but upwelling-characteristic waters during EP and CP Niños, suggesting possible coastal reproduction following advection of adults (Fig. S7m-p).

3.3.4. Subtropical offshore species

Euphausia gibboides occurs mostly in calyptopis form in upper waters of the SC region (Brinton, 1962), except before and during some Niño events (1983, 1992, 1998, 2003; Fig. 12e). Increased adult proportions during those years could suggest increased advection from offshore Baja California, where shallower waters tend to be dominated by adult rather than calyptopis forms. Subsequent increases in calyptopis phase could indicate increased *in situ* reproduction by adult populations. Unlike *E. gibboides*, however, both *E. recurva* and *S. affine* are generally dominated by the adult phase in the SC region (Fig. S6), consistent with previous measurements of shallower adult and deeper calyptopis phases (Brinton, 1962). Notably, *S. affine* occurs in entirely adult forms across all years analyzed except 1998, 2003, and four non-Niño years (Fig. S6b). Calyptopis habitat of *E. gibboides* is slightly warmer and higher-oxygen than for its total population, suggesting preferential reproduction and calyptopis dominance offshore (Fig. S7q-t). Calyptopis habitat of *E. recurva* is nearly identical to its total population, although slightly saltier and lower-oxygen, while the *S. affine* calyptopis phase inhabits fresher, higher-oxygen waters than its total population, notably during El Niño, suggesting elevated reproduction in the core California Current (Fig. S7u-bb).

Euphausia hemigibba is almost entirely adult phase in the SC region except during the 1958–59 El Niño and 2015 Warm Anomaly (Fig. 12f). As for *E. eximia*, dominance by adult forms of *E. hemigibba* may reflect preferential survival of adults and only *in situ* reproduction during periods of prolonged or sufficiently elevated temperatures in the SC region. Non-Niño calyptopis distributions of *E. hemigibba* have similar mean values to the total population, although broader distributions (Fig. 10u-x, S7cc-ff), but El Niño calyptopis abundances were too sparse to determine habitat ranges.

3.3.5. Regionwide temperate species

Nematoscelis difficilis shows predominantly calyptopis phase in the SC region, while *T. gregaria* is dominated by adult forms (Fig. 12g-h; Brinton, 1962). The exceptions are increased proportions of *N. difficilis* adult forms during some CP Niños, perhaps reflecting decreased reproduction *in situ*, and minor presences of *T. gregaria* calyptopes at the ends of two-year CP Niños and the 2015–2016 Warm Anomaly-El Niño combination. The *N. difficilis* calyptopis habitat distributions are similar to its total population, with slightly lower mean oxygen and higher Chl-*a* across all Niño categories suggesting slight preferential reproduction in upwelling waters (Figs. 10y-bb, S7gg-jj). The *T. gregaria* calyptopis habitat is higher temperature, salinity, and Chl-*a* and lower oxygen relative to its total population during both EP and CP Niños, similarly suggesting preferential reproduction in nearshore waters (Figs. 10cc-ff, S7kk-nn).

3.4. Generalized additive models and future predictions of distributional shifts

3.4.1. Generalized additive models of current habitat

We developed generalized additive models (GAMs) to evaluate dominant habitat influences on each species (see Figs. 13 and S8 for equations and component plots, and Table S9 for model statistics). Inclusion of 'Year' as a categorical variable was essential to account for substantial interannual variability in abundances of several species and to produce appropriate model residuals. Further adding Niño categories (non, EP, CP) or Niño indices (e.g., Niño3.4, San Diego Sea Level Anomaly) did not improve model results, so we considered one model for each species across all Niño categories. Models for all species except *N. difficilis* explain at least 40% of distributional deviance; *N. simplex* has highest deviance explained (70.8%; Table S9). Every GAM has a significant latitude/longitude term except for *E. recurva*.

Optimal GAMs are similar, though not identical, for spatially similar species: *E. pacifica* and *T. spinifera* both have dominant temperature terms and an influence of Chl-*a*, although *T. spinifera* is also affected by oxygen (Fig. 13). Unlike *E. pacifica,* the *N. simplex* GAM includes interaction terms of oxygen with temperature and Chl-*a*. *Euphausia eximia* and *E. hemigibba* are both modeled only by temperature-oxygen interactive effects and geographic positions, indicating the dominant effect of warm, high-oxygen waters in defining their habitats. Subtropical offshore species (*E. gibboides* [Fig. 13], *E. recurva* and *S. affine* [Fig. S8]) are best modeled by combinations of temperature, oxygen, and Chl-*a,* reflecting consistent habitats defined by specific ranges of conditions. Of the two cool-water cosmopolitan species, *N. difficilis* is strongly influenced by oxygen while *T. gregaria* shows stronger temperature and Chl-*a* effects. GAMs showed only minimal increases in AIC and decreases in percent deviance explained when latitude/longitude terms were removed, with all remaining terms still significant (Table S9, bottom rows for first four species). Cross-validation tests subsetting out a single year and using all other years to predict its abundances produced significant correlation values (measured against GAM-predicted abundance) for 80% of years.

3.4.2. Future predictions of distributional shifts

Using the GAMs developed for each species, as well as documented trends of increasing temperature and Chl-*a* and decreasing dissolved oxygen, we projected future (Year 2100) expected distributions of each species for each Niño category, including future non-Niño conditions (Figs. 14 and S9; see Methods Section 2.7). These analyses assume euphausiid associations with habitat variables will remain unchanged through time and across the spatial domain of the southern CCS.

3.4.2.1. Cool-water, coastally-associated species. Future predictions of *E. pacifica* distributions suggest moderate regionwide increases during non-Niño years but decreased abundance coastally during EP Niños compared to the present EP distribution (Fig. 14a). This change is likely due to reduced suitable habitat resulting from predicted temperature increases. Future EP Niño predictions show patchy areas of increase or decrease, while CP predictions show broader areas of minor to moderate increase (Fig. 14a, right panels). *Thysanoessa spinifera* shows similar predicted distributions for all Niño categories, with populations confined to a narrow nearshore band (Fig. 14b, left panels). Changes from present distributions vary, however: predictions for non-Niño conditions suggest distributional increases across the nearshore region, likely related to predicted increases in Chl-*a*. In contrast, future EP abundances of *T. spinifera* are lower than the present average, and total area of decrease is substantially greater than area of increase (Fig. 14b, right panels). These projected decreases are likely due to comparison to the inflated present distributional average caused by high 2016 EP abundance, as noted in Section 3.1.1.

3.4.2.2. Subtropical coastal species. Nyctiphanes simplex increases regionwide and extends northward under future non-Niño and CP Niño conditions but decreases coastally during EP Niños (Fig. 14c, left panels), with a greater total area of decrease than of increase from the current EP distribution (Fig. 14c, right panels, sum of red regions). This decrease may reflect the importance of enhanced Niño poleward advection, which our GAMs did not include, in increasing *N. simplex* populations.

3.4.2.3. Tropical Pacific-Baja California species. Euphausia eximia shows similar future non-Niño distributions to present, with lower abundance off Baja California possibly due to declining oxygen (Fig. 14d, left panels). However, total area of increase during future non-Niño conditions is substantially greater than area of decrease (Fig. 14d, first panel of right column). Future EP and CP Niño conditions also produce favorable regionwide habitat and greater total areas of increase than of decrease from corresponding present distributions (Fig. 14d, right panels). Presence of *E. eximia* calyptopes during the 1991–93 El Niño and 2014–15 Warm Anomaly suggests reproduction can occur in the SC region under sufficiently warm conditions, although populations likely

still require initial seeding via advection.

3.4.2.4. Subtropical offshore species. *Euphausia gibboides* shows substantial offshore population increases under future non-Niño conditions, perhaps due to increasing temperatures and reduced Chl-*a* (Fig. 14e, first panel of right column). However, total area of increase under future non-Niño conditions is only moderately greater than total area of decrease (Fig. 14e, red and blue regions, respectively). A similar pattern appears for CP Niños. EP Niños show only minor, patchy increases regionwide although twice as much area of increase as decrease. Future distributions for *E. recurva* and *S. affine* are nearly identical to *E. gibboides* despite different GAM equations, although *S. affine Year* 2100 predictions show regionwide decreases compared to present (Fig. S9; note lower abundance scale for *S. affine*). Both species show similar predicted Niño decreases in Year 2100 compared to current Niño averages, perhaps due to lack of advection terms, and hence population seeding, in our models. Similarly, *E. hemigibba* shows only minimal presence offshore during all predicted Year 2100 Niño states and overall moderate decreases during both EP and CP Niños, again likely due to a lack of model advection (Fig. 14f). The exception for *E. hemigibba* is non-Niño future predictions, which show increases in the southern, offshore region, likely due to increased temperatures.

3.4.2.5. Regionwide temperate species. *Nematoscelis difficilis* and *T. gregaria* are predicted to increase regionwide during non-Niño and CP Niño years, producing up to five times more area of increase than decrease. During EP Niños, total areas of decrease are modestly greater than areas of increase, although patches of increased populations appear across the nearshore and offshore SCB (Fig. 14g-h).

4. Discussion

4.1. El Niño impacts on euphausiid spatial distributions

Spatial distributions of the dominant euphausiid species in the southern California Current System (CCS) are strongly influenced by El Niño and vary to a large extent between Eastern Pacific (EP) and Central Pacific (CP) events. Euphausiid responses show additional differences among events of the same type, reflecting known physical variability in CCS expressions of El Niño.

4.1.1. Eastern Pacific (EP) El Niño events

The three major Eastern Pacific (EP) El Niño events on record (1982–83, 1997–98, 2015–16) produced corresponding greatest changes in euphausiid species abundances and spatial distributions in the southern CCS, consistent with past observations of greatest community responses during strongest El Niño events (Brinton, 1960; Brinton & Townsend, 2003; Lilly & Ohman, 2018; Pares-Escobar et al., 2018; see our Supporting Information for a full physical description of each El Niño event). However, population shifts varied between the three events, reflecting different CCS physical expressions of each EP Niño. The 1982–83 event was dominated by onshore flow into the southern CCS from southwestern offshore waters, apparently forced by anomalous local atmospheric circulation, and induced regionwide warming and freshening (Lynn, 1983; Simpson, 1983, 1984). Enhanced poleward advection occurred north of Point Conception, CA, in February 1983 (Glynn, 1988; Huyer, 1983; Ramp et al., 1997). The 1997–98 event had the strongest physical expression of any El Niño on record, particularly in the Eastern Equatorial Pacific region (L'Heureux et al., 2017; McPhaden, 1999). The El Niño signal traveled to the CCS predominantly via oceanic coastally trapped waves (CTWs) that strengthened and broadened poleward nearshore flow off California (Lynn & Bograd, 2002; Schwing et al., 2002; Schwing et al., 2005; Strub & James, 2002).

The 2015–16 EP Niño evolved more moderately than the other two EP events: it warmed waters off South America but produced greatest SST anomalies in the Central Equatorial Pacific, ultimately characterizing as a mixed EP-CP event (L'Heureux et al., 2017; Newman et al., 2018; Timmermann et al., 2019). California Current physical impacts were similarly moderate: positive SST anomalies occurred but were strongest south of Pt. Conception and attributed to alongshore advection from southern waters and possibly coastally-trapped waves (Chao et al., 2017; Frischknecht et al., 2017; Zaba et al., 2020). Downwelling also occurred, but thermocline deepening was not as strong as in 1982–83 and 1997–98, and unusual upwelling winds developed in fall 2015, moderating otherwise potentially strong El Niño effects (Jacox et al., 2016; Zaba et al., 2020).

4.1.1.1. EP Niños: Cool-water coastal and regionwide temperate species responses. Distributional shifts of euphausiid species reflect the varying contributions of enhanced shoreward and poleward flows and warming waters during each EP event. The 1982–83 and 1997–98 events induced significant poleward shifts of coastal euphausiid species, both cool-water (*Euphausia pacifica, Thysanoessa spinifera*) and subtropical (*Nyctiphanes simplex*), in narrow nearshore bands. The 1982–83 event confined coastal species to the nearshore region, likely via both anomalous onshore flow and significantly elevated offshore temperatures (+1–4 °C) (Ramp et al., 1997; Simpson, 1983, 1984). The 1997–98 event induced moderate offshore expansions of coastal populations, likely due to broadening of the Inshore Countercurrent (Lynn & Bograd, 2002). A prior study notes complete absence of *E. pacifica* and *T. spinifera* off Baja California in 1997–98 (Pares-Escobar et al., 2018), consistent with our observations of poleward retraction out of the southern CCS. Decreased total abundances of *E. pacifica* and *T. spinifera* in 1982–83 and 1997–98, and spatial retractions coastward in 1998 without any physical evidence for enhanced shoreward flow, suggest these species experienced overall population mortality and reduced reproduction in response to unfavorable habitat conditions, rather than advection-induced coastward compression of normal population levels.

In the CCS, *E. pacifica* has been shown to associate predominantly with waters below 15 °C (Brinton, 1981). We found similar habitat ranges across all years except EP Niño winters, when *E. pacifica* occurred in waters up to 18 °C. Elevated EP Niño winter temperatures, even short-term, are likely severe enough to reduce cool-water populations through the following spring. It is possible that normal population levels simply retracted northward out of the CalCOFI sampling region, but it is unlikely that the normally high abundances of *E. pacifica* observed here would be sufficiently supported in a substantially smaller region. Acoustic surveys of aggregated krill biomass (apparently dominated by *E. pacifica* and *T. spinifera*) have shown hotspots over shelf-bisecting underwater canyons, which concentrate cold, high-productivity upwelling waters (Santora et al., 2018). During EP Niños, in particular, canyons may provide refugia from warm offshore waters, but they are unlikely to shelter entire populations of *E. pacifica*, which extend into waters well offshore. Significantly elevated *E. pacifica* and *T. spinifera* abundances off Pt. Conception during the 2015–16 EP Niño, and increased proportions of *E. pacifica* calyptopis phase, were likely positive *in situ* responses to moderate spring upwelling, although effects were confined to a relatively nearshore region compared to non-Niño years, suggesting an inability to tolerate the extended 2014–16 warming offshore. Lavaniegos et al. (2019) observed continued low abundances of *E. pacifica* and *T. spinifera* off Baja California through April 2016, likely reflecting slow recovery following prolonged warm conditions.

Regionwide temperate species (*Nematoscelis difficilis, T. gregaria*) also decreased moderately in total abundances during both 1982–83 and 1997–98, although with only minor shoreward compression and poleward retraction. We note that *N. difficilis* and *T. gregaria* likely have more muted El Niño responses than other euphausiid species because they live in and below the thermocline (Brinton & Reid, 1986) and are likely less affected by El Niño-induced habitat changes to the upper 200 m. Near-normal abundances of *N. difficilis* off central and southern California in

spring 2016 suggest either a similar upwelling response to those of *E. pacifica* and *T. spinifera* or an ability to tolerate altered El Niño conditions by living at depth. Lavaniegos et al. (2019) noted significant declines in *N. difficilis* biomass off Baja California in summers 2014 and 2015 and particularly into January 2016. Our SC region may have been far enough north and experienced sufficient upwelling and cool conditions in spring 2016 to either provide a habitat refuge or induce new reproduction of *N. difficilis* off California.

Temperature was the consistent term in generalized additive models of all four cool-water species, suggesting that *in situ* temperature changes or other associated variables are the predominant influence on cool-water species distributions. A prior canonical correspondence analysis (CCA) by Pares-Escobar et al. (2018) of euphausiid species with habitat variables off Baja California revealed an inverse association of *E. pacifica* and *T. spinifera* with the dominant axis (temperature), but no covariance of *N. difficilis* and *T. gregaria* with any physical variable, perhaps due to their warmer habitat ranges or deeper distributions.

4.1.1.2. EP Niños: Subtropical coastal species responses. *Nyctiphanes simplex* responses to EP Niños reflect its unique biogeographic position between cool-water coastal and true subtropical–tropical habitats, with temperature distribution means similar to *E. pacifica* for all Niño groups but temperature ranges spanning from the *T. spinifera* means to the *E. gibboides* means and slightly cooler than the *N. difficilis* and *T. gregaria* means. These findings support the description by Brinton (1962) of *N. simplex* as a nearshore species present in coastal upwelling regions at transition zones between warm and cool regions, as well as his findings that *N. simplex* was generally limited in its northward extension in the CCS to 35°N latitude (temperatures of 11 °C at 100 m to 17 °C at the surface). Similar to cool-water coastal species, *N. simplex* shifted poleward during all EP Niños, but these shifts indicated extensions from southern habitat rather than poleward contraction. Rapid poleward expansions of *N. simplex* along the West Coast in 1982–83 (Brinton & Reid, 1986; Brodeur, 1986; Miller et al., 1985) and 1997–98 (Brinton & Townsend, 2003; Keister et al., 2005; Mackas & Galbraith, 2002; Marinovic et al., 2002; Peterson et al., 2002), as far north as Vancouver Island, British Columbia (Mackas & Galbraith, 2002), suggest initial Niño-related transport via enhanced poleward advection. Brinton and Reid (1986) noted five times higher biomass of *N. simplex* off southern California in 1983–84 than in 1969 (a non-El Niño year), which they attributed to enhanced northerly coastal flow. Marinovic et al. (2002) attribute the sudden presence of *N. simplex* off Monterey Bay, CA, in July 1997 to pre-Niño enhanced poleward flow, as described by Lynn and Bograd (2002).

However, *N. simplex* also appears capable of *in situ* reproduction in the northern CCS during El Niño. Post-larval (calyptopis, furcilia) stages were collected off Oregon between Dec 1997-Nov 1998 (Keister et al., 2005). Initial presence was attributed to northward population advection, while continued presence in summer 1998 was likely due to *in situ* reproduction despite weakening poleward flows. Populations of *N. simplex* persisted off central California through winter 1999, corroborating evidence for *in situ* northern reproduction. Elevated abundances of *N. simplex* in 2015–16 may have resulted from combined *in situ* reproduction (indicated by elevated proportions of calyptopis phase compared to the 1983 and 1998 EP Niños) during the Warm Anomaly and moderate population seeding due to moderately enhanced nearshore poleward flows into the SC region, described by Rudnick et al. (2017). However, neither mechanism was sufficient to extend populations to the northern CCS as during previous EP Niños.

4.1.1.3. EP Niños: Tropical Pacific and subtropical offshore species responses. Influxes of Tropical Pacific (*E. eximia*) and subtropical offshore (*E. gibboides, E. recurva, Stylocheiron affine, E. hemigibba*) species to the SC region suggest direct advection with enhanced onshore and poleward flows during EP Niños; magnitudes of population increase appear to be modulated by biogeographic origins and event physical magnitude. *Euphausia eximia* is known to extend northward into the Southern California Bight in fall even during non-Niño years, as shown by Brinton (1967, 1973) for falls 1949–50. These northward fall movements highlight natural spatial variability due to seasonality, which our interannual study resolution cannot capture. However, *E. eximia* is rarely observed off California in spring (Brinton, 1967, 1973; Brinton & Reid, 1986), so its presence in springs 1983–84 was significant evidence for poleward transport of southern waters, including of oceanic origin. Significant decreases in *E. eximia* temperature and salinity habitat ranges, changes in water mass associations, and absence of post-larval forms in springs 1983 and 1998 further support the hypothesis of population advection into the SC region during EP Niños, consistent with prior speculation about *E. eximia* appearances due to enhanced Countercurrent flow (McLain & Thomas, 1983). Low SC abundance of *E. eximia* in spring 1998 compared to 1983 may reflect a combination of reduced shoreward advection of oceanic waters and earlier (winter) peak event expression in 1997–98. We note the potential for sampling bias toward the adult phase due to possible calyptopis undersampling with 505 μm mesh nets, particularly for smaller species such as *E. eximia.* However, given the high proportions of calyptopis phases for other small species (e.g., *N. simplex*) across most years, and the fact that several years did show high proportions of *E. eximia* calyptopes, our adult/calyptopis proportions represent true interannual fluctuations.

As with *N. simplex,* moderate *E. eximia* presence in the southern SC region in spring 2016 may have resulted from either El Niño-enhanced poleward advection from Baja California or gradual southward population retraction following the 2014–15 Warm Anomaly. Recent analysis of pelagic mollusc populations in the SC region during 2014–16 suggests that elevated abundance in 2016 occurred due to multiyear population persistence following enhanced northward advection in 2014–2015, rather than a new seeding event (Lilly et al., 2019). However, Lavaniegos et al. (2019) measured elevated populations of *E. eximia* and *E. recurva* off Baja California in summer 2015 and through January 2016 compared to summer 2014, which they attributed to enhanced northward transport during El Niño compared to the Warm Anomaly. Our contrasting findings may indicate that enhanced transport did not extend into the SC region or that a return of moderate upwelling in spring 2016 produced unfavorable habitat for subtropical species despite northward transport. The *E. eximia* calyptopis phase had lower proportions in 2016 than 2015, suggesting reduced reproduction in the SC region. Total *E. eximia* abundance declined to zero off California by spring 2017, indicating the population could not sustain itself *in situ* due to lack of continued advection or to mortality in cooler waters.

Offshore subtropical species were likely advected into the SC region with onshore flows during all three EP Niños. Unlike coastal species, they maintain consistent habitat conditions and water mass preferences across all years and winter-spring transitions, suggesting transport with parent water masses. In addition to onshore flow, North Pacific Central Gyre waters can wrap around into the nearshore Southern California Bight and flow poleward via the Inshore Countercurrent (Bograd et al., 2019). The strongest combination of enhanced onshore and poleward flows was described for the 1982–83 EP Niño (Ramp et al., 1997; Simpson, 1984), explaining high subtropical abundances nearshore. However, increases in *E. gibboides* calyptopes during and following 1983 and through the early 1990s indicate moderate persistent post-Niño reproduction *in situ*, unlike for *E. eximia*.

The 1997–98 El Niño corroborates the importance of physical event magnitude in determining extent of euphausiid presence: offshore subtropical species were only moderately elevated and remained farther offshore in the SC region compared to 1982–83, reflecting weaker onshore flows and a stronger, broader nearshore countercurrent. Shoreward advection may have varied across the CCS, however; Keister et al. (2005) observed elevated *E. recurva* off Oregon in 1997–98, which they attribute to onshore flow. In 2016, offshore subtropical populations

appeared to be buffeted even more from shoreward expansion; their distributions mirrored coastal species, with no nearshore presence around Pt. Conception, likely prevented from shoreward movement by offshore flows of cool upwelled waters. As with *E. eximia*, subtropical offshore species distributions in spring 2016 likely reflect retractions back offshore from the SC region following significant onshore expansion in 2015.

4.1.2. Central Pacific (CP) El Niño events

Central Pacific El Niño events show substantially more variability than EP Niños in their equatorial and CCS physical impacts. Some CP Niño signals propagate to the CCS solely via atmospheric teleconnections, while others induce moderate oceanic CTWs (Ashok et al., 2007; Ramp et al., 1997; Timmermann et al., 2019). The 1957–59 CP Niño displaced the California Current offshore, depressed nearshore upwelling, and broadened the Inshore Countercurrent in winter 1958 (Lynn, 1983; Wyllie, 1966), similar to 1997–98, although event forcing was attributed to altered regional wind-driven circulation rather than CTWs (Reid, 1960). Warm conditions persisted through January 1960 (Brinton, 1981). The 1991–93 CP Niño has been characterized as mixed EP-CP (Timmermann et al., 2019) and produced both onshore flow and CTW propagation to the CCS in winter 1992 (Hayward, 1993; Ramp et al., 1997). Normal upwelling occurred in spring 1992, but elevated SSTs subsequently reappeared and persisted through spring 1993 (Chavez, 1996; Hayward, 1993).

The 2002–03 CP Niño was also characterized as mixed EP-CP (Timmermann et al., 2019) but induced strongest Kelvin wave initiation and SST anomalies in the Central Equatorial Pacific (Harrison & Chiodi, 2009; McPhaden, 2004). Its CCS expression was preceded by an anomalously cool, high-salinity subarctic water intrusion in summer 2002 (Bograd & Lynn, 2003; Wheeler et al., 2003), while the El Niño event itself was characterized by moderate warming and salinity-induced stratification (Lavaniegos, 2009; Lavaniegos & Ambriz-Arreola, 2012). The 2009–10 El Niño classified unequivocally as a CP event in the equatorial Pacific (Ashok & Yamagata, 2009; Kim et al., 2011). The Niño signal propagated to the CCS exclusively via atmospheric teleconnections, and depressed the thermocline and warmed upper ocean waters but did not induce anomalous poleward advection (Rudnick et al., 2017; Todd et al., 2011).

4.1.2.1. CP Niños: cool-water coastal and regionwide temperate species responses. As with physical signatures, euphausiid distributional responses to CP Niños separate into i) two-year events physically similar to EP Niños, and ii) cool CP Niños of the 2000s. Although cool-water coastal (*E. pacifica, T. spinifera*) and regionwide temperate (*N. difficilis, T. gregaria*) species decreased in the SC region during both 1957–59 and 1991–93, elevated populations off central California in 1958–59 suggest moderate poleward compression rather than regionwide decreases. Spatial changes during 1957–59 and 1991–93 were similar to 1997–98 but more moderate, likely due to cooler background conditions (1957–59) or weaker Niño signal transport (both events). Elevated abundances of *E. pacifica* and subtropical coastal *N. simplex* only in narrow nearshore bands around Pt. Conception in 1992, and absence of neritic *T. spinifera*, again suggest compression from onshore flows preventing outward expansion of cool and subtropical coastal populations. Shoreward compression appeared to weaken by spring 1993, in line with diminished onshore flows compared to 1992, although impacts of warm temperatures persisted.

Both the 2002–03 and 2009–10 CP Niño events changed CCS euphausiid community composition in opposite ways from past El Niño events. Cool-water species maintained average abundances or increased during both events and expanded outward from the coast in spring 2010. Lavaniegos and Ambriz-Arreola (2012) note similar increases in *E. pacifica* and *T. spinifera* off Baja California in July 2002-spring 2003, which they attribute to increased southward flow via Subarctic water intrusions and cooler habitat conditions.

4.1.2.2. CP Niños: subtropical coastal, tropical Pacific, and subtropical offshore species responses. Subtropical and tropical species increases were more muted and showed less poleward expansion during 1957–59 and 1991–93 compared to 1982–83 and 1997–98. However, subtropical–tropical intrusions appeared to persist and even strengthen by the second spring of each event (1959, 1993), even for the usually rare *E. eximia*, likely due to some *in situ* reproduction under prolonged warm conditions. Elevated post-Niño subtropical abundances persisted through winter 1960 (data not shown) but decreased by spring, suggesting return of upwelling. The 1957–59 event occurred against cool conditions of a negative Pacific Decadal Oscillation (PDO) phase (McGowan, 1998), which likely explains why subtropical species did not persist longer-term as for the 1982–83 El Niño. Surprisingly, despite strong onshore flows in February 1992, two subtropical offshore species (*E. gibboides, S. affine*) did not show significant shoreward expansions, although *E. recurva* did. *Stylocheiron affine* is not a vertically migrating species, which may explain its difference from *E. recurva.* The distributions of *E. gibboides* and *E. recurva* are nearly identical, so we cannot explain this apparent temporary divergence.

Subtropical-tropical species, both coastal and offshore, were near-zero or absent in nearshore waters during the 2002–03 and 2009–10 CP Niños. Offshore subtropical species did expand poleward offshore of the California Current during both events, more so in 2009–10. Subtropical euphausiid responses to the 2002–03 and 2009–10 CP Niños are consistent with past El Niño responses if we consider the anomalous physical characteristics of these two events. Stronger southward flow of the California Current in 2002–03 and lack of enhanced poleward flow in 2009–10 eliminated poleward and shoreward advection of subtropical–tropical euphausiid species into the SC region. Any populations that arrived or already existed *in situ* were likely unable to grow and reproduce under cooler temperatures. Offshore subtropical species and *N. simplex* did increase in the SC region in springs 2005 and 2007, which classified as equatorial CP Niños but fell short of our 'CCS El Niño' classification. Analyzing these years may provide further insight into mechanisms that cause subtropical species movements during CP-like events.

Physically atypical El Niño events such as the 2009–10 CP Niño, which did not show anomalous poleward advection in the southern CCS but had elevated temperatures (Rudnick et al., 2017) and sea level anomaly (Lilly & Ohman, 2018), highlight the importance of developing 'CCS El Niño indices' that consider multiple physical factors in both the equatorial Pacific and CCS, as we have done here. The two regions may show markedly different responses, or a region may have different physical signals depending on the specific El Niño event, so we developed an index to distinguish events that show one or more of a suite of anomalous characteristics in both regions. Likewise, analyzing CCS zooplankton responses during these events can provide greater clues to the physical forcing mechanisms that cause population changes by evaluating how the community responds differently when one of those physical mechanisms (e.g., anomalous advection) is absent.

4.1.3. 2014–15 Warm Anomaly

The anomalously warm conditions in the Eastern North Pacific from late 2013–15 were not attributed to direct El Niño forcing (Bond et al., 2015), but they produced unprecedented surface-enhanced warming (+1–5 °C), onshore flows, and stratified, low-productivity conditions in the CCS on par with major El Niño events (Gentemann et al., 2017; Lilly et al., 2019; Zaba & Rudnick, 2016). Anomalous warming appeared definitively in nearshore waters off California by late spring 2014 and persisted through summer 2015, temporarily interrupted by moderate upwelling in spring 2015 (Gentemann et al., 2017; Jacox et al., 2016; Leising et al., 2015; Lilly et al., 2019; Robinson, 2016; Zaba & Rudnick, 2016). All cool-water euphausiid species and *N. simplex* responded to the

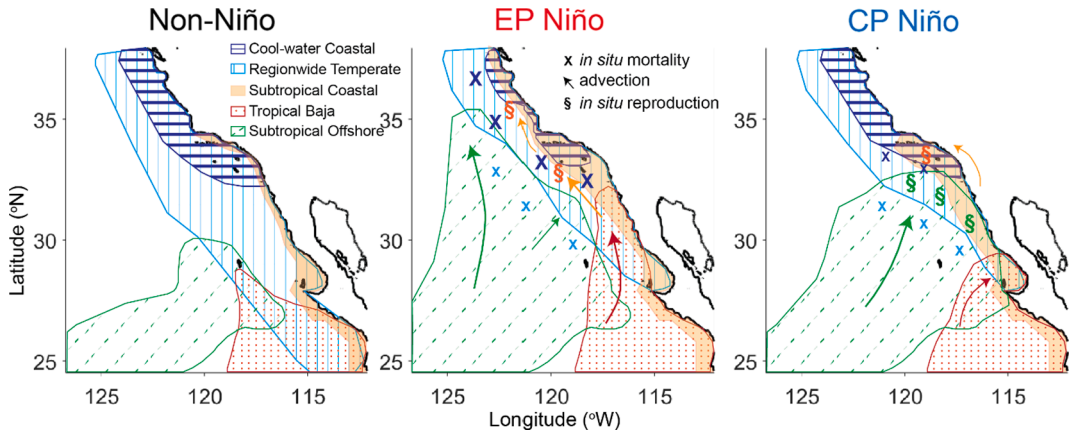

Fig. 15. Schematic distributions of the five main types of euphausiid species spring responses to Eastern Pacific (EP) and Central Pacific (CP) El Niño events. *(center and right panels)* 'X' symbols indicate inferred *in situ* mortality or reduced reproduction, causing coastward compression or poleward retraction; arrows indicate population transport via enhanced advection; '§' indicates inferred *in situ* reproduction and population growth. Symbol colors correspond to the group they affect. Larger symbols indicate a hypothesized larger influence of that process.

Warm Anomaly in a similar manner to past El Niño events characterized by regionwide warming and onshore flow (e.g., 1957–59, 1982–83, 1991–93). Cool-water species contracted to nearshore Pt. Conception but maintained moderate abundances there, suggesting nearshore refugia from the offshore warming, further reinforced by upwelling in spring 2015. Subtropical species flooded the SC region by spring 2015, increasing from near-zero abundances in 2014; three offshore species (*E. gibboides, E. recurva, S. affine*) reached coastal waters. *Euphausia eximia* and subtropical offshore species reached their highest levels in the entire timeseries. Increased proportions of *E. eximia* and *E. gibboides* calyptopis phases compared to EP Niños suggest that persistent warm conditions and shallow stratification promoted significant *in situ* reproduction, as was also described for Baja California (Pares-Escobar et al., 2018).

4.2. Proposed El Niño forcing mechanisms on euphausiids

Our analyses suggest that cool-water euphausiid species respond predominantly to altered *in situ* habitat conditions during El Niño events, while subtropical and tropical species appear in the SC region initially due to anomalous advection. Under non-Niño conditions, cool-water species dominate CCS waters off California (Fig. 15, left panel; dark and light blue shapes), with only minor poleward intrusions of subtropical coastal species (light orange band) into the SC region. During EP Niños, regionwide decreases and nearshore compression of cool-water coastal species into only upwelling areas suggest that negative *in situ* habitat conditions induce population mortality or reduced reproduction in offshore and southern waters (Fig. 15, middle panel; dark blue shape; 'x' indicates inferred *in situ* population mortality or reduced growth). Cool-water coastal species decreases are not as severe during CP Niños, reflecting less extreme habitat changes, although some amount of reduced population growth likely occurs in the southern part of the distribution (Fig. 15, right panel; dark blue shape and symbols). Regionwide temperate species appear overall less impacted by El Niño events, as previously noted (Lilly & Ohman, 2018), but still appear to experience some *in situ* die-off or reduced population growth in the southern and offshore parts of their ranges during both EP and CP Niños (Fig. 15; light blue shape and symbols; small 'x's indicate minor population mortality).

In contrast, subtropical coastal species (*N. simplex*) and Tropical Pacific-Baja California species (*E. eximia*) likely move northward into novel CCS habitats during El Niño events predominantly due to advection. The most significant poleward extensions of subtropical coastal species during EP Niños are apparently due to strongest levels of poleward advection during those events (Fig. 15, middle and right panels; light orange and red arrows). However, subsequent *in situ* reproduction by *N. simplex* likely occurs during and following major El Niños, even when it extends anomalously northward, prolonging its anomalous northern presence (Fig. 15, middle panel; light orange '§' symbols). In contrast, offshore subtropical species (*E. gibboides*, *E. recurva, S. affine, E. hemigibba*) are likely advected shoreward to varying degrees with their parent water masses, depending on the specific strength of onshore flow during each El Niño event (Fig. 15; green shape and arrows). They appear to reach the nearshore SCB only during years of anomalously strong onshore flow, which occurred more often in our timeseries during CP Niños (e.g., 1958) and the Warm Anomaly than during EP Niños, although spring 1983 showed substantial shoreward species incursions in line with observed onshore flow.

As with subtropical coastal species, subtropical offshore species appear to secondarily undergo *in situ* reproduction during and following El Niño events that have sustained warm conditions or a warm background PDO phase (i.e., 1982–83, 1991–93, 2014–16; Fig. 15, green '§' in right panel). However, more southerly tropical species (*E. eximia, E. hemigibba*) show little post-Niño persistence except following multiyear anomalous warming (e.g., 1992–93, 2014–15), likely due to their requirement for significantly warmer reproductive habitat. Thus, although all subtropical and tropical species are influenced by anomalous El Niño-related advection, the extent of advective transport and resulting population persistence depends on a species' biogeographic origins and tolerance for El Niño-induced habitat changes, as well as the physical characteristics of each event. We note that our conclusions are limited by a lack of higher temporal resolution (i.e., seasonality) of sampling, so we cannot truly track *in situ* reproduction or advection. However, our proposed forcing mechanisms are based on patterns in the available data and are intended to be framework hypotheses to be tested in future studies of modeled advection or further measurements of *in situ* population growth.

4.3. Future species distributions and implications for higher trophic levels

Long-term abundance trends combined with predictions of future distributions suggest that cool-water euphausiids will maintain or moderately expand population levels and distributional patterns under non-Niño conditions, while subtropical species will expand into the SC region. The combination of minimal predicted warming in the nearshore southern CCS (compared to regions farther offshore) and increasing Chl-*a* due to enhanced upwelling (Hazen et al., 2013; Rykaczewski & Dunne, 2010) likely explains our findings of cool-water species increases long-term despite temporary El Niño-related population decreases. Pares-Escobar et al. (2018) note that, given predictions that global warming

will induce stronger coastal upwelling (see Bakun et al., 2015; Wang et al., 2015), upwelling-adapted species such as *T. spinifera* will likely continue to increase in the future. Cool-water species will likely tolerate moderate temperature increases and benefit from elevated primary production, while subtropical species may better reproduce under sustained warmer temperatures, as already shown for 1993 and 2015. Although *N. difficilis* and *T. gregaria* live deeper in the water column and are less likely to be affected by changes in coastal upwelling, their long-term increases are likely also due to increasing primary production. Future El Niño events, superimposed on long-term climate trends in the CCS, may continue to result in marked short-term declines in cool-water euphausiid abundances during EP Niños but moderate regionwide increases in all species during CP Niños.

Our predictions of future increases in both cool-water and subtropical species by Year 2100 highlight the importance of understanding the specific mechanisms that cause sub-regional changes in species distributions in the southern CCS. Our observations of long-term increases in cool-water euphausiids over the past 70 years, but no long-term trends for subtropical species in the southern CCS, are contrary to recent findings of increasing subtropicalization of mesopelagic forage fishes in the southern CCS (McClatchie et al., 2018). Strong El Niño-related variability in subtropical euphausiid species suggests they currently depend predominantly on advection into the SC region and cannot yet sustainably reproduce *in situ* long-term. The lack of advective terms in our GAM predictions limits our ability to fully forecast future changes in subtropical species distributions. Assessing advective influences on euphausiids via particle-tracking models will be a topic of future study.

Seasonal-to-interannual variations in euphausiid distributions can significantly affect highly mobile planktivore foraging patterns and management strategies. Whales, seabirds, and mobulid rays off California and Baja California show distinct preferences for certain species of euphausiids, particularly *E. pacifica* (by humpback whales, *Megaptera novaeangliae*: Fleming et al., 2016; Santora et al., 2020; Cassin's auklets, *Ptychoramphus aleuticus*: Lee et al., 2007, Sydeman et al., 2006), *T. spinifera* (blue whales, *Balaenoptera musculus*: Croll et al., 1998, Fiedler et al., 1998, Nickels et al., 2018, 2019; Cassin's auklets, *Ptychoramphus aleuticus*: Lee et al., 2007, Sydeman et al., 2006), and *N. simplex* (fin whales, *Balaenoptera physalus*, and mobulids, *Mobula mobular*: Croll et al., 2012; Stewart et al., 2017). Some highly mobile species face significant threats from ship strikes and fishing gear entanglements (Abrahms et al., 2019; Hazen et al., 2017; Office of Protected Resources, 2018a, 2018b; Santora et al., 2020). Oceanography-based models (e.g., WhaleWatch, Abrahms et al., 2019; Hazen et al., 2017) are emerging to track blue whale movements in the CCS using physical habitat conditions, but do not yet include zooplankton distributional information (but see Szesciorka et al., 2020). Lack of appropriate zooplankton data limits model accuracy by only establishing 'habitat suitability', not potentially variable whale densities due to targeted foraging on krill hotspots. Zooplanktivorous consumers may also preferentially forage on certain growth stages of euphausiids, which may vary spatially within a species (Nickels et al., 2018). Such models need also to account for rapid switching to alternative prey (i.e., humpback whales to anchovy when *E. pacifica* is low; Santora et al., 2020; Santora et al., 2011) that may not simply correspond to physical oceanographic conditions. Incorporating euphausiid spatial distributions and life-histories into foraging models may clarify highly mobile species preferences and produce more accurate spatiotemporal predictions to reduce needs for fishery closures and vessel diversions.

Declaration of Competing Interest

The authors declare that they have no known competing financial interests or personal relationships that could have appeared to influence the work reported in this paper.

Acknowledgements and author contributions

We thank all contributors to CalCOFI data collection and analysis, particularly the at-sea technicians and ship crews for rigorous and high-quality sampling sustained over so many decades. We dedicate this study to the late E. Brinton in recognition of his career's work and extensive insight into euphausiid biogeography and biology, without which this analysis would not have been possible. We thank A. Townsend, and currently L. Sala, for continued detailed enumerations. S. Bograd and I. Schroeder developed and generously provided the water mass indices used here. We thank D. L. Rudnick, B. D. Cornuelle, and K. D. Zaba for extensive help with objective mapping and spatial statistics, and J. B. Shurin, S. Gastauer, and J. P. Zwolinski for assistance with GAMs. This work was supported by an NSF Graduate Research Fellowship to L. E. Lilly, by NSF OCE-1614359 and OCE-1637632 to the California Current Ecosystem-LTER site, and by Gordon and Betty Moore Foundation support to M. D. Ohman.

L.E.L. and M.D.O. developed the study. L.E.L. conducted all analyses and wrote the manuscript. L.E.L. and M.D.O. analyzed results and edited the manuscript. The authors declare no competing interests.

Appendix A. Multi-sample averaging per station and year

CalCOFI cruises have occasionally sampled the same station multiple times within a single season, either on multiple cruises or as multiple samples on one cruise, so we used a two-part system to produce only one abundance value per station per year: for spring samples, 1) if multiple samples existed at the same station but only in different months (i.e., one April sample and one March sample at Station 90.50), we used a selection hierarchy of: i) April sample (if present), ii) if not, then March sample, iii) if neither, then May sample, iv) if no other months, then February sample. All four months are considered 'spring' in CalCOFI because spring cruises can start as early as February 15 and extend into May; 2) if multiple samples still existed at a station within the same month after we completed the selection hierarchy (i.e., two April samples at Stn 90.50), we averaged those samples to get one mean abundance value for the station. We chose the above month hierarchy to obtain each year's sample as close as possible to April for consistency and because we expect April to be the peak of biological responses to January peak CCS El Niño physical signals, assuming an average three-month lag of biological responses behind physical change. We used the same method for winter zooplankton samples, with a month hierarchy of i) January, ii) December, iii) February (Days 1–15). Enumerated winter samples are only available for 1951–2002 and 2009.

Appendix B. Objective mapping decorrelation length-scales

To determine object mapping input parameters, we calculated an autocovariance matrix for each species from all available abundance values (averaged to one value per station per year; see Appendix A). For each species, we first removed a plane mean from all values in the timeseries to obtain anomalies from the mean. We chose a rotation angle of -60° based on visual determination of the angle that produced the straightest x/y orientation of the CalCOFI sampling grid, to align the cross-shore and alongshore components to x and y. Using the rotated values, we calculated all station-station covariance values within a year and binned those values by their station-station distances, using bin increments of 95 and 80 km for the x- and y-

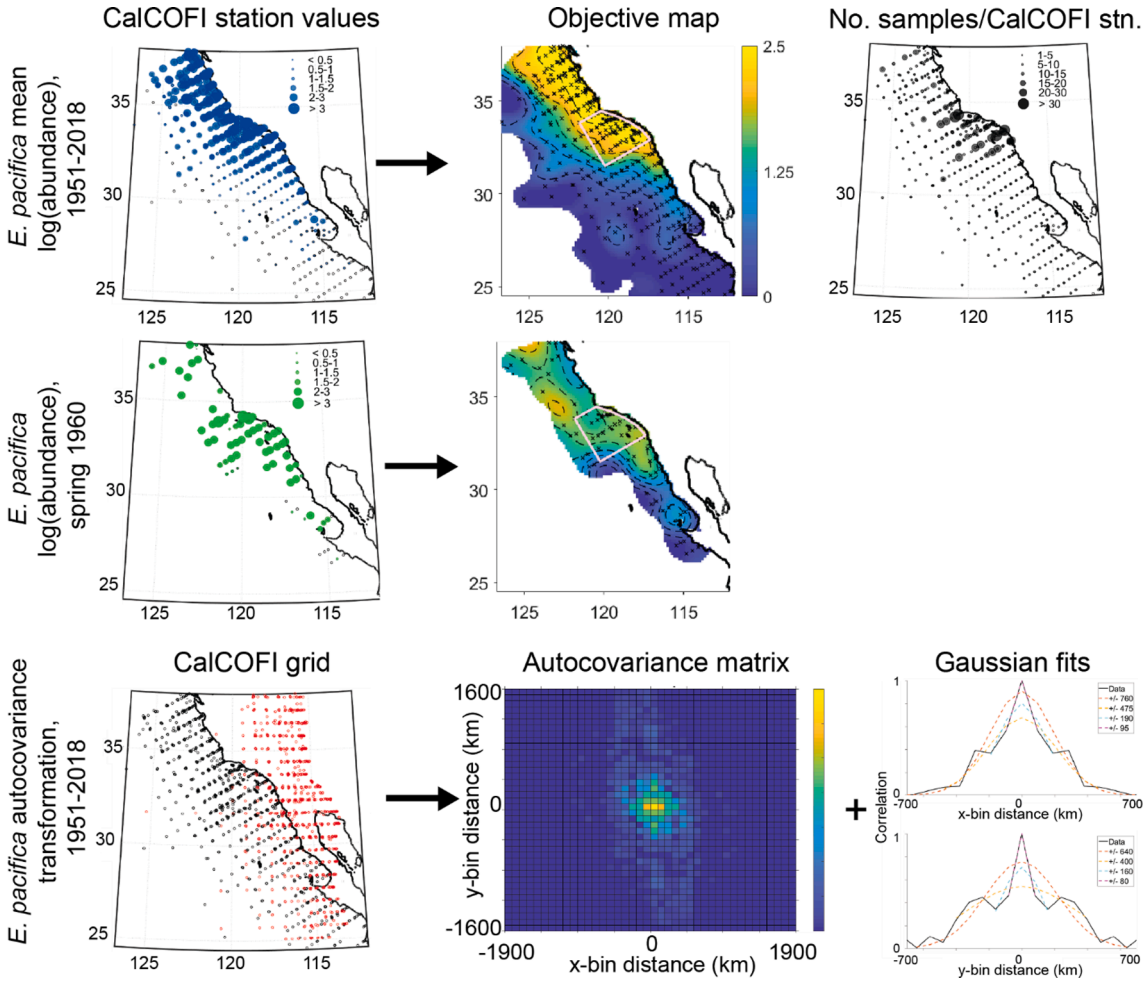

Fig. B1. Objective mapping fit steps and explanation: *(top row)* comparison of *E. pacifica* CalCOFI station-by-station datapoints (left panel) and objectively mapped distribution (center panel) for the 1951–2018 mean; right panel shows the number of times each CalCOFI station was sampled; *(middle row)* same comparison but for a single year (1960); *(bottom row)* −60° rotation of CalCOFI grid for objective mapping (left panel), autocovariance matrix of all station-station covariances for *E. pacifica* (center panel), and Gaussian fits of decorrelation lengths (colored lines, in km) to actual data (black lines) for x (top) and y (bottom) directions (right panel).

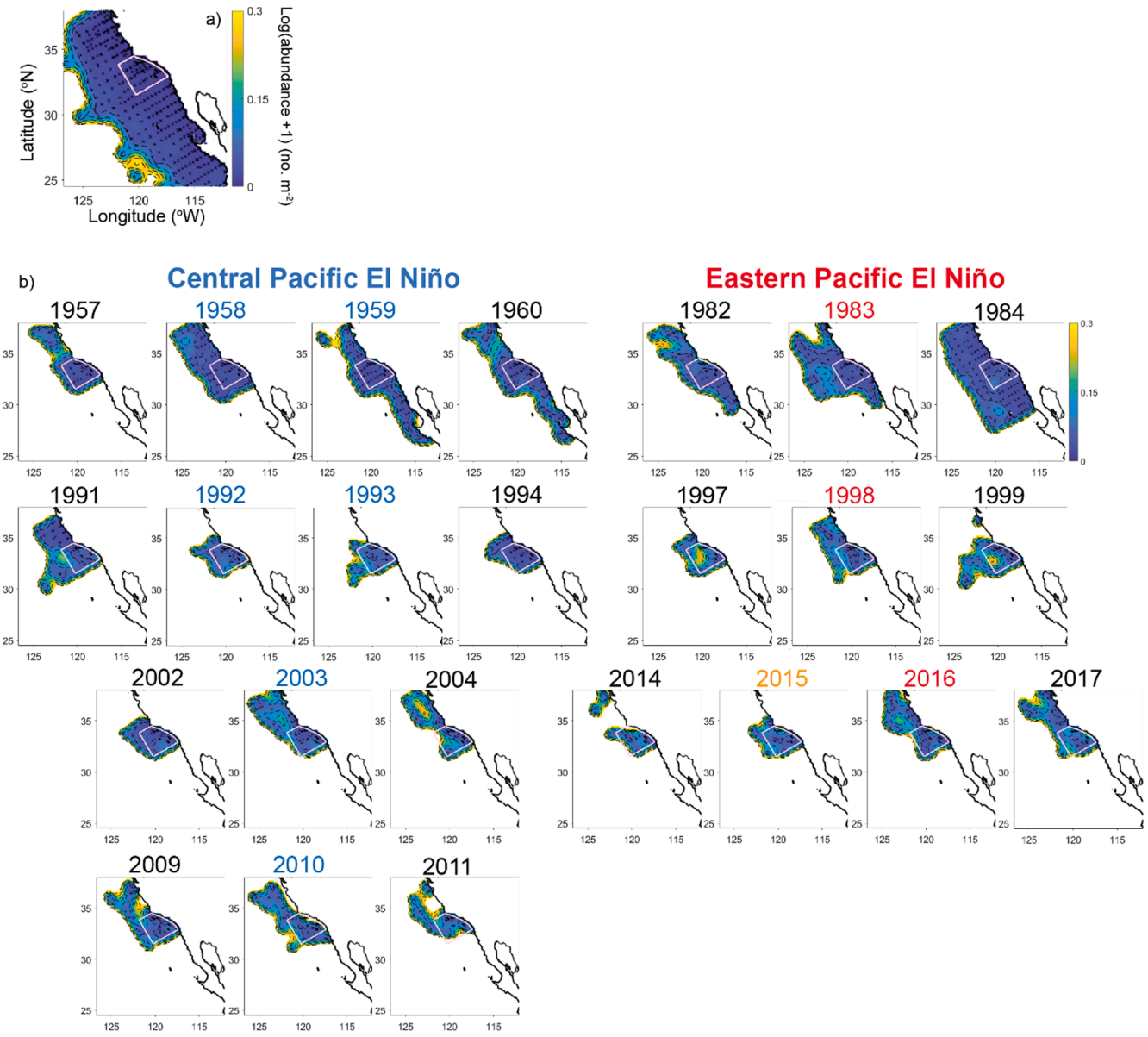

Fig. B2. Error maps associated with yearly objective maps for all species. Error threshold is 0.3 for all years.

directions, respectively. For each distance bin, we averaged all covariance values within a year and then summed all yearly mean covariance values within that bin to obtain its autocovariance. The full autocovariance matrix consists of each distance bin's sum of all yearly averages in that bin. As a secondary check on our selection of optimal input angle, we visually assessed each autocovariance matrix under different input rotation angles to ensure closest alignment to an x/y grids. To determine optimal x and y decorrelation length-scales for mapping, we fit Gaussian curves to the zero-bin (center) distributions separately for the x- and y-directions, and varied the numbers of input bins (i.e., distances from zero) to determine optimal curve fits. Decorrelation scales of 160 km (x-direction) and 190 km (y-direction) produced the best overall fits, so we used those distances as our optimal decorrelation length-scales for objective maps. All species showed similar optimal bin numbers, so we used the same decorrelation length-scales and rotation angles for each species.

Appendix C. Spatial statistical calculations

To determine annual changes in the spatial distribution of each species, we calculated yearly mean regionwide abundance and centers of gravity (COG) in the x (cross-shore) and y (alongshore) directions. We present results from both the 'Southern California only' and 'full CalCOFI' regions (see Section 2.1 for region descriptions). We calculated yearly means and standard errors using $\log_{10}$-transformed abundance (see Figs. 2–9c, S2-S3c). We calculated changes in x- and y-centers of gravity using untransformed abundance data, to emphasize centroid shifts without damping effects from log-transformation. We used the rotated CalCOFI grid (−60°) for COG calculations so that x- and y-directional changes would correspond to cross-shore and alongshore. We used a 'zero point' of lat0 = 32.84°N, lon0 = −118.73°W (the approximate center point of the SC region) from which to calculate

all other station distances. For center of gravity calculations, we converted each station's coordinates from latitude/longitude to kilometers, and used the following equation:

$$\mathrm{cogx} = \left(1/\mathrm{sum}\left(\mathrm{abd_{yr}}\right)\right) * \mathrm{sum}\left(\mathrm{abd_{yr}}. * \mathrm{xn}\right)$$

where 'cogx' is the vector of center of gravity offsets in the x-direction from the zero point, '$\mathrm{abd_{yr}}$' is the vector of zooplankton untransformed abundance values at each station for that year, and 'xn' is the vector of x-distance values from the zero point. The same equation applies to changes in y-direction center of gravity, replacing 'xn' with 'yn'. We estimated the effects of sampling error on yearly change in center of gravity using a random normal distribution multiplied by the abundance data and iterated 1000 times to produce 1000 'pseudo-shifts' in center of gravity, from which we calculated a standard deviation.

For distance values in center of gravity calculations, we converted each station's coordinates from latitude/longitude to km as described in Appendix B. To estimate the effects of sampling errors on yearly change in center of gravity ('$\mathrm{err_{abd}}$'), we calculated the standard deviations from each COG value (separate for x and y) using the following steps: 1) we produced a random normal distribution of the same length as the number of occupied stations for a year; 2) we multiplied this random normal distribution by the abundance value at each station and by 0.1 to incorporate an expected 10% sampling error into the distribution; 3) we added these 'error' distribution values to the station abundances; 4) we calculated the changes in x and y centers of gravity:

$$\mathrm{err_{abd}} = \left(\mathrm{abd_{yr}}\right) + \left(\left(\mathrm{dist_{rnd}}\right) * \left(\mathrm{abd_{yr}}\right) * 0.1\right)$$

$$\mathrm{cogx_{err}} = \left(1/\mathrm{sum}\left(\mathrm{err_{abd}}\right)\right) * \mathrm{sum}\left(\mathrm{err_{abd}} * \mathrm{xn}\right)$$

We repeated these steps 1000 times to produce a distribution changes in center of gravity, from which we calculated the standard deviation as a metric of likely sampling error.

To calculate the 'area of influence' of each CalCOFI station for total areas of population increase or decrease in 'EP Niño-non Niño' maps (e.g., Fig. 2e), we assumed individual station 'area boxes' which represent the total area around each station that we expected to have the same abundance as the station does. We assumed that each station represents an area around it out to halfway to the next station or line. The average inter-station and inter-line distances in the SC region are 30 km and 70 km, respectively, and we expect each station to have a halfway distance (15 km and 35 km) on each side, so we used 30 km and 70 km for box length and width, giving us a total 'area of influence' of 2100 km^2.

We did not include 1968 in our statistical calculations because CalCOFI only sampled off southern Baja California in that year, which skewed those centers of gravity significantly southward.

Appendix D. Supplementary material

Supplementary data to this article can be found online at https://doi.org/10.1016/j.pocean.2021.102544.

References

Abrahms, B., Welch, H., Brodie, S., Jacox, M.G., Becker, E.A., Bograd, S.J., et al., 2019. Dynamic ensemble models to predict distributions and anthropogenic risk exposure for highly mobile species. Divers. Distrib. 25 (8), 1182–1193. https://doi.org/10.1111/ddi.12940.

Aksnes, D.L., Ohman, M.D., 2009. Multi-decadal shoaling of the euphotic zone in the southern sector of the California Current System. Limnol. Oceanogr. 54 (4), 1272–1281. https://doi.org/10.4319/lo.2009.54.4.1272.

Alexander, M.A., Blade, I., Newman, M., Lanzante, J.R., Lau, N.C., Scott, J.D., 2002. The atmospheric bridge: The influence of ENSO teleconnections on air-sea interaction over the global oceans. J. Clim. 15 (16), 2205–2231.

Amante, C., Eakins, B.W., 2009. ETOPO1 1 Arc-Minute Global Relief Model: Procedures, Data Sources and Analysis. Retrieved from: https://www.ngdc.noaa.gov/mgg/global/.

Ashok, K., Behera, S.K., Rao, S.A., Weng, H., Yamagata, T., 2007. El Niño Modoki and its possible teleconnection. J. Geophys. Res. Oceans 112 (C11).

Ashok, K., Yamagata, T., 2009. The El Niño with a difference. Nature 461 (7263), 481–484.

Bakun, A., Black, B.A., Bograd, S.J., Garcia-Reyes, M., Miller, A.J., Rykaczewski, R.R., Sydeman, W.J., 2015. Anticipated effects of climate change on coastal upwelling ecosystems. Curr. Climate Change Rep. 1 (2), 85–93. https://doi.org/10.1007/s40641-015-0008-4.

Bograd, S.J., Castro, C.G., Di Lorenzo, E., Palacios, D.M., Bailey, H., Gilly, W., Chavez, F. P., 2008. Oxygen declines and the shoaling of the hypoxic boundary in the California Current. Geophys. Res. Lett. 35 (12) https://doi.org/10.1029/2008gl034185.

Bograd, S.J., Checkley, D.A., Wooster, W.S., 2003. CalCOFI: a half century of physical, chemical, and biological research in the California current system. Deep-Sea Res. Part Ii-Topical Stud. Oceanography 50 (14–16), 2349–2353. https://doi.org/10.1016/S0967-0645(03)00122-X.

Bograd, S.J., Lynn, R.J., 2001. Physical-biological coupling in the California Current during the 1997–99 El Niño-La Niña cycle. Geophys. Res. Lett. 28 (2), 275–278.

Bograd, S.J., Lynn, R.J., 2003. Anomalous subarctic influence in the southern California Current during 2002. Geophys. Res. Lett. 30 (15) https://doi.org/10.1029/2003gl017446.

Bograd, S.J., Schroeder, I.D., Jacox, M.G., 2019. A water mass history of the Southern California current system. Geophys. Res. Lett. 46 (12), 6690–6698. https://doi.org/10.1029/2019gl082685.

Bond, N.A., Cronin, M.F., Freeland, H., Mantua, N., 2015. Causes and impacts of the 2014 warm anomaly in the NE Pacific. Geophys. Res. Lett. 42 (9), 3414–3420. https://doi.org/10.1002/2015gl063306.

Bretherton, F.P., Davis, R.E., Fandry, C.B., 1976. A technique for objective analysis and design of oceanographic experiments applied to MODE-73. Deep Sea Res. Oceanographic Abstracts 23 (7), 559–582.

Brinton, E., 1960. Changes in the distribution of euphausiid crustaceans in the region of the California Current. CalCOFI Rep. 7, 137–146.

Brinton, E., 1962. The distribution of Pacific euphausiids. Bulletin of the Scripps Institution of Oceanography, University of California, San Diego(8), 51-270.

Brinton, E., 1967. Distributional atlas of Euphausiacea (Crustacea) in the California current region, Part I. In California Cooperative Oceanic Fisheries Investigations Atlas (Vol. 5, pp. 275 p.).

Brinton, E., 1973. Distributional atlas of euphausiacea (crustacean) in the California Current region, Part II. CalCOFI Atlas, 18.

Brinton, E., 1976. Population biology of Euphausia-Pacifica Off Southern-California. Fish. Bull. 74 (4), 733–762.

Brinton, E., 1979. Parameters relating to the distributions of planktonic organisms, especially euphausiids in the eastern tropical Pacific. Prog. Oceanogr. 8 (3), 125–189.

Brinton, E., 1981. Euphausiid distributions in the California Current during the warm winter-spring of 1977–78, in the context of a 1949–1966 time series. California Cooperative Oceanic Fisheries Investigations Reports 22, 135–154.

Brinton, E., Ohman, M.D., Townsend, A.W., Knight, M.D., Bridgeman, A.L. (Producer), 2000. Euphausiid of the World Ocean.

Brinton, E., Reid, J.L., 1986. On the effects of interannual variations in circulation and temperature upon euphausiids of the California Current. UNESCO Tech. Pap. Mar. Sci 49 (25–34).

Brinton, E., Townsend, A., 2003. Decadal variability in abundances of the dominant euphausiid species in southern sectors of the California Current. Deep-Sea Rese. Part Ii-Topical Stud. Oceanography 50 (14–16), 2449–2472. https://doi.org/10.1016/S0967-0645(03)00126-7.

Brinton, E., Townsend, A.W., 1981. A comparison of euphausiid abundances from bongo and 1-m CalCOFI nets. California Cooperative Oceanic Fisheries Investigations Reports 22, 111–125.

Brodeur, R.D., 1986. Northward Displacement of the Euphausiid Nyctiphanes-Simplex Hansen to Oregon and Washington Waters Following the El-Nino Event of 1982–83. J. Crustac. Biol. 6 (4), 686–692. https://doi.org/10.2307/1548382.

Cane, M.A., 1986. El-Nino. Annu. Rev. Earth Planet. Sci. 14, 43–70. https://doi.org/10.1146/annurev.ea.14.050186.000355.
Capotondi, A., 2013. ENSO diversity in the NCAR CCSM4 climate model. J. Geophys. Res.-Oceans 118 (10), 4755–4770. https://doi.org/10.1002/jgrc.20335.
Capotondi, A., Wittenberg, A.T., Newman, M., Di Lorenzo, E., Yu, J.Y., Braconnot, P., et al., 2015. Understanding ENSO diversity. Bull. Am. Meteorol. Soc. 96 (6), 921–938.
Chao, Y., Farrara, J.D., Bjorkstedt, E., Chai, F., Chavez, F., Rudnick, D.L., et al., 2017. The origins of the anomalous warming in the California coastal ocean and San Francisco Bay during 2014–2016. J. Geophys. Res.-Oceans 122 (9), 7537–7557. https://doi.org/10.1002/2017jc013120.
Chavez, F.P., 1996. Forcing and biological impact of onset of the 1992 El Niño in central California. Geophys. Res. Lett. 23 (3), 265–268.
Croll, D.A., Marinovic, B., Benson, S., Chavez, F., Black, N., Temullo, R., Tershy, B.R., 2005. From wind to whales: trophic links in a coastal upwelling ecosystem. Mar. Ecol. Prog. Ser. 289, 117–130. https://doi.org/10.3354/meps289117.
Croll, D.A., Newton, K.M., Weng, K., Galvan-Magana, F., O'Sullivan, J., Dewar, H., 2012. Movement and habitat use by the spine-tail devil ray in the Eastern Pacific Ocean. Mar. Ecol. Prog. Ser. 465, 193–200. https://doi.org/10.3354/meps09900.
Croll, D.A., Tershy, B.R., Hewitt, R.P., Demer, D.A., Fiedler, P.C., Smith, S.E., et al., 1998. An integrated approach to the foraging ecology of marine birds and mammals. Deep-Sea Research Part Ii-Topical Studies in Oceanography, 45(7), 1353-+. doi: 10.1016/S0967-0645(98)00031-9.
Davis, R.E., 1985. Objective mapping by least squares fitting. J. Geophys. Res. Oceans 90 (C3), 4773–4777.
Di Lorenzo, E., Mantua, N., 2016. Multi-year persistence of the 2014/15 North Pacific marine heatwave. Nat. Clim. Change 6 (11), 1042–1047.
Di Lorenzo, E., Ohman, M.D., 2013. A double-integration hypothesis to explain ocean ecosystem response to climate forcing. Proc. Natl. Acad. Sci. 110 (7), 2496–2499.
Dorman, J.G., Powell, T.M., Sydeman, W.J., Bograd, S.J., 2011. Advection and starvation cause krill (Euphausia pacifica) decreases in 2005 Northern California coastal populations: Implications from a model study. Geophys. Res. Lett. 38 (L04605).
Fasiolo, M., Nedellec, R., Goude, Y., Wood, S.N., 2019. Scalable visualization methods for modern generalized additive models. J. Comput. Graphical Statistics. https://doi.org/10.1080/10618600.2019.1629942.
Fiedler, P.C., Reilly, S.B., Hewitt, R.P., Demer, D., Philbrick, V.A., Smith, S., et al., 1998. Blue whale habitat and prey in the California Channel Islands. Deep-Sea Res. Part Ii-Topical Stud. Oceanography 45 (8–9), 1781–1801. https://doi.org/10.1016/S0967-0645(98)80017-9.
Fleming, A.H., Clark, C.T., Calambokidis, J., Barlow, J., 2016. Humpback whale diets respond to variance in ocean climate and ecosystem conditions in the California Current. Global Change Biol. 22 (3), 1214–1224.
Frischknecht, M., Munnich, M., Gruber, N., 2017. Local atmospheric forcing driving an unexpected California Current System response during the 2015–2016 El Nino. Geophys. Res. Lett. 44 (1), 304–311. https://doi.org/10.1002/2016gl071316.
Gentemann, C.L., Fewings, M.R., Garcia-Reyes, M., 2017. Satellite sea surface temperatures along the West Coast of the United States during the 2014–2016 northeast Pacific marine heat wave. Geophys. Res. Lett. 44 (1), 312–319. https://doi.org/10.1002/2016gl071039.
Glynn, P.W., 1988. El-Nino Southern Oscillation 1982–1983 - Nearshore Population, Community, and Ecosystem Responses. Annu. Rev. Ecol. Syst. 19, U309-+.
Gomez, J.G., 1995. Distribution patterns, abundance and population-dynamics of the Euphausiids Nyctiphanes-simplex and Euphausia-Eximia Off the West-Coast of Baja-California, Mexico. Mar. Ecol. Prog. Series 119 (1–3), 63–76. https://doi.org/10.3354/meps119063.
Harrison, D.E., Chiodi, A.M., 2009. Pre-and post-1997/98 westerly wind events and equatorial Pacific cold tongue warming. J. Clim. 22 (3), 568–581.
Hastie, T., Tibshirani, R., 1987. Generalized additive-models - some applications. J. Am. Stat. Assoc. 82 (398), 371–386. https://doi.org/10.2307/2289439.
Hayward, T.L., 1993. Preliminary observations of the 1991–1992 El Niño in the California Current. California Cooperative Oceanic Fisheries Investigations Reports 34 (21–29).
Hazen, E.L., Jorgensen, S., Rykaczewski, R.R., Bograd, S.J., Foley, D.G., Jonsen, I.D., et al., 2013. Predicted habitat shifts of Pacific top predators in a changing climate. Nat. Clim. Change 3 (3), 234–238. https://doi.org/10.1038/Nclimate1686.
Hazen, E.L., Palacios, D.M., Forney, K.A., Howell, E.A., Becker, E., Hoover, A.L., et al., 2017. WhaleWatch: a dynamic management tool for predicting blue whale density in the California Current. J. Appl. Ecol. 54 (5), 1415–1428. https://doi.org/10.1111/1365-2664.12820.
Huyer, A., 1983. Coastal upwelling in the California current system. Prog. Oceanogr. 12, 259–284.
Jacox, M.G., Fiechter, J., Moore, A.M., Edwards, C.A., 2015. ENSO and the California Current coastal upwelling response. J. Geophys. Res.-Oceans 120 (3), 1691–1702. https://doi.org/10.1002/2014jc010650.
Jacox, M.G., Hazen, E.L., Zaba, K.D., Rudnick, D.L., Edwards, C.A., Moore, A.M., Bograd, S.J., 2016. Impacts of the 2015–2016 El Nino on the California Current System: Early assessment and comparison to past events. Geophys. Res. Lett. 43 (13), 7072–7080. https://doi.org/10.1002/2016gl069716.
Kao, H.Y., Yu, J.Y., 2009. Contrasting Eastern-Pacific and Central-Pacific Types of ENSO. J. Clim. 22 (3), 615–632. https://doi.org/10.1175/2008jcli2309.1.
Karnauskas, K.B., 2013. Can we distinguish canonical El Nino from Modoki? Geophys. Res. Lett. 40 (19), 5246–5251. https://doi.org/10.1002/grl.51007.
Keister, J.E., Johnson, T.B., Morgan, C.A., Peterson, W.T., 2005. Biological indicators of the timing and direction of warm-water advection during the 1997/1998 El Nino off the central Oregon coast, USA. Mar. Ecol. Prog. Ser. 295, 43–48. https://doi.org/10.3354/meps295043.
Kim, W., Yeh, S.W., Kim, J.H., Kug, J.S., Kwon, M., 2011. The unique 2009–2010 El Niño event: A fast phase transition of warm pool El Niño to La Niña. Geophys. Res. Lett. 38 (15).
Kug, J.S., Jin, F.F., An, S.I., 2009. Two types of El Nino Events: cold tongue El Nino and Warm Pool El Nino. J. Clim. 22 (6), 1499–1515. https://doi.org/10.1175/2008jcli2624.1.
L'Heureux, M.L., Takahashi, K., Watkins, A.B., Barnston, A.G., Becker, E.J., Di Liberto, T. E., et al., 2017. Observing and predicting the 2015/16 El Nino. Bull. Am. Meteorol. Soc. 98 (7), 1363–1382. https://doi.org/10.1175/Bams-D-16-0009.1.
Larkin, N.K., Harrison, D.E., 2005. On the definition of El Niño and associated seasonal average US weather anomalies. Geophys. Res. Lett. 32 (12).
Lavaniegos, B.E., 1992. Growth and larval development of Nyctiphanes simplex in laboratory conditions. CalCOFI Rep. 33, 162–171.
Lavaniegos, B.E., 2009. Influence of a multiyear event of low salinity on the zooplankton from Mexican eco-regions of the California Current. Prog. Oceanogr. 83 (1–4), 369–375.
Lavaniegos, B.E., Ambriz-Arreola, I., 2012. Interannual variability in krill off Baja California in the period 1997–2005. Prog. Oceanogr. 97, 164–173. https://doi.org/10.1016/j.pocean.2011.11.008.
Lavaniegos, B.E., Jiménez-Herrera, M., Ambriz-Arreola, I., 2019. Unusually low euphausiid biomass during the warm years of 2014–2016 in the transition zone of the California Current. Deep Sea Res. Part II: Topical Stud. Oceanography, 104638.
Lavaniegos, B.E., Jimenez-Perez, L.C., Gaxiola-Castro, G., 2002. Plankton response to El Nino 1997–1998 and La Nina 1999 in the southern region of the California Current. Prog. Oceanogr. 54 (1–4), 33–58. https://doi.org/10.1016/S0079-6611(02)00042-3.
Lavaniegos, B.E., Ohman, M.D., 2007. Coherence of long-term variations of zooplankton in two sectors of the California Current System. Prog. Oceanogr. 75 (1), 42–69.
Lee, D.E., Nur, N., Sydeman, W.J., 2007. Climate and demography of the planktivorous Cassin's auklet Ptychoramphus aleuticus off northern California: implications for population change. J. Anim. Ecol. 76 (2), 337–347. https://doi.org/10.1111/j.1365-2656.2007.01198.x.
Leising, A.W., Schroeder, I.D., Bograd, S.J., Abell, J., Durazo, R., Warybok, P., 2015. State of the California Current 2014–15: Impacts of the Warm-Water" Blob". California Cooperative Oceanic Fisheries Investigations Reports 56, 31–68.
Lilly, L.E., Ohman, M.D., 2018. CCE IV: El Niño-related zooplankton variability in the southern California Current System. Deep-Sea Research Part I: Oceanographic Research Papers.
Lilly, L.E., Send, U., Lankhorst, M., Martz, T.R., Feely, R.A., Sutton, A.J., Ohman, M.D., 2019. Biogeochemical anomalies at two southern California Current System moorings during the 2014–16 Warm Anomaly-El Niño sequence. J. Geophys. Res. Oceans.
Lynn, R.J., 1983. The 1982–83 warm episode in the California current. Geophys. Res. Lett. 10 (11), 1093–1095.
Lynn, R.J., Bograd, S.J., 2002. Dynamic evolution of the 1997-1999 El Nino-La Nina cycle in the southern California current system. Prog. Oceanography, 54(1-4), 59-75. doi:Pii S0079-6611(02)00043-5.
Mackas, D.L., Galbraith, M., 2002. Zooplankton community composition along the inner portion of Line P during the 1997–1998 El Nino event. Prog. Oceanogr. 54 (1–4), 423–437. https://doi.org/10.1016/S0079-6611(02)00062-9.
Mackas, D.L., Peterson, W.T., Ohman, M.D., Lavaniegos, B.E., 2006. Zooplankton anomalies in the California Current system before and during the warm ocean conditions of 2005. Geophys. Res. Lett. 33 (22).
Marinovic, B.B., Croll, D.A., Gong, N., Benson, S.R., Chavez, F.P., 2002. Effects of the 1997–1999 El Nino and La Nina events on zooplankton abundance and euphausiid community composition within the Monterey Bay coastal upwelling system. Prog. Oceanogr. 54 (1–4), 265–277. https://doi.org/10.1016/S0079-6611(02)00053-8.
Matthews, S.A., Goetze, E., Ohman, M.D., 2020. Cross-shore changes in vertical habitats of Mesozoplankton: A paired metabarcoding and morphological approach. Paper presented at the Ocean Sciences Meeting 2020, San Diego, CA, USA.
McClatchie, S., Gao, J., Drenkard, E.J., Thompson, A.R., Watson, W., Ciannelli, L., et al., 2018. Interannual and secular variability of larvae of mesopelagic and forage fishes in the Southern California current system. J. Geophys. Res. Oceans 123 (9), 6277–6295.
McGowan, J.A., 1998. Climate-ocean variability and ecosystem response in the northeast Pacific (vol 281, pg 210, 1998). Science 282 (5388), 417.
McLain, D.R., Thomas, D.H., 1983. Year-to-year fluctuations of the California Countercurrent and effects on marine organisms. CalCOFI Rep. 24 (165–181).
McPhaden, M.J., 1999. Genesis and evolution of the 1997–98 El Nino. Science 283 (5404), 950–954. https://doi.org/10.1126/science.283.5404.950.
McPhaden, M.J., 2004. Evolution of the 2002/03 El Nino. Bull. Am. Meteorol. Soc. 85 (5), 677–695. https://doi.org/10.1175/Bams-85-5-677.
Miller, C.B., Batchelder, H.P., Brodeur, R.D., Pearcy, W.G., 1985. Response of the zooplankton and ichthyoplankton off Oregon to the El Niño event of 1983. In: Wooster, W.S., Fluharty, A.L. (Eds.), El Niño North. Washington Sea Grant Program, pp. 185–187.
Newman, M., Wittenberg, A.T., Cheng, L.Y., Compo, G.P., Smith, C.A., 2018. The extreme 2015/16 El Nino, in the context of historical climate variability and change. Bull. Am. Meteorol. Soc. 99 (1), S16–S20. https://doi.org/10.1175/Bams-D-17-0116.1.
Nickels, C.F., Sala, L.M., Ohman, M.D., 2018. The morphology of euphausiid mandibles used to assess selective predation by blue whales in the southern sector of the California Current System. J. Crustac. Biol. 38 (5), 563–573.
Nickels, C.F., Sala, L.M., Ohman, M.D., 2019. The euphausiid prey field for blue whales around a steep bathymetric feature in the southern California current system. Limnol. Oceanogr. 64 (1), 390–405. https://doi.org/10.1002/lno.11047.

Notarbartolo-di-Sciara, G., 1988. Natural history of the rays of the genus Mobula in the Gulf of California. Fish. Bull. 86 (1), 45–66.
Office of Protected Resources, N., 2018a. BLUE WHALE (Balaenoptera musculus musculus): Eastern North Pacific Stock. Retrieved from https://www.fisheries.noaa.gov/national/marine-mammal-protection/marine-mammal-stock-assessment-reports-species-stock#cetaceans—large-whales.
Office of Protected Resources, N., 2018b. HUMPBACK WHALE (Megaptera novaeangliae): California/Oregon/Washington Stock.
Ohman, M.D., Lavaniegos, B.E., 2002. Comparative zooplankton sampling efficiency of a ring net and bongo net with comments on pooling of subsamples. California Cooperative Oceanic Fisheries Investigations Reports 162–173.
Ohman, M.D., Mantua, N., Keister, J., Garcia-Reyes, M., McClatchie, S., 2017. ENSO impacts on ecosystem indicators in the California Current System. US Clivar Variations 15 (1), 8–15.
Ohman, M.D., Romagnan, J.B., 2016. Nonlinear effects of body size and optical attenuation on Diel Vertical Migration by zooplankton. Limnol. Oceanogr. 61 (2), 765–770. https://doi.org/10.1002/lno.10251.
Ohman, M.D., Smith, P.E., 1995. A comparison of zooplankton sampling methods in the CalCOFI time series. California Cooperative Oceanic Fisheries Investigations Reports 153–158.
Pares-Escobar, F., Lavaniegos, B.E., Ambriz-Arreola, I., 2018. Interannual summer variability in oceanic euphausiid communities off the Baja California western coast during 1998–2008. Prog. Oceanogr. 160, 53–67. https://doi.org/10.1016/j.pocean.2017.11.009.
Peterson, W.T., Keister, J.E., Feinberg, L.R., 2002. The effects of the 1997–99 El Nino/La Nina events on hydrography and zooplankton off the central Oregon coast. Prog. Oceanogr. 54 (1–4), 381–398. https://doi.org/10.1016/S0079-6611(02)00059-9.
Ramp, S.R., McClean, J.L., Collins, C.A., Semtner, A.J., Hays, K.A.S., 1997. Observations and modeling of the 1991–1992 El Nino signal off central California. J. Geophys. Res.-Oceans 102 (C3), 5553–5582. https://doi.org/10.1029/96jc03050.
Reid, J.L., 1960. Oceanography of the eastern North Pacific in the last 10 years. Retrieved from.
Ren, H.L., Jin, F.F., 2011. Niño indices for two types of ENSO. Geophys. Res. Lett. 38 (4).
Robinson, C.J., 2016. Evolution of the 2014–2015 sea surface temperature warming in the central west coast of Baja California, Mexico, recorded by remote sensing. Geophys. Res. Lett. 43 (13), 7066–7071.
Ross, R.M., 1982. Energetics of Euphausia-Pacifica. 1. Effects of body carbon and nitrogen and temperature on measured and predicted production. Mar. Biol. 68 (1), 1–13. https://doi.org/10.1007/Bf00393135.
Rudnick, D.L., Zaba, K.D., Todd, R.E., Davis, R.E., 2017. A climatology of the California Current System from a network of underwater gliders. Prog. Oceanogr. 154, 64–106. https://doi.org/10.1016/j.pocean.2017.03.002.
Rykaczewski, R.R., Dunne, J.P., 2010. Enhanced nutrient supply to the California Current Ecosystem with global warming and increased stratification in an earth system model. Geophys. Res. Lett. 37 https://doi.org/10.1029/2010gl045019.
Santora, J.A., Mantua, N.J., Schroeder, I.D., Field, J.C., Hazen, E.L., Bograd, S.J., et al., 2020. Habitat compression and ecosystem shifts as potential links between marine heatwave and record whale entanglements. Nat. Commun. 11 (1) https://doi.org/10.1038/s41467-019-14215-w.
Santora, J.A., Sydeman, W.J., Schroeder, I.D., Wells, B.K., Field, J.C., 2011. Mesoscale structure and oceanographic determinants of krill hotspots in the California Current: Implications for trophic transfer and conservation. Prog. Oceanogr. 91 (4), 397–409. https://doi.org/10.1016/j.pocean.2011.04.002.
Santora, J.A., Zeno, R., Dorman, J.G., Sydeman, W.J., 2018. Submarine canyons represent an essential habitat network for krill hotspots in a large marine ecosystem. Sci. Rep. 8 (1), 1–9.
Schwing, F.B., Murphree, T., Green, P.M., 2002. The evolution of oceanic and atmospheric anomalies in the northeast Pacific during the El Niño and La Niña events of 1995–2001. Prog. Oceanogr. 54 (1), 459–491.
Schwing, F.B., Palacios, D.M., Bograd, S.J., 2005. El Nino impacts of the California current ecosystem. US CLIVAR Newsletter 3 (2), 5–8.
Simpson, J.J., 1983. Large-scale thermal anomalies in the California Current during the 1982–1983 El-Nino. Geophys. Res. Lett. 10 (10), 937–940. https://doi.org/10.1029/GL010i010p00937.
Simpson, J.J., 1984. El-Nino-induced onshore transport in the California Current during 1982–1983. Geophys. Res. Lett. 11 (3), 241–242.
Smiles, M.C., Pearcy, W.G., 1971. Size structure and growth rate of Euphausia-Pacifica off oregon coast. United States Fish and Wildlife Service Fishery Bulletin, 69(1), 79-&.
Stewart, J.D., Rohner, C.A., Araujo, G., Avila, J., Fernando, D., Forsberg, K., et al., 2017. Trophic overlap in mobulid rays: insights from stable isotope analysis. Mar. Ecol. Prog. Ser. 580, 131–151. https://doi.org/10.3354/meps12304.
Strub, P.T., James, C., 2002. The 1997–1998 oceanic El Niño signal along the southeast and northeast Pacific boundaries - an altimetric view. Prog. Oceanogr. 54 (1–4), 439–458.
Sydeman, W.J., Bradley, R.W., Warzybok, P., Abraham, C.L., Jahncke, J., Hyrenbach, K.D., et al., 2006. Planktivorous auklet Ptychoramphus aleuticus responses to ocean climate, 2005: Unusual atmospheric blocking? Geophys. Res. Lett. 33 (22) https://doi.org/10.1029/2006gl026736.
Szesciorka, A.R., Ballance, L.T., Širović, A., Rice, A., Ohman, M.D., Hildebrand, J.A., Franks, P.J., 2020. Timing is everything: Drivers of interannual variability in blue whale migration. Sci. Rep. 10 (1), 1–9.
Tanasichuk, R.W., 1998. Interannual variations in the population biology and productivity of Euphausia pacifica in Barkley Sound, Canada, with special reference to the 1992 and 1993 warm ocean years. Mar. Ecol. Prog. Ser. 173, 163–180. https://doi.org/10.3354/Meps173163.
Timmermann, A., An, S.-I., Kug, J.S., Jin, F.F., Cai, W., Capotondi, A., et al., 2019. El Niño-Southern Oscillation complexity. Nature 559, 535–545.
Todd, R.E., Rudnick, D.L., Davis, R.E., Ohman, M.D., 2011. Underwater gliders reveal rapid arrival of El Nino effects off California's coast. Geophys. Res. Lett. 38 https://doi.org/10.1029/2010gl046376.
Wang, D.W., Gouhier, T.C., Menge, B.A., Ganguly, A.R., 2015. Intensification and spatial homogenization of coastal upwelling under climate change. Nature 518 (7539), 390–394. https://doi.org/10.1038/nature14235.
Wheeler, P.A., Huyer, A., Fleischbein, J., 2003. Cold halocline, increased nutrients and higher chlorophyll off Oregon in 2002. Geophys. Res. Lett. 30 (14) https://doi.org/10.1029/2003gl017395.
Wickett, W.P., 1967. Ekman transport and zooplankton concentration in the North Pacific Ocean. J. Fisheries Board of Canad 24 (3), 581–594.
Wood, S.N., Li, Z.Y., Shaddick, G., Augustin, N.H., 2017. Generalized additive models for Gigadata: Modeling the UK black smoke network daily data. J. Am. Stat. Assoc. 112 (519), 1199–1210. https://doi.org/10.1080/01621459.2016.1195744.
Wyllie, J.G., 1966. Geostrophic flow of the California Current at the surface and at 200 m. In: CalCOFI Atlas (Vol. 4). University of California, San Diego.
Wyrtki, K., 1975. El Nino - dynamic-response of equatorial Pacific Ocean to atmospheric forcing. J. Phys. Oceanography, 5(4), 572–584. doi:10.1175/1520-0485(1975)005<0572:Entdro>2.0.Co;2.
Yeh, S.W., Kug, J.S., Dewitte, B., Kwon, M.H., Kirtman, B.P., Jin, F.F., 2009. El Nino in a changing climate (vol 461, pg 511, 2009). Nature, 462(7273). doi:10.1038/nature08546.
Zaba, K.D., Rudnick, D.L., 2016. The 2014–2015 warming anomaly in the Southern California Current System observed by underwater gliders. Geophys. Res. Lett. 43 (3), 1241–1248. https://doi.org/10.1002/2015gl067550.
Zaba, K.D., Rudnick, D.L., Cornuelle, B., Gopalakrishnan, G., Mazloff, M., 2020. Volume and heat budgets in the coastal California Current System: Means, annual cycles and interannual anomalies of 2014–2016. J. Phys. Oceanography.

Euphausiid spatial displacements and habitat shifts in the southern California Current System in response to El Niño variability

Laura E. Lilly* and Mark D. Ohman

SUPPLEMENTAL TABLES AND FIGURES

Table S1. Mean values (± standard error) of habitat variables (temp @ 50 m, sal @ 50 m, oxygen @ 100 m, ln(Chl-a) @ 10 m) for each euphausiid species' spring total abundance distribution in figures 10 and S4 (lower rows), during non-Niño years (grey bars and black vertical line), EP Niño years (pink bars and line), and CP Niño years (blue bars and line).

	Temperature @ 50 m			Salinity @ 50 m			Oxygen @ 100 m			ln(Chl-a) @ 10 m		
Species	**Non**	**EP**	**CP**	**Non**	**EP**	**CP**	**Non**	**EP**	**CP**	**Non**	**EP**	**CP**
Euphausia pacifica	11.47 (0.001)	10.61 (0.003)	12.09 (0.003)	33.54 (<0.001)	33.59 (<0.001)	33.43 (<0.001)	3.26 (0.001)	2.87 (0.001)	3.39 (0.003)	0.06 (0.001)	0.90 (0.003)	0.52 (0.005)
Thysanoessa spinifera	10.72 (0.005)	10.77 (0.011)	10.82 (0.014)	33.66 (0.001)	33.66 (0.001)	33.72 (0.003)	2.83 (0.004)	2.68 (0.003)	3.08 (0.011)	0.74 (0.005)	0.78 (0.013)	1.51 (0.014)
Nyctiphanes simplex	12.16 (0.005)	11.87 (0.008)	12.56 (0.015)	33.63 (0.001)	33.57 (0.001)	33.54 (0.001)	3.18 (0.003)	3.07 (0.005)	3.64 (0.008)	0.13 (0.004)	0.32 (0.007)	0.52 (0.016)
Euphausia eximia	16.05 (0.015)	14.36 (0.026)	13.33 (0.051)	33.79 (0.003)	33.41 (0.003)	33.40 (0.006)	4.30 (0.009)	4.01 (0.024)	3.77 (0.017)	-1.88 (0.014)	-1.64 (0.025)	-1.07 (0.031)
Euphausia gibboides	14.87 (0.011)	15.03 (0.034)	15.17 (0.022)	33.43 (0.002)	33.27 (0.009)	33.49 (0.003)	4.80 (0.008)	4.86 (0.023)	4.69 (0.014)	-1.99 (0.008)	-1.93 (0.023)	-1.37 (0.095)
Euphausia recurva	14.51 (0.010)	14.80 (0.018)	14.66 (0.020)	33.39 (0.002)	33.26 (0.004)	33.44 (0.003)	4.79 (0.008)	5.09 (0.015)	4.43 (0.014)	-1.79 (0.008)	-1.71 (0.015)	-1.76 (0.041)
Stylocheiron affine	14.61 (0.018)	14.34 (0.043)	14.37 (0.057)	33.42 (0.003)	33.32 (0.006)	33.43 (0.007)	4.69 (0.012)	4.65 (0.039)	4.36 (0.034)	-1.79 (0.013)	-1.53 (0.029)	-1.18 (0.104)
Euphausia hemigibba	15.13 (0.032)	15.01 (0.046)	15.36 (0.066)	33.45 (0.006)	33.27 (0.010)	33.40 (0.017)	5.28 (0.019)	5.33 (0.025)	5.10 (0.046)	-2.20 (0.022)	-1.80 (0.042)	-2.49 (0.079)
Nematoscelis difficilis	12.56 (0.003)	12.99 (0.012)	13.11 (0.010)	33.46 (<0.001)	33.41 (0.003)	33.40 (0.001)	3.72 (0.002)	3.50 (0.009)	3.76 (0.005)	-0.62 (0.003)	-0.30 (0.011)	-0.48 (0.012)
Thysanoessa gregaria	12.90 (0.007)	13.65 (0.021)	13.50 (0.021)	33.40 (0.001)	33.32 (0.004)	33.31 (0.003)	4.03 (0.005)	4.31 (0.018)	4.11 (0.014)	-1.01 (0.006)	-0.85 (0.021)	-0.87 (0.025)

Table S2. Kruskal-Wallis and post-hoc multicomparison test values (p-values in parentheses) for spring total abundance distributions of the three El Niño categories (non, EP=Eastern Pacific, CP=Central Pacific) at four habitat variables (temp @ 50 m, sal @ 50 m, oxygen @ 100 m, ln(Chl-a) @ 10 m) shown in figures 10 and S4 (lower rows). See Table S1 for mean values.

Species	K-W X^2	Δ(non-EP)	Δ(non-CP)	Δ(EP-CP)	K-W X^2	Δ(non-EP)	Δ(non-CP)	Δ(EP-CP)	K-W X^2	Δ(non-EP)	Δ(non-CP)	Δ(EP-CP)	K-W X^2	Δ(non-EP)	Δ(non-CP)	Δ(EP-CP)
Euphausia pacifica	3.64 (0.16)	110.88 (0.19)	36.38 (0.65)	-74.50 (0.57)	6.49 (0.04)	128.98 (0.10)	66.22 (0.23)	-62.76 (0.66)	8.06 (0.02)	140.84 (0.02)	38.24 (0.51)	-102.61 (0.21)	6.58 (0.04)	-65.71 (0.13)	-59.77 (0.16)	5.94 (0.99)
Nyctiphanes simplex	31.03 (2e-7)	-328.91 (2e-16)	-62.18 (0.25)	266.73 (4e-4)	30.30 (2e-7)	-317.95 (2e-16)	-66.03 (0.20)	251.91 (1e-3)	24.58 (5e-6)	-243.49 (2e-16)	-37.54 (0.49)	205.95 (1e-3)	4.36 (0.11)	7.15 (0.97)	-64.34 (0.10)	-71.49 (0.22)
Euphausia eximia	13.85 (1e-3)	-124.28 (7e-3)	-62.97 (0.04)	61.31 (0.40)	15.63 (4e-4)	-125.56 (5e-3)	-68.62 (0.02)	56.94 (0.44)	15.75 (4e-4)	-109.31 (3e-3)	-53.74 (0.04)	55.57 (0.32)	12.32 (2e-3)	53.60 (0.02)	-39.56 (0.10)	-93.15 (1e-3)
Euphausia gibboides	31.96 (1e-7)	-187.29 (3e-3)	-172.67 (<2e-16)	14.62 (0.97)	33.22 (6e-8)	-181.57 (3e-3)	-177.42 (2e-16)	4.15 (0.99)	21.28 (2e-5)	-152.04 (3e-3)	-108.65 (1e-3)	43.39 (0.70)	12.33 (2e-3)	70.73 (0.05)	-68.15 (0.05)	-138.87 (1e-3)
Thysanoessa spinifera	10.55 (5e-3)	-120.20 (0.06)	-84.03 (0.04)	36.37 (0.82)	7.58 (0.02)	-110.08 (0.09)	-65.01 (0.14)	45.07 (0.74)	7.87 (0.02)	-81.79 (0.15)	-64.52 (0.07)	17.26 (0.94)	0.24 (0.89)	-14.16 (0.88)	0.14 (0.99)	14.30 (0.93)
Euphausia recurva	39.48 (3e-9)	-222.75 (4e-4)	-197.70 (<2e-16)	25.05 (0.93)	39.79 (2e-9)	-213.06 (1e-3)	-200.51 (2e-16)	12.56 (0.98)	28.48 (7e-7)	-183.86 (5e-4)	-131.21 (1e-4)	52.65 (0.62)	9.13 (0.01)	66.22 (0.09)	-59.65 (0.12)	-125.87 (7e-3)
Stylocheiron affine	22.30 (1e-5)	-264.12 (2e-16)	-41.63 (0.49)	222.49 (2e-3)	21.09 (3e-5)	-253.52 (2e-16)	-38.78 (0.54)	214.74 (3e-3)	21.20 (2e-5)	-215.90 (2e-16)	-24.11 (0.72)	191.79 (1e-3)	19.01 (7e-5)	90.04 (8e-3)	-85.35 (0.01)	-175.39 (2e-16)
Euphausia hemigibba	6.32 (0.04)	-73.90 (0.16)	-47.24 (0.16)	26.65 (0.83)	7.08 (0.03)	-74.30 (0.14)	-50.95 (0.11)	23.35 (0.87)	5.58 (0.06)	-62.05 (0.16)	-36.58 (0.23)	25.47 (0.79)	2.08 (0.35)	25.18 (0.45)	-14.15 (0.77)	-39.33 (0.34)
Nematoscelis difficilis	12.45 (2e-3)	-220.54 (2e-3)	-37.35 (0.63)	183.18 (0.03)	8.52 (0.01)	-182.36 (0.01)	1.03 (0.99)	183.38 (0.03)	7.06 (0.03)	-139.23 (0.02)	-7.17 (0.98)	132.06 (0.07)	2.79 (0.25)	-12.98 (0.92)	-54.02 (0.23)	-41.04 (0.64)
Thysanoessa gregaria	13.04 (2e-3)	-227.21 (1e-3)	6.45 (0.99)	233.66 (4e-3)	12.40 (2e-3)	-212.07 (2e-3)	26.98 (0.78)	239.05 (3e-3)	9.61 (8e-3)	-156.04 (7e-3)	19.98 (0.83)	176.02 (0.01)	3.18 (0.20)	42.89 (0.41)	-37.20 (0.49)	-80.09 (0.18)

Table S3. Mean values (± standard error) of habitat variables (temp @ 50 m, sal @ 50 m, oxygen @ 100 m, ln(Chl-a) @ 10 m) for each euphausiid species' winter total abundance distribution in figure S4 (top rows) during non-Niño years (corresponding to grey bars and black vertical line), EP Niño years (pink bars and line), and CP Niño years (blue bars and line).

	Temperature @ 50 m			**Salinity @ 50 m**			**Oxygen @ 100 m**			**ln(Chl-a) @ 10 m**		
Species	**Non**	**EP**	**CP**	**Non**	**EP**	**CP**	**Non**	**EP**	**CP**	**Non**	**EP**	**CP**
Euphausia pacifica	12.17 (0.002)	15.84 (0.168)	13.51 (0.004)	33.45 (<0.001)	33.34 (0.033)	33.29 (<0.001)	3.48 (0.002)	4.41 (0.070)	4.03 (0.002)	-0.08 (0.003)	-0.52 (0.042)	-0.83 (0.002)
Thysanoessa spinifera	11.99 (0.013)	16.62 (<0.001)	12.85 (0.086)	33.50 (0.002)	NaN	33.43 (0.014)	3.15 (0.008)	3.84 (<0.001)	3.65 (0.052)	0.32 (0.017)	-0.19 (<0.001)	-0.04 (<0.001)
Nyctiphanes simplex	13.91 (0.008)	16.15 (0.002)	13.97 (0.011)	33.51 (0.001)	33.64 (<0.001)	33.35 (0.002)	3.71 (0.003)	3.94 (0.008)	4.08 (0.006)	-0.11 (0.005)	-0.53 (0.006)	-0.56 (0.008)
Euphausia eximia	16.00 (0.034)	16.59 (0.027)	15.30 (0.125)	33.63 (0.005)	33.62 (0.005)	33.57 (0.014)	4.22 (0.012)	4.05 (0.011)	3.96 (0.023)	-1.24 (0.021)	-0.72 (0.024)	-0.59 (0.026)
Euphausia gibboides	14.80 (0.029)	15.99 (0.084)	14.85 (0.081)	33.39 (0.005)	33.38 (0.028)	33.43 (0.011)	4.69 (0.015)	4.91 (0.059)	4.25 (0.033)	-1.40 (0.020)	-1.18 (0.055)	-0.95 (0.043)
Euphausia recurva	14.92 (0.014)	15.68 (0.024)	15.00 (0.026)	33.38 (0.002)	33.37 (0.008)	33.41 (0.004)	4.90 (0.007)	5.07 (0.016)	4.50 (0.015)	-1.59 (0.008)	-1.26 (0.020)	-1.16 (0.019)
Stylocheiron affine	15.30 (0.021)	16.54 (0.035)	15.42 (0.043)	33.46 (0.003)	33.51 (0.010)	33.45 (0.006)	4.78 (0.010)	4.46 (0.026)	4.61 (0.022)	-1.51 (0.013)	-0.86 (0.028)	-1.24 (0.040)
Euphausia hemigibba	15.65 (0.052)	15.88 (0.045)	16.23 (0.089)	33.45 (0.008)	33.51 (0.001)	33.49 (0.021)	5.22 (0.023)	5.26 (0.043)	5.01 (0.064)	-1.77 (0.030)	-1.60 (0.078)	-1.92 (0.047)
Nematoscelis difficilis	12.93 (0.005)	16.27 (0.016)	13.99 (0.011)	33.42 (0.001)	33.43 (0.006)	33.35 (0.002)	3.80 (0.003)	4.16 (0.007)	4.25 (0.006)	-0.59 (0.004)	-0.54 (0.008)	-0.88 (0.007)
Thysanoessa gregaria	13.38 (0.010)	15.60 (0.034)	13.86 (0.020)	33.38 (0.001)	33.28 (0.009)	33.31 (0.003)	4.15 (0.006)	4.61 (0.016)	4.37 (0.013)	-0.98 (0.007)	-0.91 (0.016)	-0.85 (0.011)

Table S4. Kruskal-Wallis and post-hoc multicomparison test values (p-values in parentheses) for winter total abundance distributions of the three El Niño categories (non, EP=Eastern Pacific, CP=Central Pacific) at four habitat variables (temp @ 50 m, sal @ 50 m, oxygen @ 100 m, ln(Chl-a) @ 10 m) shown in figure S4 (top rows). See Table S3 for mean values.

	Temperature @ 50 m				**Salinity @ 50 m**				**Oxygen @ 100 m**				**ln(Chl-a) @ 10 m**			
Species	**K-W X^2**	**Δ(non-EP)**	**Δ(non-CP)**	**Δ(EP-CP)**	**K-W X^2**	**Δ(non-EP)**	**Δ(non-CP)**	**Δ(EP-CP)**	**K-W X^2**	**Δ(non-EP)**	**Δ(non-CP)**	**Δ(EP-CP)**	**K-W X^2**	**Δ(non-EP)**	**Δ(non-CP)**	**Δ(EP-CP)**
Euphausia pacifica	46.37 (9e-9)	360.37 (2e-16)	106.46 (1e-3)	-253.91 (3e-4)	24.47 (5e-6)	293.51 (1e-3)	96.24 (1e-3)	-197.28 (0.06)	35.51 (2e-8)	266.94 (2e-16)	71.22 (0.01)	-195.72 (1e-3)	14.27 (1e-3)	-95.96 (0.01)	52.95 (0.06)	148.91 (1e-3)
Thysanoessa spinifera	7.54 (0.02)	44.34 (0.37)	40.10 (0.04)	-4.24 (0.99)	6.35 (0.04)	54.50 (0.45)	33.18 (0.06)	-21.33 (0.89)	5.51 (0.06)	28.97 (0.51)	28.32 (0.08)	-0.64 (0.99)	0.09 (0.96)	5.39 (0.95)	-0.55 (0.99)	-5.93 (0.96)
Nyctiphanes simplex	11.31 (4e-3)	-58.99 (0.57)	-92.93 (3e-3)	-33.94 (0.85)	10.18 (6e-3)	27.53 (0.94)	-81.47 (5e-3)	-109.00 (0.38)	3.92 (0.14)	-43.28 (0.63)	-43.57 (0.17)	-0.28 (0.99)	11.39 (3e-3)	53.57 (0.22)	66.63 (7e-3)	13.06 (0.94)
Euphausia eximia	26.03 (2e-6)	-229.11 (2e-16)	-4.83 (0.97)	224.29 (2e-16)	2.42 (0.30)	-89.75 (0.32)	-12.35 (0.81)	77.39 (0.45)	25.86 (2e-6)	-186.42 (2e-16)	5.56 (0.95)	191.97 (2e-16)	15.09 (1e-3)	94.65 (4e-4)	-7.04 (0.91)	-101.69 (1e-3)
Euphausia gibboides	13.12 (1e-3)	-160.24 (0.01)	-65.09 (0.05)	95.15 (0.26)	7.21 (0.03)	-92.20 (0.45)	-61.12 (0.04)	31.09 (0.92)	10.81 (5e-3)	-128.15 (0.02)	-45.97 (0.12)	82.19 (0.24)	4.45 (0.11)	65.37 (0.10)	12.21 (0.84)	-53.16 (0.32)
Euphausia recurva	42.93 (5e-9)	-193.08 (3e-3)	-168.25 (2e-16)	24.83 (0.92)	27.53 (1e-6)	-112.74 (0.34)	-133.51 (2e-16)	-20.77 (0.97)	32.56 (8e-8)	-164.41 (2e-3)	-117.14 (<1e-3)	47.27 (0.64)	10.46 (5e-3)	77.31 (0.05)	53.41 (0.05)	-23.90 (0.81)
Stylocheiron affine	24.35 (5e-6)	-259.64 (2e-16)	-58.45 (0.09)	201.19 (3e-3)	3.18 (0.29)	-24.52 (0.95)	-39.55 (0.26)	-15.03 (0.98)	25.17 (3e-6)	-221.78 (<1e-3)	-48.13 (0.11)	173.65 (2e-3)	8.40 (0.02)	92.52 (0.01)	-1.17 (0.99)	-93.69 (0.03)
Euphausia hemigibba	6.82 (0.03)	-64.39 (0.26)	-43.45 (0.08)	20.94 (0.89)	3.18 (0.20)	-8.85 (0.99)	-32.74 (0.18)	-23.90 (0.91)	4.83 (0.09)	-59.17 (0.20)	-25.85 (0.30)	33.32 (0.65)	2.98 (0.23)	35.90 (0.27)	-10.74 (0.78)	-46.64 (0.20)
Nematoscelis difficilis	4.24 (0.12)	-121.23 (0.11)	10.64 (0.93)	131.87 (0.11)	1.82 (0.40)	-28.17 (0.94)	34.85 (0.40)	63.02 (0.74)	6.01 (0.05)	-118.23 (0.05)	10.64 (0.91)	128.87 (0.05)	19.27 (6e-5)	85.53 (0.03)	87.08 (5e-4)	1.55 (0.99)
Thysanoessa gregaria	11.55 (3e-3)	-175.03 (0.01)	47.46 (0.25)	222.48 (2e-3)	4.12 (0.13)	-12.67 (0.99)	54.21 (0.11)	66.88 (0.72)	11.41 (3e-3)	-158.04 (4e-3)	22.26 (0.65)	180.30 (2e-3)	12.57 (2e-3)	82.33 (0.04)	63.20 (0.02)	-19.13 (0.88)

Table S5. Mean values (± standard error) of associations of each euphausiid species' spring total abundance with proportions of three water masses (PSUW @ 150 m, PEW @ 200 m, ENPCW @ 100 m) shown in figures 11 and S5 during non-Niño years (corresponding to grey bars and black vertical line), EP Niño years (pink bars and line), and CP Niño years (blue bars and line).

	PSUW @ 150 m			**PEW @ 200 m**			**ENPCW @ 100 m**		
Species	**Non**	**EP**	**CP**	**Non**	**EP**	**CP**	**Non**	**EP**	**CP**
Euphausia pacifica	0.50 (<0.001)	0.51 (<0.001)	0.38 (<0.001)	0.38 (<0.001)	0.33 (<0.001)	0.51 (0.001)	0.12 (0.001)	0.12 (0.001)	0.07 (0.001)
Thysanoessa spinifera	0.46 (0.001)	0.35 (0.001)	0.37 (0.001)	0.40 (0.001)	0.48 (0.001)	0.49 (0.003)	0.10 (0.001)	0.19 (0.001)	0.07 (0.001)
Nyctiphanes simplex	0.49 (0.001)	0.45 (0.001)	0.41 (0.003)	0.37 (0.001)	0.41 (0.001)	0.46 (0.003)	0.17 (0.001)	0.18 (0.001)	0.08 (0.002)
Euphausia eximia	0.50 (0.004)	0.42 (0.003)	0.45 (0.004)	0.32 (0.004)	0.40 (0.006)	0.44 (0.003)	0.28 (0.006)	0.32 (0.006)	0.12 (0.002)
Euphausia gibboides	0.57 (0.001)	0.55 (0.004)	0.62 (0.007)	0.32 (0.001)	0.36 (0.004)	0.36 (0.006)	0.37 (0.003)	0.45 (0.006)	0.31 (0.014)
Euphausia recurva	0.58 (0.001)	0.54 (0.002)	0.63 (0.005)	0.30 (0.001)	0.33 (0.003)	0.34 (0.003)	0.36 (0.002)	0.59 (0.005)	0.26 (0.008)
Stylocheiron affine	0.56 (0.002)	0.49 (0.005)	0.60 (0.009)	0.30 (0.002)	0.40 (0.004)	0.33 (0.006)	0.34 (0.003)	0.44 (0.008)	0.19 (0.014)
Euphausia hemigibba	0.53 (0.005)	0.56 (0.006)	0.67 (0.008)	0.27 (0.004)	0.33 (0.006)	0.31 (0.006)	0.50 (0.008)	0.63 (0.010)	0.46 (0.021)
Nematoscelis difficilis	0.51 (<0.001)	0.40 (0.001)	0.50 (0.002)	0.37 (0.001)	0.44 (0.002)	0.42 (0.001)	0.19 (0.001)	0.31 (0.002)	0.11 (0.001)
Thysanoessa gregaria	0.52 (0.001)	0.49 (0.001)	0.51 (0.001)	0.36 (0.001)	0.38 (0.001)	0.42 (0.003)	0.23 (0.003)	0.41 (0.001)	0.13 (0.003)

Table S6. Kruskal-Wallis and post-hoc multicomparison test values (p-values in parentheses) for spring total abundance distributions of the three El Niño categories (non, EP=Eastern Pacific, CP=Central Pacific) at three water mass proportions (PSUW @ 150 m, PEW @ 200 m, ENPCW @ 100 m) shown in figures 11 and S5. See Table S5 for mean values.

	PSUW @ 150 m				PEW @ 200 m				ENPCW @ 100 m			
Species	**K-W X^2**	**Δ(non-EP)**	**Δ(non-CP)**	**Δ(EP-CP)**	**K-W X^2**	**Δ(non-EP)**	**Δ(non-CP)**	**Δ(EP-CP)**	**K-W X^2**	**Δ(non-EP)**	**Δ(non-CP)**	**Δ(EP-CP)**
Euphausia pacifica	22.63 (1e-5)	135.15 (2e-16)	44.45 (0.15)	-90.70 (0.03)	14.50 (7e-4)	112.39 (4e-4)	15.45 (0.79)	-96.94 (0.02)	11.36 (3e-3)	56.93 (0.13)	68.50 (0.01)	11.58 (0.94)
Thysanoessa spinifera	4.98 (0.08)	-26.01 (0.56)	-41.31 (0.10)	-15.30 (0.87)	6.82 (0.03)	-30.53 (0.44)	-47.62 (0.04)	-17.09 (0.84)	3.48 (0.18)	-32.73 (0.36)	-26.75 (0.34)	5.98 (0.98)
Nyctiphanes simplex	26.25 (2e-6)	-126.96 (2e-16)	42.91 (0.13)	169.87 (2e-16)	25.90 (2e-6)	-127.82 (2e-16)	37.01 (0.21)	164.84 (2e-16)	35.33 (2e-8)	-145.77 (2e-16)	46.91 (0.08)	192.68 (2e-16)
Euphausia eximia	67.99 (2e-15)	-126.04 (2e-16)	-20.37 (0.22)	105.68 (2e-16)	65.06 (2e-16)	-119.57 (2e-16)	-21.31 (0.17)	98.26 (2e-16)	58.45 (2e-12)	-118.07 (2e-16)	-18.01 (0.31)	100.06 (2e-16)
Euphausia gibboides	8.21 (0.02)	-71.26 (0.02)	14.42 (0.77)	85.68 (0.02)	8.47 (0.01)	-72.44 (0.01)	12.47 (0.82)	84.90 (0.02)	14.81 (6e-4)	-90.80 (1e-3)	25.10 (0.44)	11.60 (7e-4)
Euphausia recurva	5.64 (0.06)	-65.45 (0.05)	4.31 (0.98)	69.76 (0.10)	6.44 (0.04)	-69.70 (0.03)	1.65 (0.99)	71.35 (0.09)	12.02 (3e-3)	-91.00 (3e-3)	14.79 (0.77)	105.79 (4e-3)
Stylocheiron affine	17.49 (2e-4)	-88.22 (4e-3)	52.07 (0.04)	140.29 (1e-4)	21.46 (2e-5)	-103.72 (4e-3)	49.20 (0.06)	152.92 (2e-16)	25.82 (2e-6)	-110.81 (1e-4)	53.94 (0.03)	164.74 (2e-16)
Euphausia hemigibba	3.10 (0.21)	-30.21 (0.260	10.22 (0.78)	40.43 (0.20)	2.48 (0.29)	-26.01 (0.36)	9.97 (0.79)	35.98 (0.27)	3.87 (0.14)	-34.05 (0.17)	9.58 (0.80)	43.64 (0.14)
Nematoscelis difficilis	8.73 (0.01)	11.83 (0.92)	70.11 (9e-3)	58.27 (0.25)	3.00 (0.22)	-12.25 (0.91)	38.58 (0.23)	50.83 (0.34)	25.70 (3e-6)	-112.04 (4e-4)	70.97 (7e-3)	183.01 (2e-16)
Thysanoessa gregaria	3.24 (0.20)	-40.20 (0.37)	25.41 (0.53)	65.61 (0.17)	7.44 (0.02)	-80.63 (0.02)	-5.07 (0.97)	75.56 (0.09)	17.76 (1e-4)	-106.40 (8e-4)	42.54 (0.16)	148.94 (1e-4)

Table S7. Mean values (± standard error) of habitat variables (temp @ 50 m, sal @ 50 m, oxygen @ 100 m, ln(Chl-a) @ 10 m) for each euphausiid species' spring calyptopis abundance distribution in figure S7 during non-Niño years (corresponding to grey bars and black vertical line), EP Niño years (pink bars and line), and CP Niño years (blue bars and line).

	Temperature @ 50 m			**Salinity @ 50 m**			**Oxygen @ 100 m**			**ln(Chl-a) @ 10 m**		
Species	**Non**	**EP**	**CP**	**Non**	**EP**	**CP**	**Non**	**EP**	**CP**	**Non**	**EP**	**CP**
Euphausia pacifica	11.35 (0.003)	10.45 (0.002)	12.00 (0.010)	33.55 (0.001)	33.60 (<0.001)	33.44 (0.002)	3.18 (0.003)	2.83 (<0.001)	3.49 (0.009)	0.52 (0.003)	1.04 (0.003)	0.96 (0.013)
Thysanoessa spinifera	10.82 (0.013)	10.85 (0.013)	11.58 (0.055)	33.64 (0.002)	33.57 (0.001)	33.61 (0.005)	2.76 (0.010)	2.88 (0.004)	2.74 (0.030)	0.72 (0.014)	0.79 (0.017)	1.64 (0.052)
Nyctiphanes simplex	12.20 (0.008)	12.03 (0.011)	12.81 (0.051)	33.56 (0.001)	33.55 (0.001)	33.54 (0.004)	3.25 (0.007)	2.94 (0.007)	3.57 (0.026)	0.32 (0.008)	0.64 (0.010)	-0.01 (0.080)
Euphausia eximia	16.2 (0.038)	13.30 (0.135)	13.07 (0.124)	33.76 (0.006)	33.51 (0.022)	33.38 (0.015)	4.41 (0.020)	2.87 (0.067)	3.80 (0.038)	-2.14 (0.015)	-0.70 (0.182)	-1.20 (0.064)
Euphausia gibboides	15.01 (0.019)	15.48 (0.047)	15.11 (0.035)	33.41 (0.004)	33.37 (0.009)	33.50 (0.004)	4.92 (0.013)	4.85 (0.031)	4.72 (0.020)	-2.12 (0.011)	-2.02 (0.034)	-1.58 (0.177)
Euphausia recurva	14.57 (0.025)	14.88 (0.101)	14.79 (0.057)	33.37 (0.005)	33.31 (0.016)	33.55 (0.005)	4.88 (0.021)	4.60 (0.085)	4.33 (0.034)	-1.79 (0.027)	-1.89 (0.056)	-1.50 (0.192)
Stylocheiron affine	15.05 (0.077)	14.76 (0.102)	13.66 (0.132)	33.29 (0.017)	33.24 (0.034)	33.12 (0.001)	5.23 (0.056)	5.00 (0.061)	4.56 (0.113)	-2.19 (0.052)	-1.76 (0.122)	-1.47 (0.122)
Euphausia hemigibba	15.04 (0.233)	NaN	NaN	33.48 (0.034)	NaN	NaN	4.82 (0.153)	NaN	NaN	-1.77 (0.124)	NaN	NaN
Nematoscelis difficilis	12.51 (0.006)	12.86 (0..019)	13.22 (0.019)	33.46 (0.001)	33.47 (0.003)	33.37 (0.003)	3.62 (0.005)	3.21 (0.012)	3.85 (0.011)	-0.39 (0.006)	0.07 (0.016)	-0.74 (0.023)
Thysanoessa gregaria	12.86 (0.058)	12.87 (0.112)	13.08 (0.090)	33.45 (0.010)	33.49 (0.005)	33.21 (0.021)	4.11 (0.055)	3.52 (0.102)	4.29 (0.073)	-0.60 (0.074)	0.15 (0.105)	-1.06 (0.065)

Table S8. Kruskal-Wallis and post-hoc multicomparison test values (p-values in parentheses) for spring calyptopis abundance distributions of the three El Niño categories (non, EP=Eastern Pacific , CP=Central Pacific) at four habitat variables (temp @ 50 m, sal @ 50 m, oxygen @ 100 m, ln(Chl-a) @ 10 m) shown in figure S6. See Table S7 for mean values.

	Temperature @ 50 m				**Salinity @ 50 m**				**Oxygen @ 100 m**				**ln(Chl-a) @ 10 m**			
Species	**K-W X^2**	**Δ(non-EP)**	**Δ(non-CP)**	**Δ(EP-CP)**	**K-W X^2**	**Δ(non-EP)**	**Δ(non-CP)**	**Δ(EP-CP)**	**K-W X^2**	**Δ(non-EP)**	**Δ(non-CP)**	**Δ(EP-CP)**	**K-W X^2**	**Δ(non-EP)**	**Δ(non-CP)**	**Δ(EP-CP)**
Euphausia pacifica	4.52 (0.10)	-101.87 (0.17)	-46.20 (0.42)	55.67 (0.67)	2.50 (0.29)	-83.94 (0.30)	-22.82 (0.81)	61.12 (0.62)	3.70 (0.16)	-60.89 (0.40)	-47.07 (0.28)	13.81 (0.97)	1.11 (0.57)	-33.01 (0.55)	-8.09 (0.96)	24.92 (0.83)
Thysanoessa spinifera	35.91 (2e-7)	-204.32 (2e-16)	-9.34 (0.91)	194.98 (2e-16)	32.73 (8e-8)	-195.54 (2e-16)	0.22 (0.99)	195.76 (2e-16)	30.63 (2e-7)	-154.33 (2e-16)	-17.58 (0.61)	136.76 (1e-4)	0.32 (0.85)	-10.14 (0.88)	-6.51 (0.94)	3.63 (0.99)
Nyctiphanes simplex	21.17 (3e-5)	-208.71 (2e-16)	-22.52 (0.72)	186.18 (1e-3)	20.00 (4e-5)	201.91 (2e-16)	-19.99 (0.78)	181.93 (2e-3)	15.40 (5e-4)	-141.84 (3e-4)	-20.54 (0.67)	121.31 (0.011)	5.36 (0.07)	-58.90 (0.05)	-2.22 (0.99)	56.68 (0.22)
Euphausia eximia	0.07 (0.96)	0.95 (0.99)	3.92 (0.96)	2.98 (0.99)	0.10 (0.95)	2.12 (0.99)	4.49 (0.95)	2.36 (0.99)	0.08 (0.96)	-4.83 (0.96)	0.63 (0.99)	5.46 (0.96)	0.51 (0.77)	-7.71 (0.76)	-1.50 (0.99)	6.21 (0.90)
Euphausia gibboides	16.87 (2e-4)	-12.50 (0.95)	-107.33 (1e-4)	-94.82 (0.11)	16.47 (3e-4)	-8.73 (0.97)	-106.21 (1e-4)	-97.48 (0.09)	9.66 (8e-3)	-14.79 (0.90)	-68.80 (6e-3)	-54.01 (0.35)	5.23 (0.07)	-13.16 (0.80)	-45.41 (0.06)	-32.26 (0.48)
Euphausia recurva	14.50 (7e-4)	-68.97 (0.14)	-79.96 (2e-3)	-10.99 (0.96)	14.36 (8e-4)	-65.98 (0.16)	-80.20 (2e-3)	-14.22 (0.94)	9.84 (7e-3)	-59.85 (0.12)	-52.04 (0.03)	7.81 (0.97)	4.71 (0.09)	28.26 (0.33)	-29.57 (0.28)	-57.83 (0.08)
Stylocheiron affine	8.00 (0.02)	-44.35 (0.03)	10.99 (0.58)	55.34 (0.01)	8.01 (0.02)	-43.80 (0.03)	10.43 (0.61)	54.23 (0.01)	8.57 (0.01)	-38.91 (0.02)	7.41 (0.71)	46.32 (0.01)	4.43 (0.11)	21.68 (0.09)	0.30 (0.99)	-21.37 (0.27)
Euphausia hemigibba	NaN	NaN	NaN	NaN	NaN	NaN	NaN	NaN	NaN	NaN	NaN	NaN	NaN	NaN	NaN	NaN
Nematoscelis difficilis	5.93 (0.05)	-147.80 (0.04)	-21.27 (0.85)	126.53 (0.17)	4.53 (0.10)	-126.65 (0.09)	10.62 (0.96)	137.27 (0.12)	2.75 (0.25)	-80.83 (0.25)	-18.48 (0.84)	62.35 (0.53)	1.95 (0.38)	-41.97 (0.41)	-21.01 (0.79)	20.96 (0.88)
Thysanoessa gregaria	18.25 (1e-4)	-104.22 (1e-4)	-5.57 (0.93)	98.64 (1e-3)	15.94 (3e-4)	-99.01 (2e-4)	-2.66 (0.99)	96.34 (2e-3)	13.56 (0.001)	-76.01 (7e-4)	-6.78 (0.87)	69.23 (0.01)	0.58 (0.75)	10.14 (0.73)	1.87 (0.99)	-8.27 (0.89)

Table S9. Parameters for optimal generalized additive model (GAM) equation for each species (see figures 13 and S8 for equations). 'd.f.' is the total degrees of freedom of the model; 'AIC' is Akaike Information Criterion; '-REML' indicates the score using the method of maximum likelihood (ML) for smoothing selection, treating smooth components as random effects; '%dev. exp.' is the percent deviance explained by the model (akin to adjusted R^2); and 'Terms' indicate knots ('kts'), degrees of freedom, and significance of each term ('p'). Terms were only included in a model if they reached a significance of $p < 0.05$. For first four species, top row is term values for GAM with lat/lon terms; bottom row is for GAM without lat/lon terms.

Species	d.f.	AIC	-REML	%dev. exp.	Term 1		Term 2		Term 3	
					kts	d.f. (p)	kts	d.f. (p)	kts	d.f. (p)
Euphausia pacifica	44.9	798.0	397.2	63.6%	(5)	3.09 (4e-11)**	(5)	3.00 (6e-5)**	(5,5)	4.79 (1e-4)**
no (Lat,Lon)	41.6	823.0	403.9	60.8%		4.76 (2e-08)***		2.88 (1e-06)***	---	---
Nyctiphanes simplex	49.9	742.2	360.6	70.8%	(5,5)	3.00 (8e-8)**	(5,5)	9.01 (6e-4)**	(5,5)	3.90 (7e-3)**
no (Lat,Lon)	40.5	764.4	371.9	67.1%		3 (<2e-16)***	---	---		3.472 (0.046)*
Euphausia eximia	44.0	212.3	120.7	44.2%	(7,6)	6.50 (5e-3)**	(6,5)	6.05 (0.046)*	---	---
no (Lat,Lon)	40.0	229.6	131.8	38.2%	---	---		5.97 (0.014)*		---

Euphausia gibboides	46.4	501.9	256.2	56.9%	(6,5)	3.30 (6e-7)**	(6,6)	7.37 (0.022)*	(3)	1.77 (0.044)*
no (Lat,Lon)	39.0	510.9	261.7	54.0%		3.28 (1e-11)***	---	---		1.79 (1e-3)**
Thysanoessa spinifera	42.3	941.9	454.2	51.6%	7	1.00 (2e-3)**	(7,7)	4.17 (0.014)*	(7,7)	3.17 (0.05)^
Euphausia recurva	42.7	583.4	294.0	60.8%	(5,5)	3.00 (4e-3)**	(5,5)	3.13 (4e-3)**	(5,6)	2.54 (0.04)*
Stylocheiron affine	42.5	583.4	293.0	40.5%	(5,5)	5.54 (9e-5)***	(5,5)	3.00 (3e-4)***	---	---
Euphausia hemigibba	42.0	-190.4	-57.0	49.3%	(5,5)	5.91 (2e-16)***	5	2.12 (0.02)*	---	---
Nematoscelis difficilis	40.7	696.2	348.2	34.2%	(6,5)	4.40 (2e-10)**	6	1.00 (4e-4)**	6	1.30 (0.014)*
Thysanoessa gregaria	45.9	780.1	382.9	48.2%	(5,5)	5.21 (3e-5)***	(5,5)	6.66 (2e-4)***	---	---

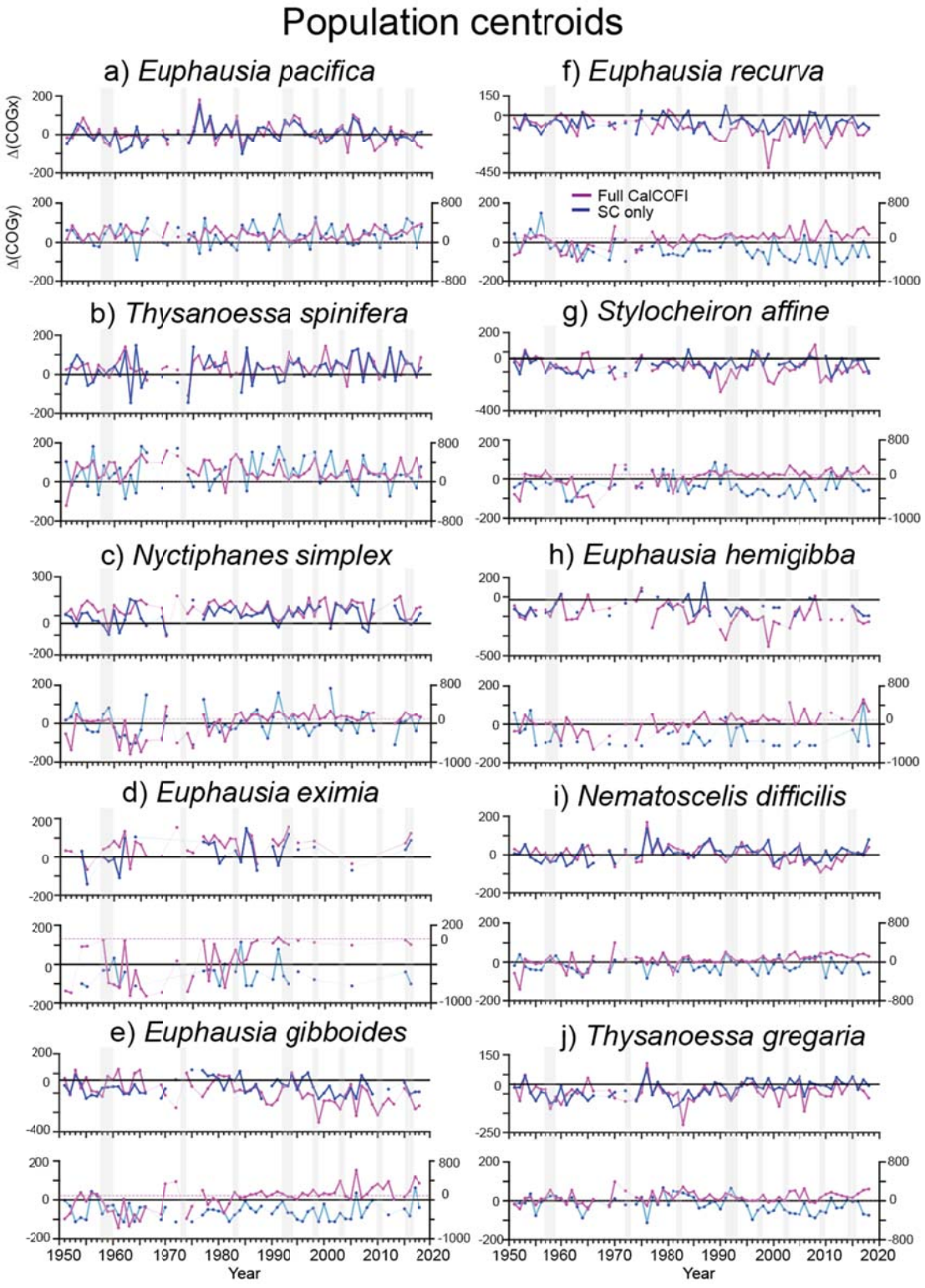

Figure S1. Metrics of population distribution change for the 10 species analyzed, corresponding to individual year distribution maps in Figs. S10-S19. Plots are (*top*) changes in x-direction

center of gravity (COGx) and (*bottom*) y-direction center of gravity (COGy). All centers of gravity are calculated from a constant centroid (x = -118.73^{o}W, y= 32.84^{o}N), so a species may have consistently negative values if its population is always offset from that centroid. Positive values denote shoreward (x) and northward (y) shifts. Pink lines show values for the full CalCOFI region (variable sampling); blue lines are for the SC region only. Vertical grey bars denote El Niño events. See Appendix C for explanation of calculations.

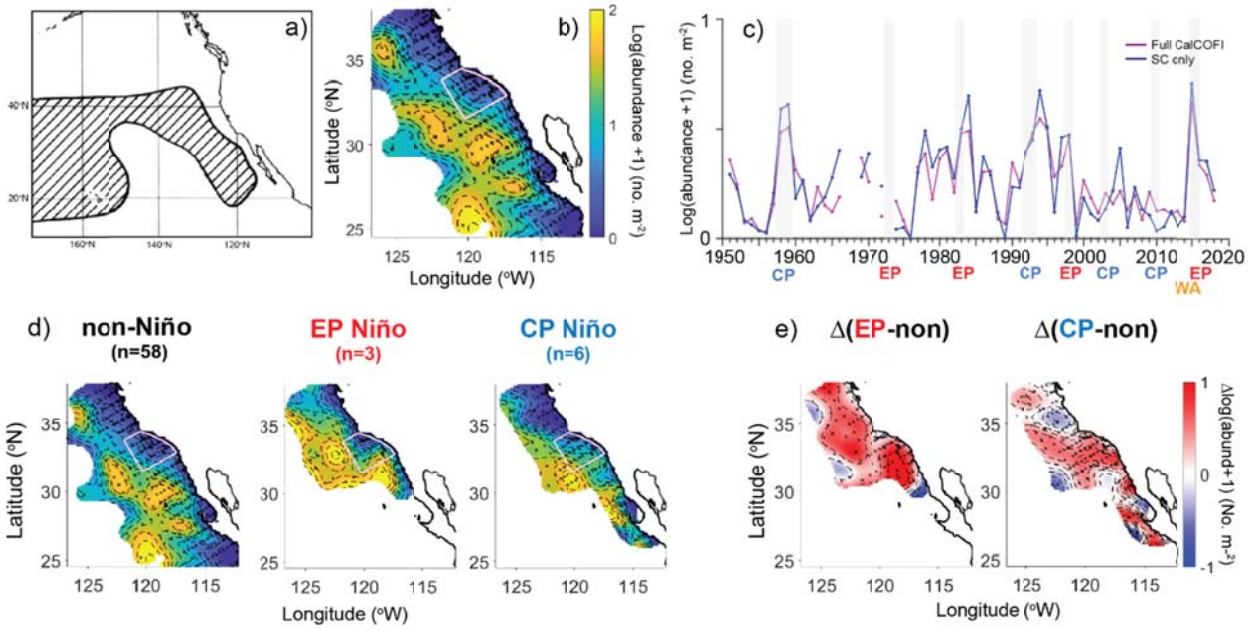

Figure S2. As in figure 2, but for *Euphausia recurva*. Lack of linear trendline in 'c' indicates no significant long-term trend ($p > 0.05$).

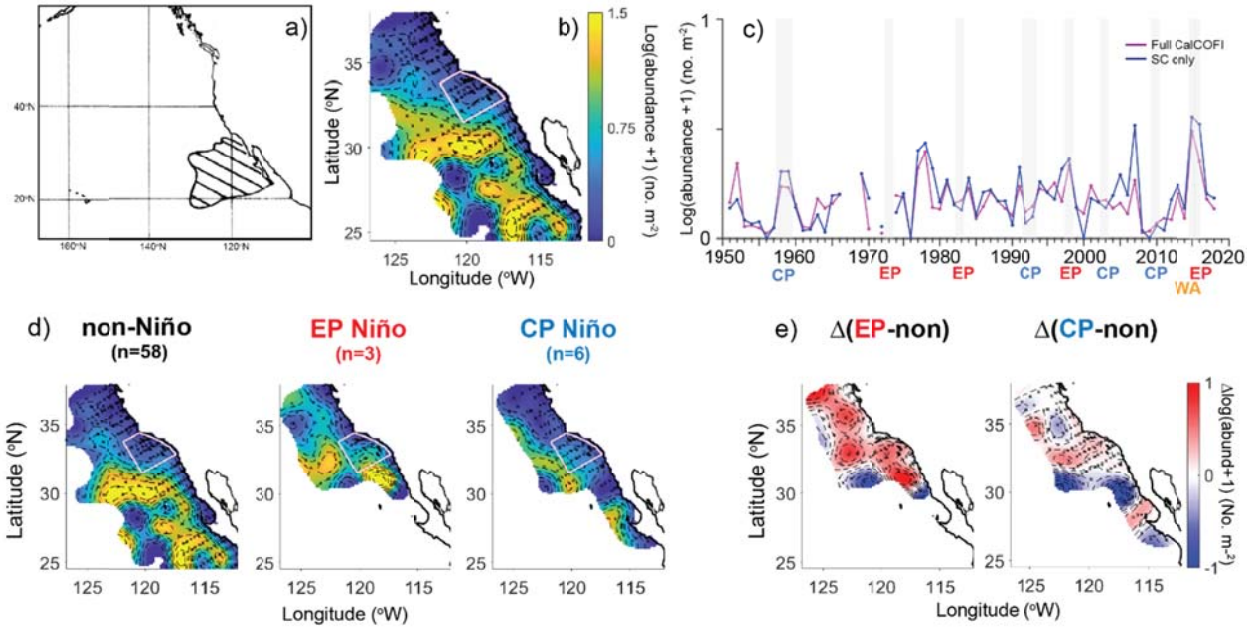

Figure S3. As in figure 2, but for *Stylocheiron affine.* Lack of linear trendline in 'c' indicates no significant long-term trend ($p > 0.05$).

Habitat Variables - Winter and Spring Comparison

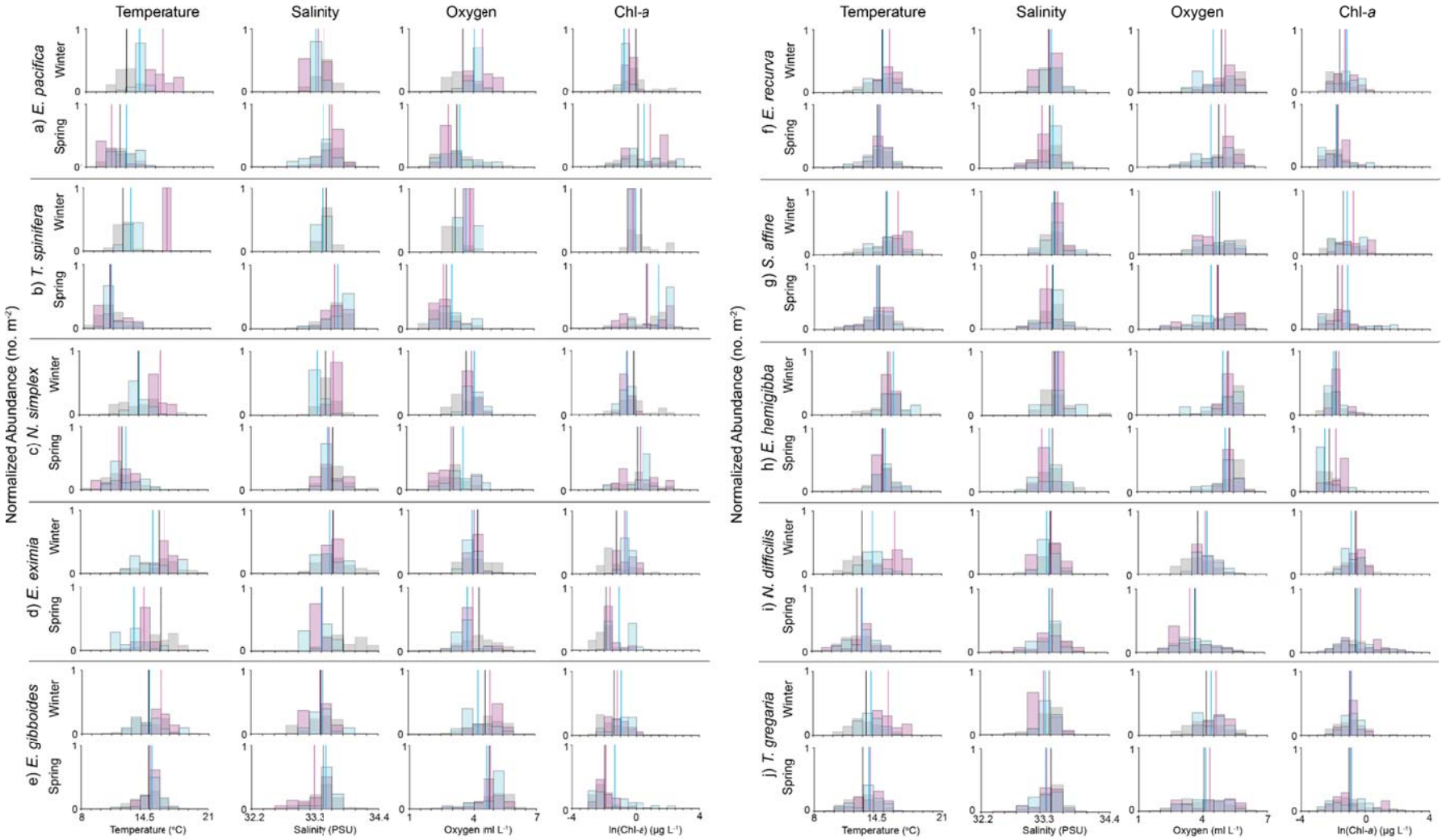

Figure S4. As in figure 10 but for both winter (*top row, each species*) and spring (bottom rows) habitat distributions. Spring plots are identical to figure 10 but are shown for direct comparison to winter distributions.

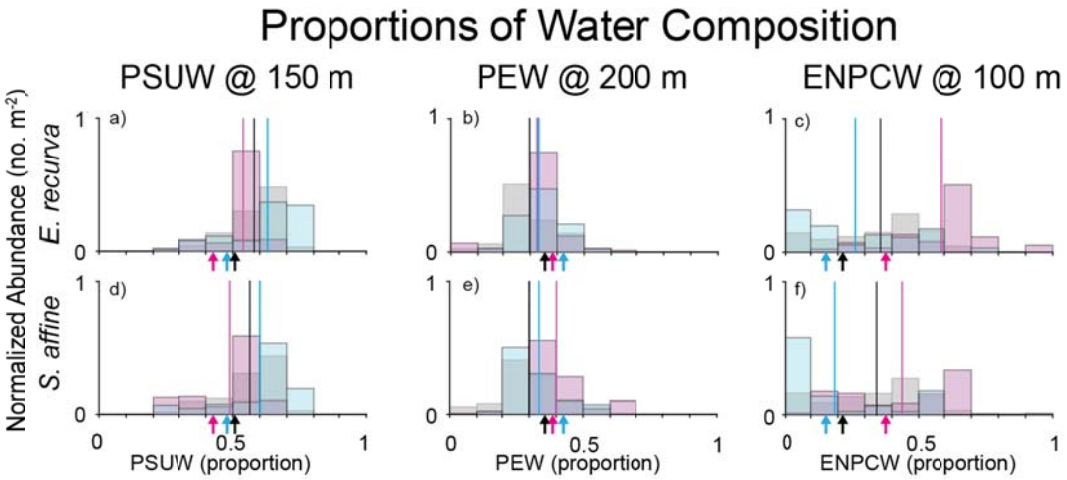

Figure S5. As in figure 11 but for the remaining two species.

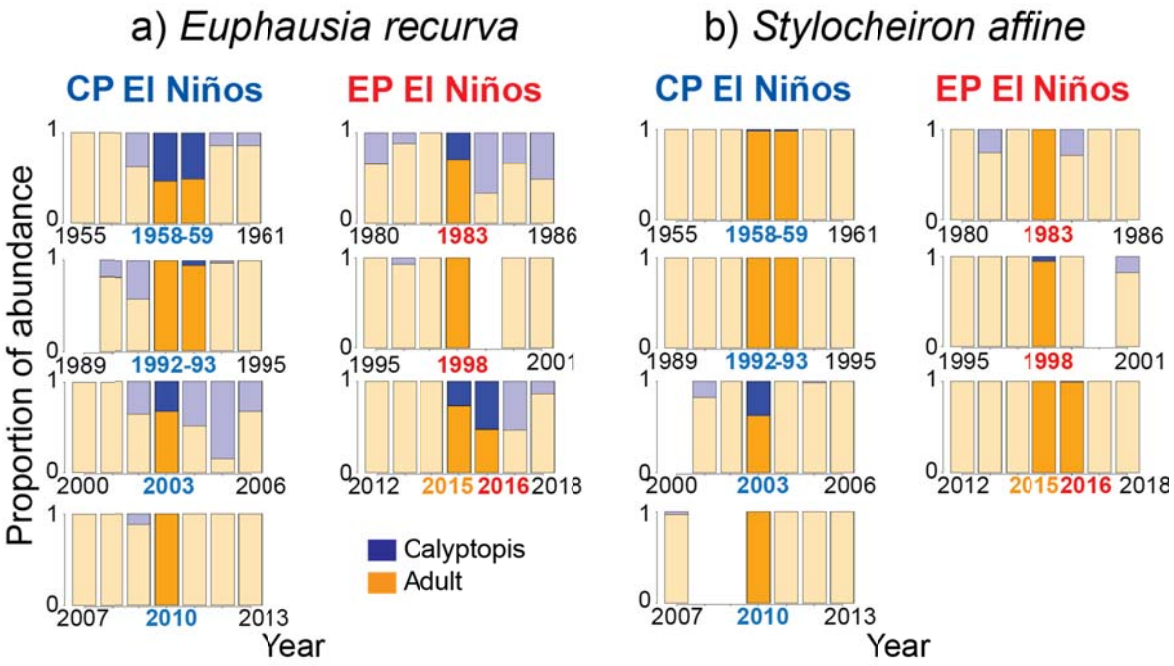

Figure S6. As in figure 12 but for the remaining two species.

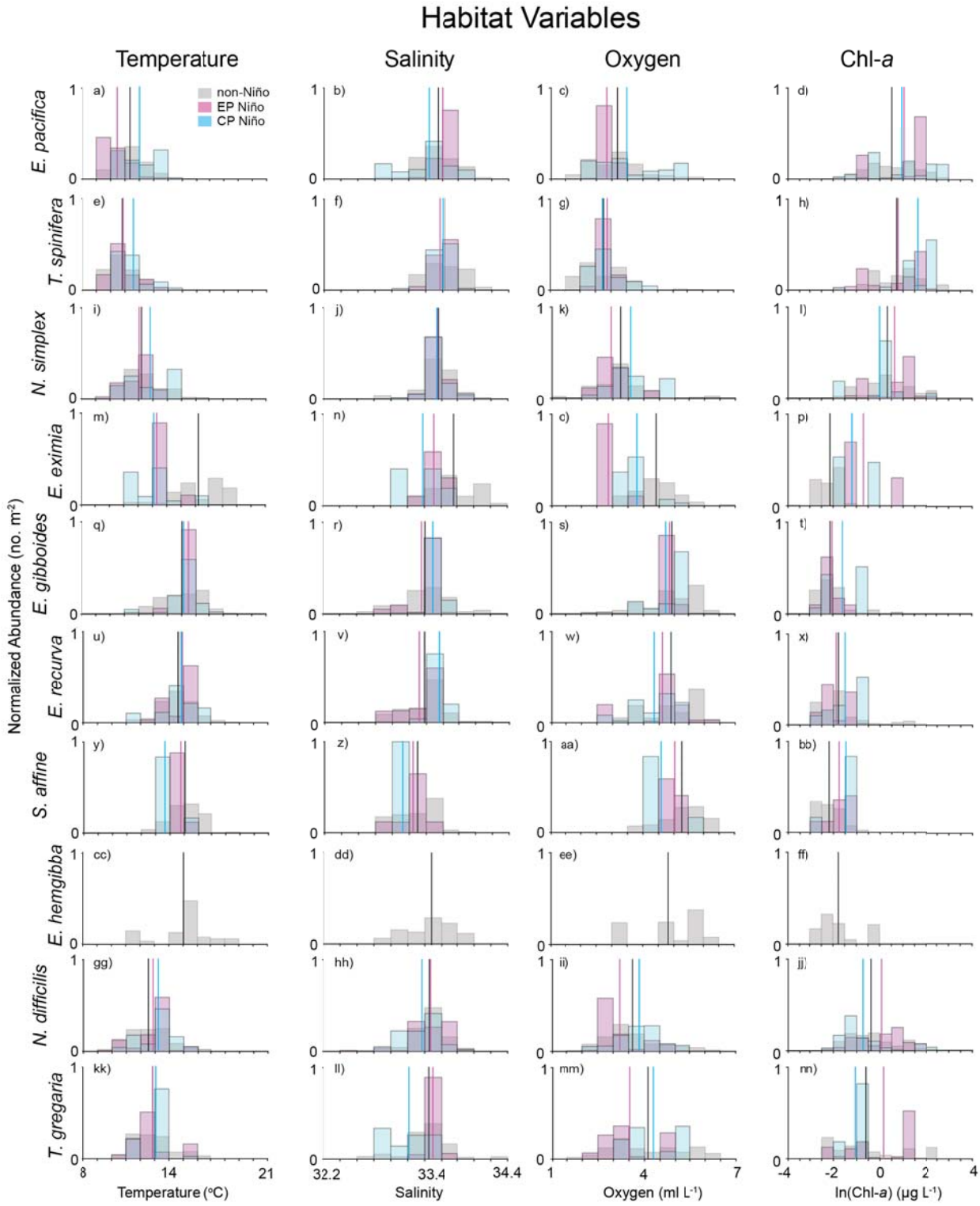

Figure S7. As in figure 10 but spring habitat distributions for calyptopis phase only.

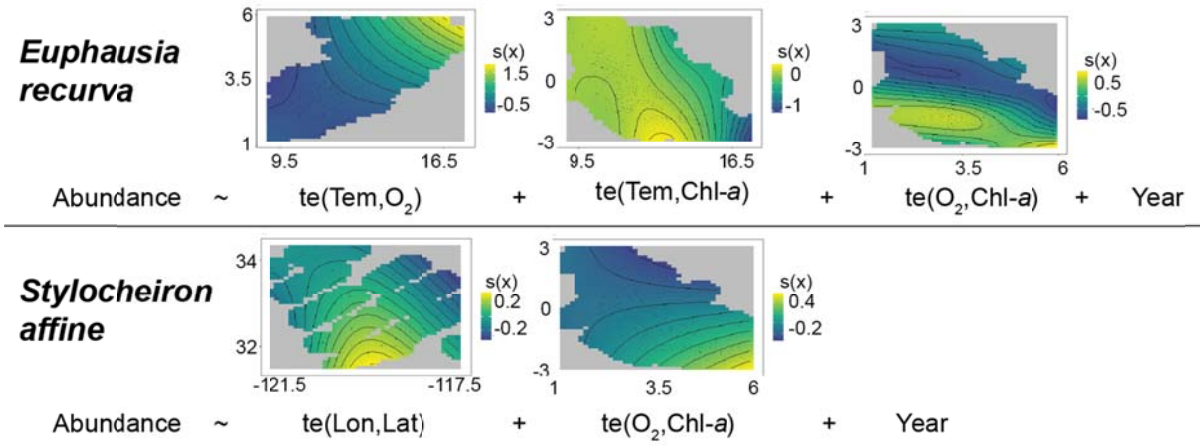

Figure S8. As in figure 13 but for the remaining two species.

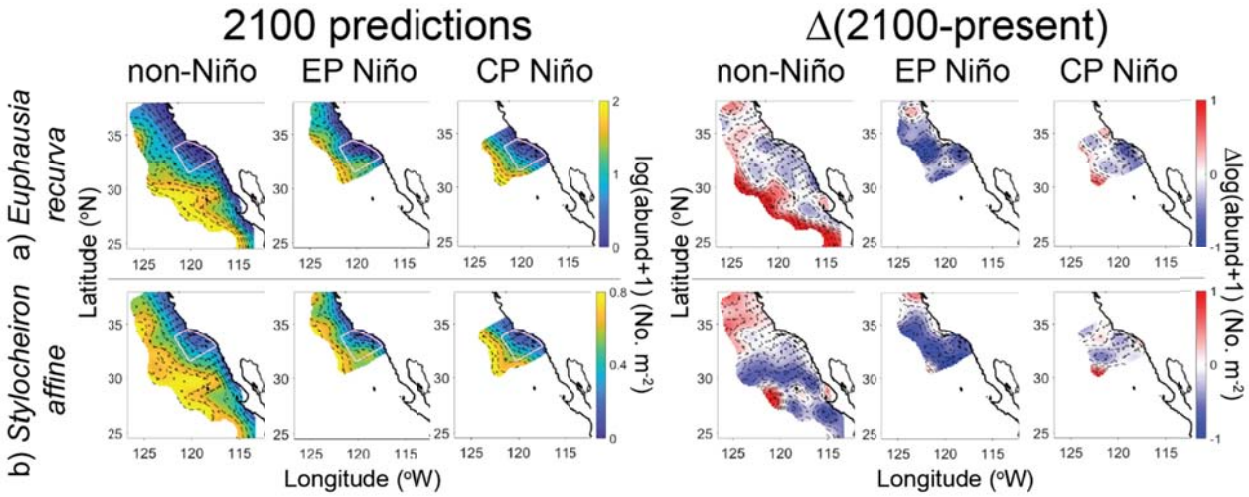

Figure S9. As in figure 14 but for the remaining two species.

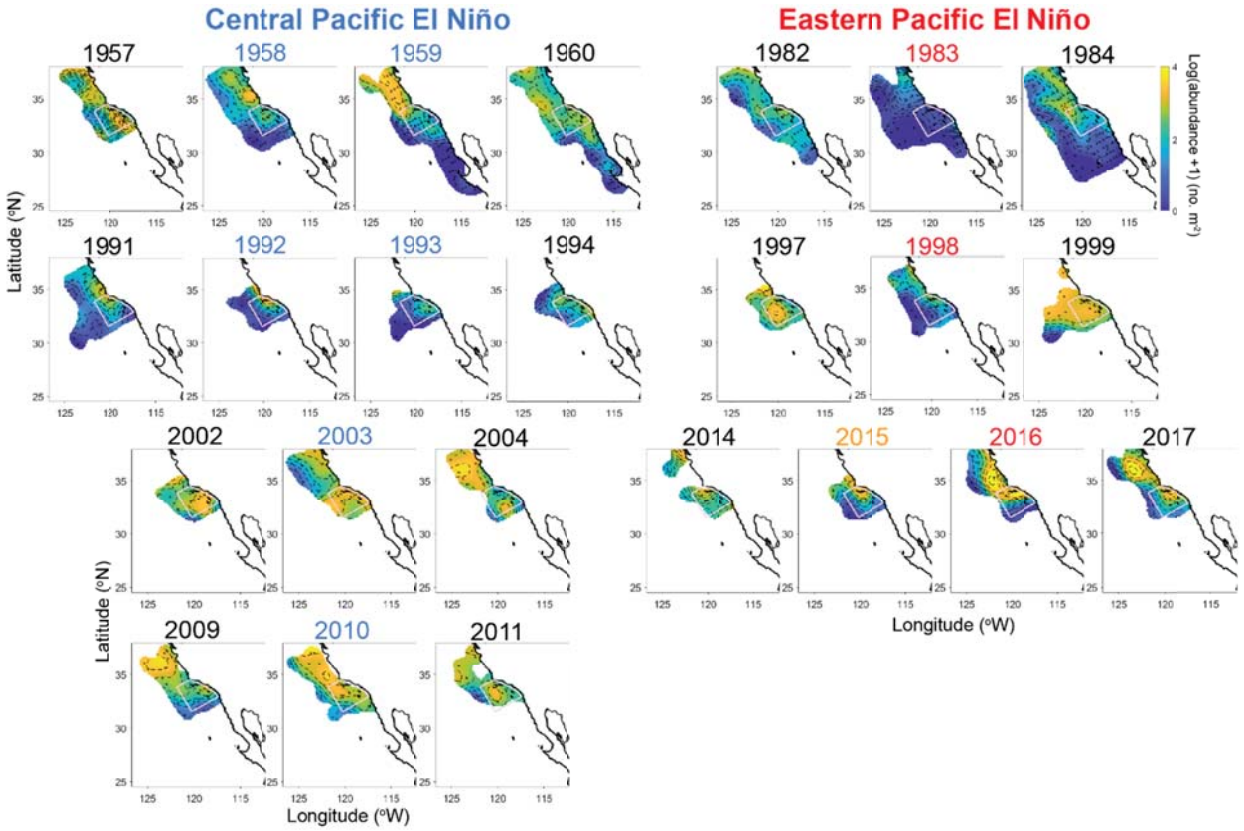

Figure S10. Individual year spring distributions for *E. pacifica*. Color scale shown for 1984 is the same for all years. El Niño springs are shown as central plots with colored year-labels. Spring 2015 was the Warm Anomaly (orange label), although it was also a precursor to the 2015-16 Eastern Pacific El Niño.

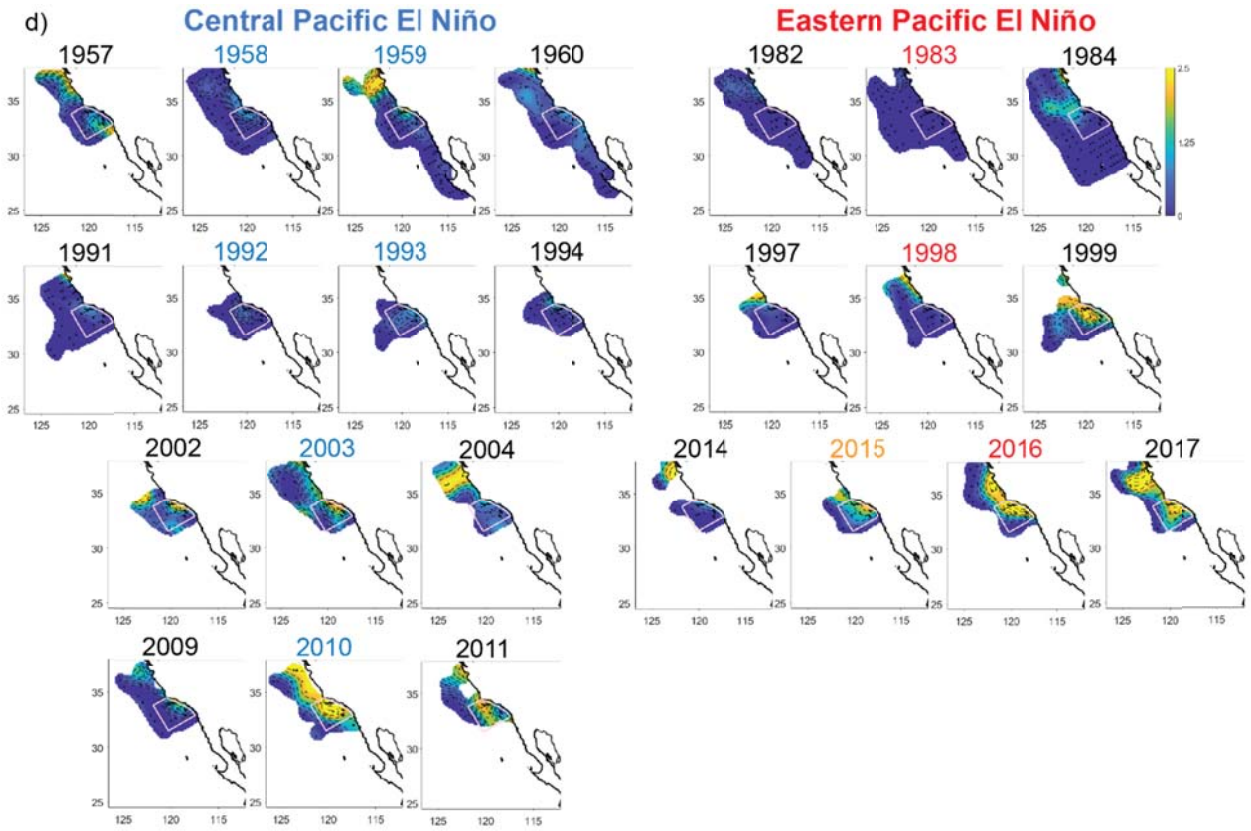

Figure S11. As in figure S10, but for *T. spinifera*.

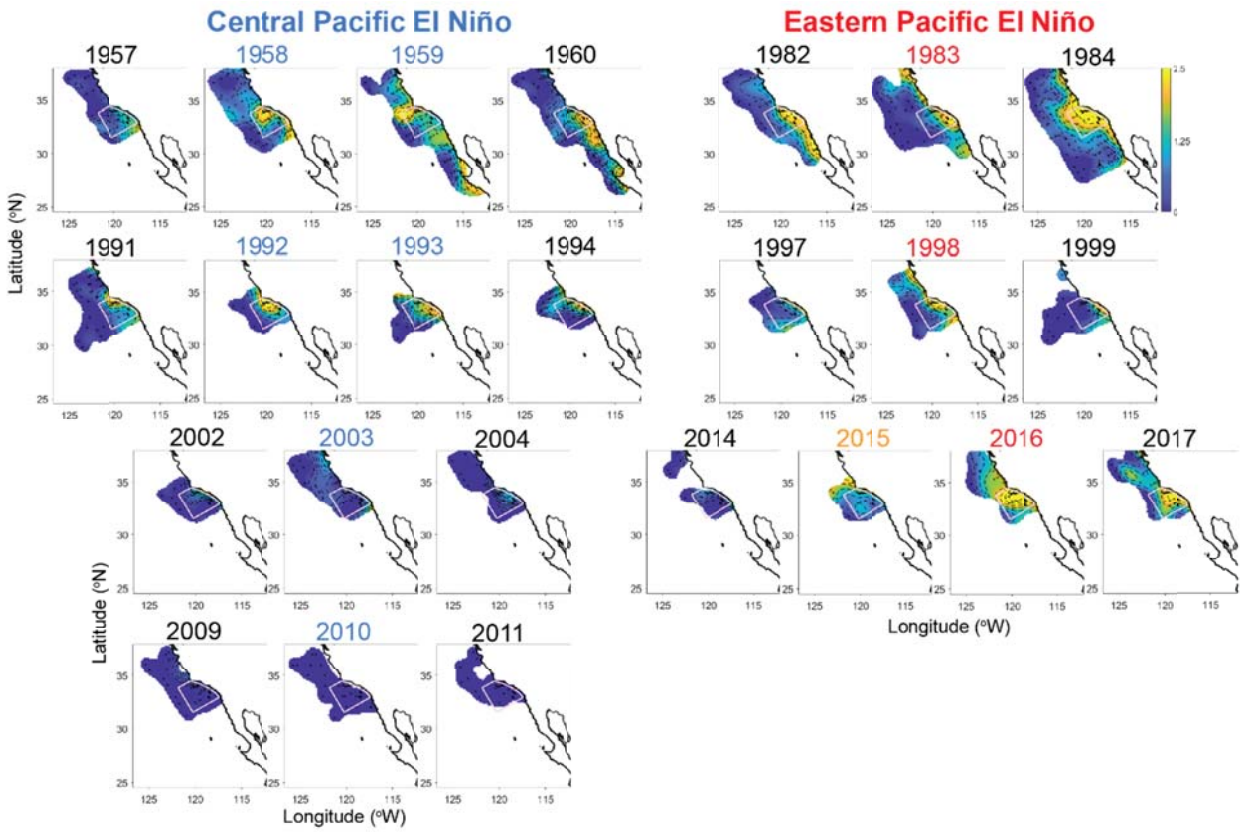

Figure S12. As in figure S10, but for *N. simplex*

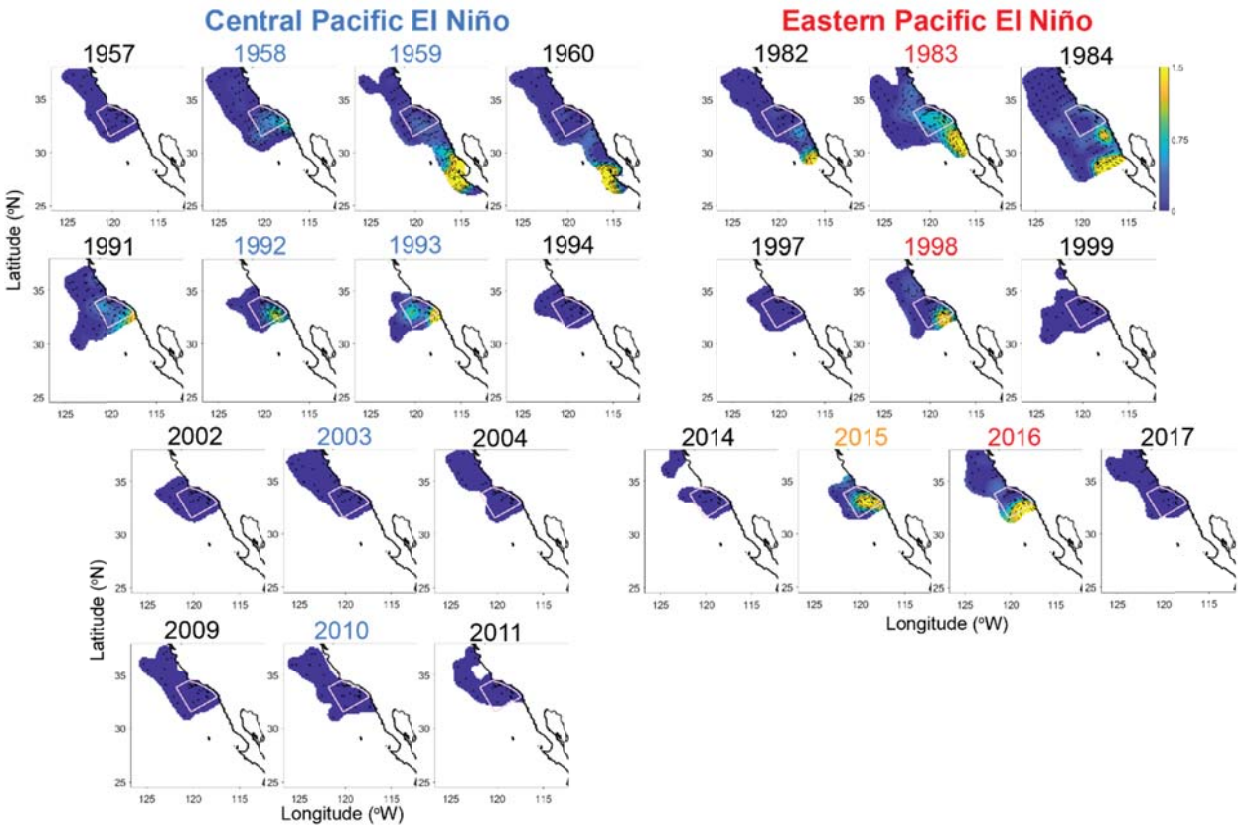

Figure S13. As in figure S10, but for *E. eximia*.

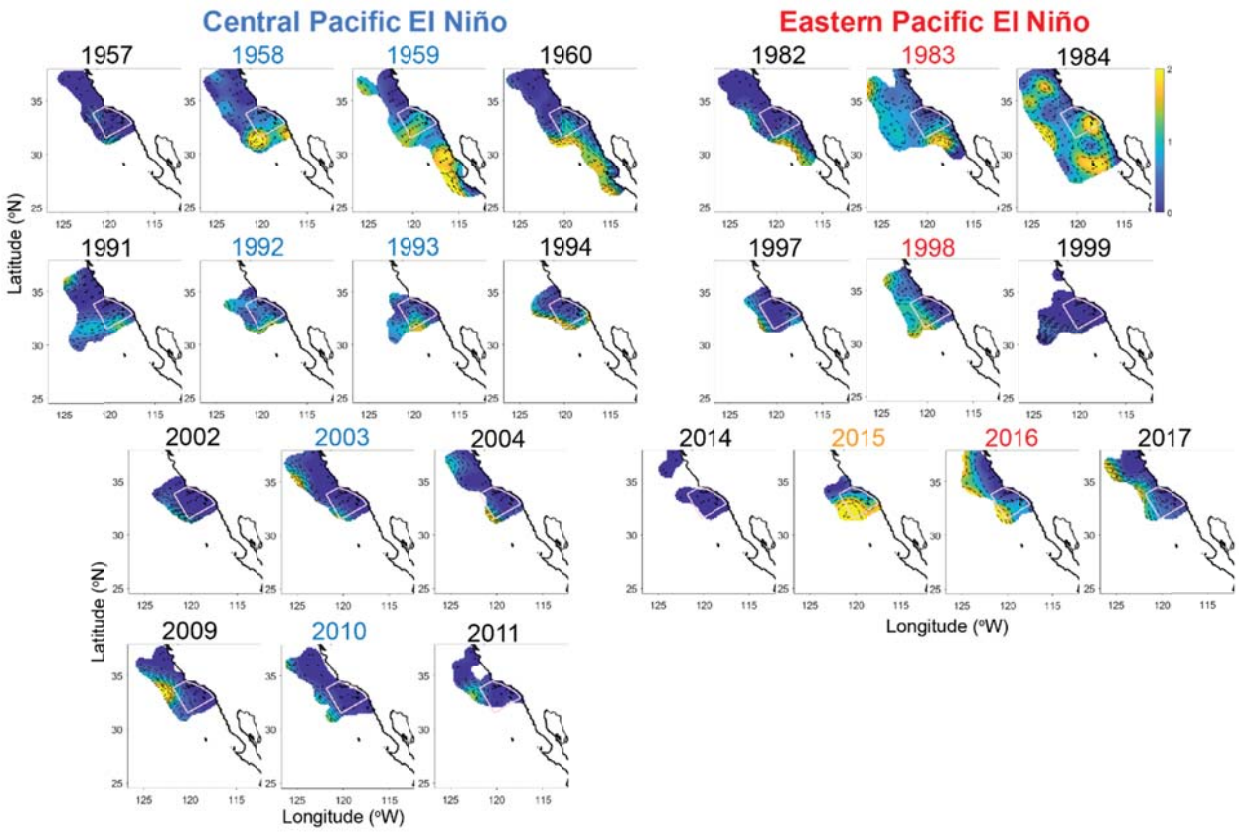

Figure S14. As in figure S10, but for *E. gibboides.*

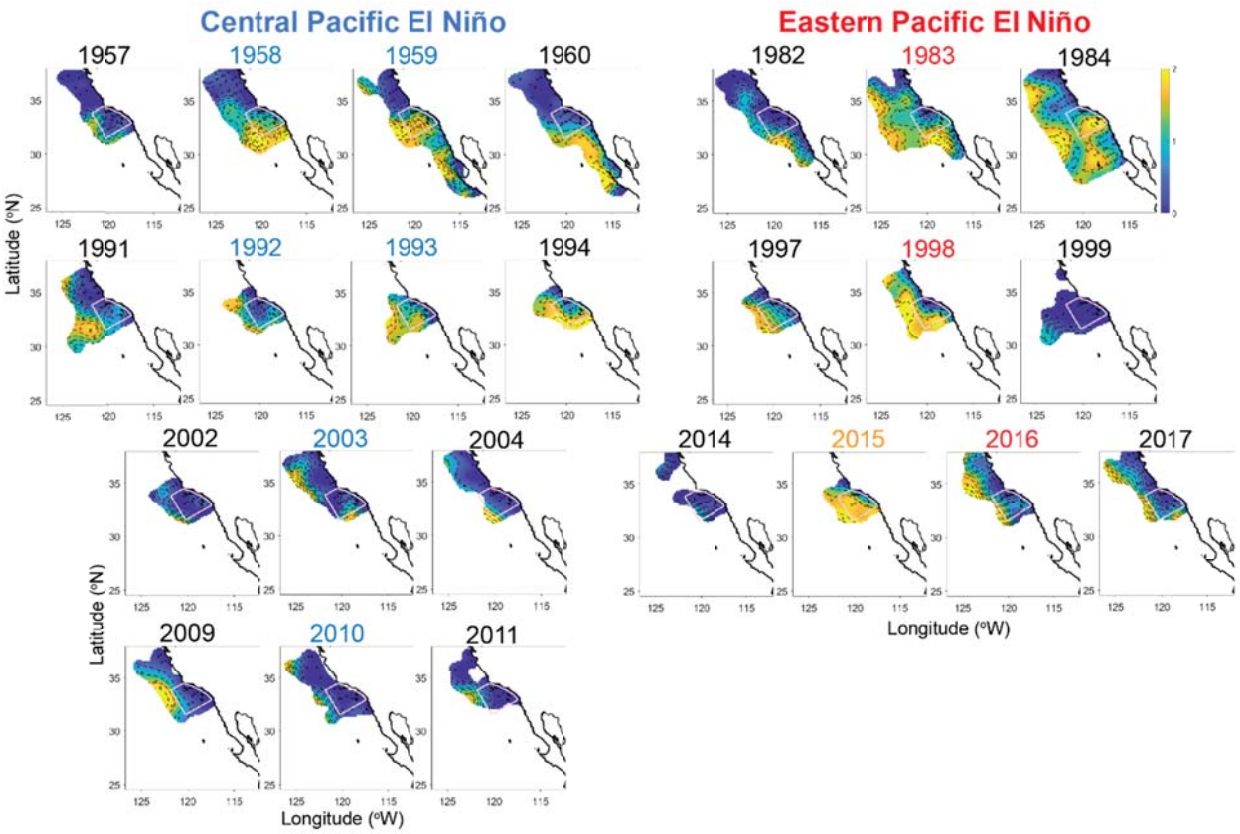

Figure S15. As in figure S10, but for *E. recurva.*

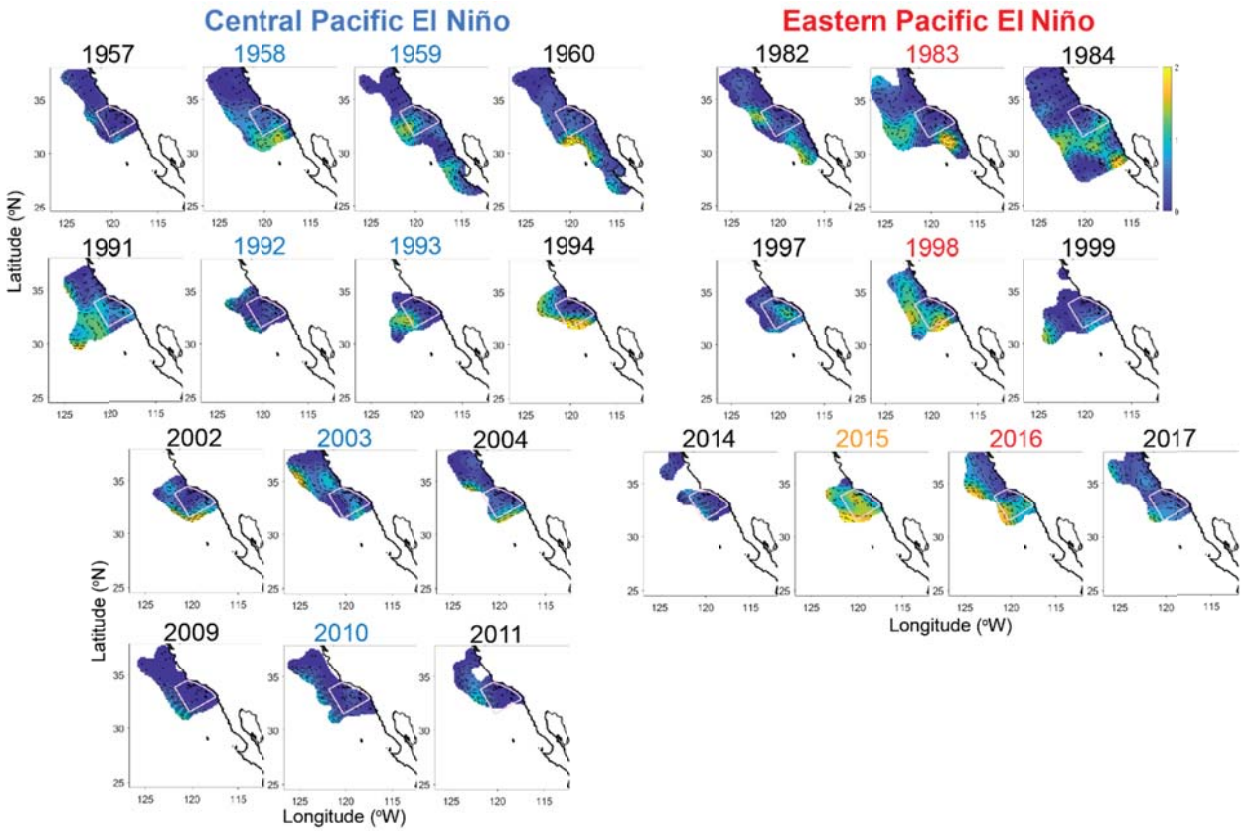

Figure S16. As in figure S10, but for *S. affine*.

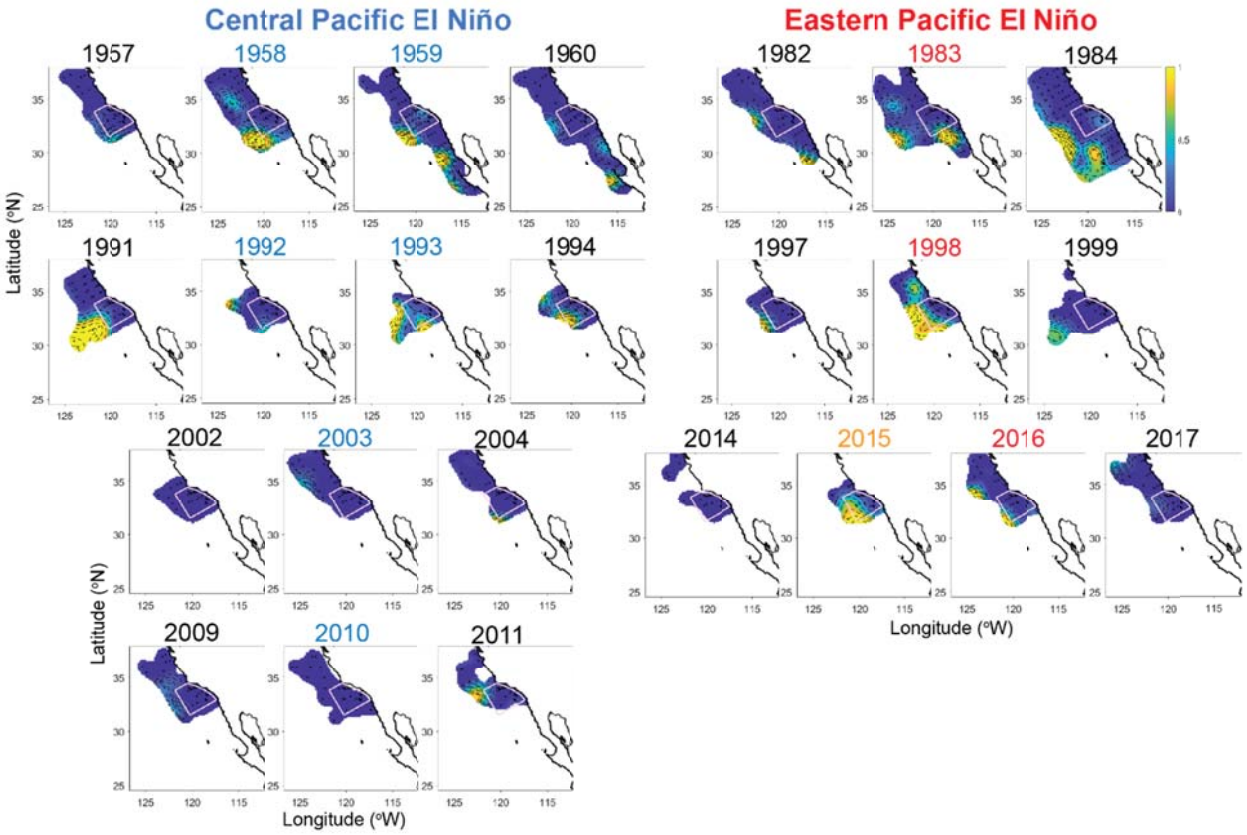

Figure S17. As in figure S10, but for *E. hemigibba*.

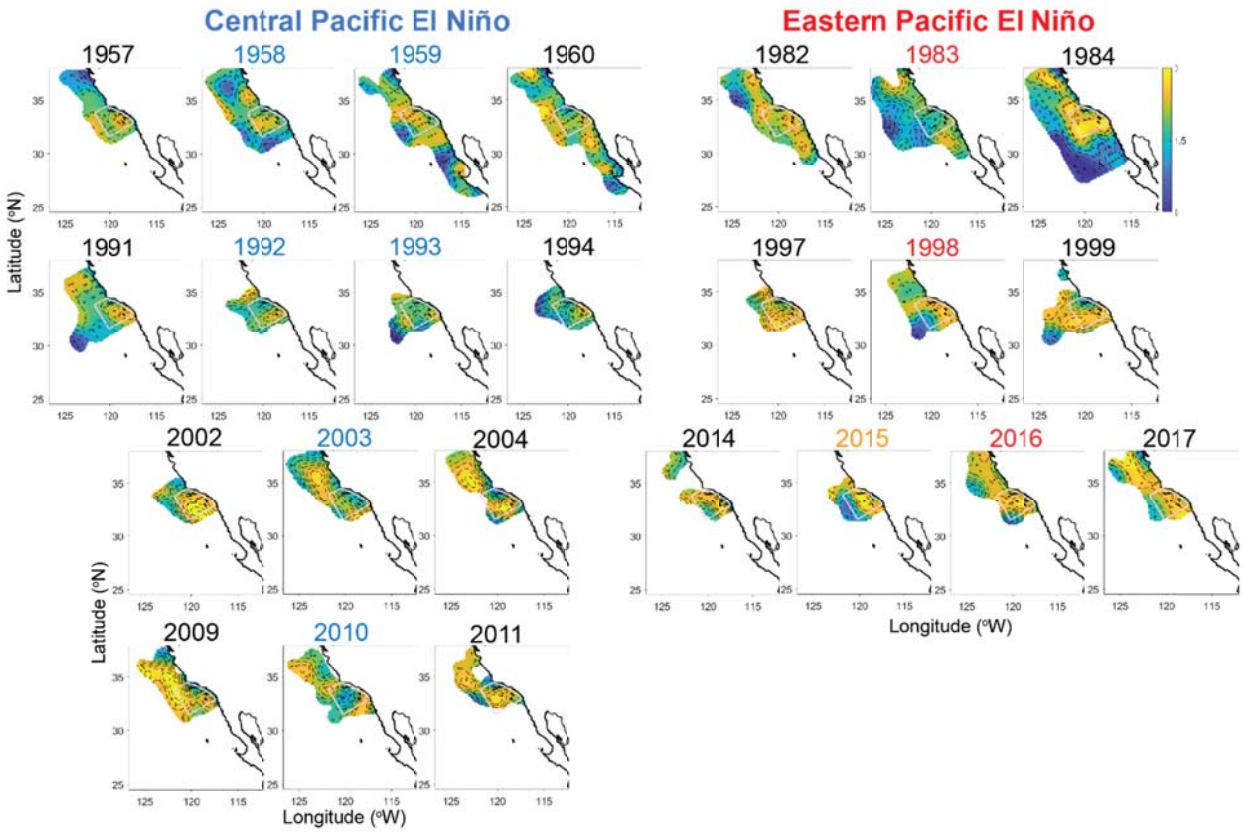

Figure S18. As in figure S10, but for *N. difficilis*.

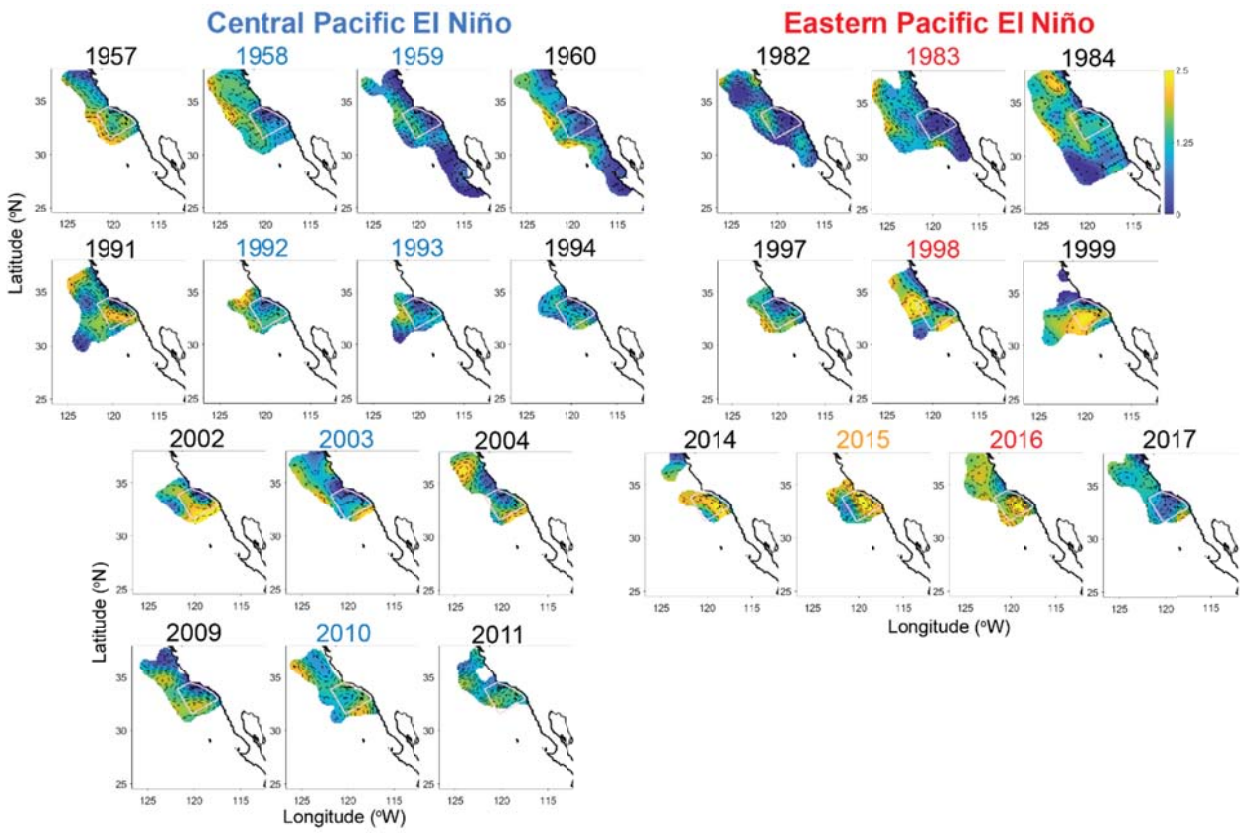

Figure S19. As in figure S10, but for *T. gregaria.*

Euphausiid spatial displacements and habitat shifts in the southern California Current System in response to El Niño variability

Laura E. Lilly, Mark D. Ohman

SUPPORTING INFORMATION: Physical characterizations of individual El Niño events, 1951-2018

We present here additional information on the physical development and impacts in the equatorial Pacific and California Current System of each El Niño event considered in our analyses. See references for detailed event descriptions.

S.1. Eastern Pacific El Niño events

S.1.1. 1982-83

The 1982-82 Eastern Pacific (EP) Niño was one of the two strongest events on record in the equatorial Pacific. It was the first El Niño for which the initial development of warm conditions was observed in the western equatorial Pacific (WEP) rather than the eastern equatorial Pacific (EEP) off South America, although whether that development sequence was unprecedented or was simply the first record is not clear (Barber & Chavez, 1986; Philander, 1983). The 1982-83 EP Niño produced the strongest temperature anomalies besides the 1997-98 El Niño in the

Niño1+2 region off South America, but anomalies occurred much later in event development (fall through following summer, rather than initial spring-summer) (L'Heureux et al., 2017). The 1982-83 EP Niño was dominated by onshore flow into the southern CCS from southwestern offshore waters, apparently forced by anomalous local atmospheric circulation, although it also showed characteristics of enhanced poleward advection north of Point Conception, CA, in February 1983. Poleward flow was also attributed predominantly to altered local atmospheric circulation rather than coastally trapped wave (CTW) propagation (Huyer, 1983; Simpson, 1983, 1984). Nearshore flows reversed to their normal spring equatorward direction in March, driven by the return of normal upwelling (Ramp et al., 1997). Significant surface and subsurface warming, freshening, and oxygen increases occurred regionwide (Lynn, 1983; Ramp et al., 1997).

S.1.2. 1997-98

The 1997-98 EP Niño is considered the canonical El Niño event in both the equatorial Pacific and CCS. Its physical signature remains the strongest on record, particularly in the EEP region (L'Heureux et al., 2017; McPhaden, 1999b). In the normal cold tongue region off South America, sea surface temperature anomalies were +4^{o}C in summer-fall 1997, and eastward-propagating Kelvin waves depressed the thermocline by 90 m (McPhaden, 1999b). Positive event feedback occurred due to eastward expansion of the Western Pacific Warm Pool, which increased the area over which westerly wind bursts blew, further strengthening the event (McPhaden, 1999a, 1999b) The El Niño signal traveled to the CCS predominantly via oceanic coastally trapped waves (CTWs) that strengthened and broadened the poleward nearshore flow off California

(Lynn & Bograd, 2002; Schwing et al., 2002; Schwing et al., 2005; Strub & James, 2002). Nearshore dynamic height increased significantly and nutricline depth decreased by > 80 m, and upper layer waters warmed +3-4^{o}C regionwide, due to both changes in flow patterns and thermal expansion in winter 1997-98 (Bograd & Lynn, 2001; Lynn & Bograd, 2002). The 1997-98 El Niño was also followed by the most dramatic reversal to a significant La Niña event (1998-99) on record (McPhaden, 1999a, 1999b).

S.1.3. 2015-16

The 2015-16 El Niño developed in the Equatorial Pacific initially in line with the 1997-98 event, although temperature anomalies did not develop as strongly in the EEP. In contrast, SST anomalies in the Central Equatorial Pacific (CEP) were the strongest of any El Niño on record (L'Heureux et al., 2017; Newman et al., 2018). Although our method of El Niño classification labels the 2015-16 El Niño as an EP event, it weighed equally on the E and C indices, suggesting a mixture of EP and CP characteristics (Takahashi et al., 2011; Timmermann et al., 2019). Similarly, the 2015-16 El Niño impact in the CCS was more moderate than the previous two EP Niños: positive SST anomalies did occur, strongest south of Pt. Conception, but they were weaker and also had a smaller cross-shore temperature gradient because offshore temperatures were still elevated from the 2014-15 Warm Anomaly (Jacox et al., 2016). Thermocline depression was similarly established in mid-2014 during the Warm Anomaly and remained constant and moderate (~1 standard deviation shallower than predicted) through spring 2016, suggesting weak oceanic teleconnections from the tropical Pacific (Jacox et al., 2016).

S.2. Central Pacific El Niño events

S.2.1. 1957-59

The 1957-59 El Niño was the first event recognized and studied as a significant global phenomenon with impacts beyond the equatorial Pacific (Schwing et al., 2005). The event was anomalous in that it produced significant regionwide upper ocean warming across the southern CCS but occurred against the cool background conditions of a negative Pacific Decadal Oscillation (PDO) phase (McGowan, 1998). Similar to the 1997-98 El Niño, the core California Current was displaced offshore and reduced in strength in winter 1958, and nearshore upwelling was depressed, while the Inshore Countercurrent surface flow intensified and broadened (Brinton, 1981; Lynn, 1983; Wyllie, 1966). However, Reid (1960) posited that the 1957-59 El Niño was forced in the CCS by changes in wind-driven regional circulation rather than oceanic CTWs. Warm El Niño conditions persisted in the California Current through January 1960, over a year beyond the end of the equatorial Pacific event (Brinton, 1981).

S.2.2. 1991-93

The 1991-93 El Niño was just below our Niño1+2 cutoff for EP Niño events, and has been characterized in the equatorial Pacific as a mixed EP-CP event (Timmermann et al., 2019). Kelvin waves propagated east at the equator, though more weakly than in true EP events, and induced poleward CTW propagation (Chavez, 1996; Ramp et al., 1997). Two CTWs arrived in

the CCS between Feb-Apr 1992 (Ramp et al., 1997); their arrival later in the event sequence likely induced the prolonged warm anomalies that lasted through spring 1993. The CCS experienced warm, fresh anomalies and isopycnal depression in February 1992 due to onshore flows driven by the southward-displaced Aleutian Low. Hayward (1993) described elevated SSTs and strong poleward countercurrent flows off California during fall 1991-Apr 1992, with low total zooplankton displacement volume. This period was followed by a rapid reversal to strong upwelling, decreased nearshore sea surface height (SSH), and a strong southward California Current. However, elevated SSTs persisted throughout 1992, and El Niño-related high SSH anomalies returned from late 1992-early 1993, prolonging the impact of the event in the CCS. Sea surface height anomalies from 1991-92 were comparable to those during 1982-83, but of shorter duration (eight months), at least during the initial event onset. Hayward (1993) also noted that no large salinity anomalies occurred during 1991-92, which would suggest a lack of advection of southern waters from the Eastern Tropical Pacific; this appears to contradict the assertion by Ramp et al. (1997) that two CTWs arrived to the CCS in spring 1992, although the timings of the two studies may not overlap.

S.2.3. 2002-03

As with 1991-93, the 2002-03 El Niño characterized as a mixed EP-CP event of moderate strength in the equatorial Pacific (Timmermann et al., 2019), although its signature was very different than 1991-93 (Harrison & Chiodi, 2009). Westerly wind bursts induced subsurface Kelvin waves that generated the event, but they were weaker and farther west than during past major El Niños. Resulting strongest SST anomalies occurred in the CEP region, and the event

most resembled the equatorial 1994-95 El Niño, which did not classify as a 'CCS Niño' by our metrics (McPhaden, 2004). Physical event development in the CCS in 2002-03 was preceded by an anomalously cool, high-salinity Subarctic water intrusion and strengthening of the southward core California Current in summer 2002 (Bograd & Lynn, 2003; Wheeler et al., 2003). Cool subarctic waters reached Baja California by October 2002 and induced high phytoplankton production but low zooplankton biomass (Lavaniegos, 2009; Lavaniegos & Ambriz-Arreola, 2012). The PDO also switched to a positive phase in 2002 (Lavaniegos, 2009). The 2002-03 El Niño itself was characterized by moderate warming, although low-salinity surface waters and resulting stratification persisted throughout and following the event (Lavaniegos, 2009; Lavaniegos & Ambriz-Arreola, 2012).

S.2.4. 2009-10

The 2009-10 El Niño characterizes unequivocally as a CP event in the equatorial Pacific, with record-breaking SST anomalies in the CEP (Kim et al., 2011; Lee & McPhaden, 2010). Unlike other CP events, it had a rapid decay phase to cool conditions resembling a strong EP Niño but no off-equator heat discharge as in major EP events (Kim et al., 2011). Instead, El Niño signals propagated to the CCS exclusively via atmospheric teleconnections, depressing the thermocline and warming upper ocean waters but not inducing anomalous poleward advection (Todd et al., 2011).

S.3. 2014-15 Warm Anomaly

The 2014-15 Warm Anomaly was not attributed to direct equatorial El Niño forcing. Equatorial El Niño conditions developed in spring 2014 but stalled and weakened over the summer due to anomalous eastward wind bursts (Hu & Fedorov, 2016; Li et al., 2015). However, the 2014-15 event produced unprecedented surface-enhanced warming ($> +1^{o}C$) and stratified, low-productivity conditions in the CCS, on par with major El Niño events. Anomalously warm conditions appeared offshore of California as early as January 2014 (Gentemann et al., 2017; Zaba & Rudnick, 2016), and definitively in the nearshore region by late spring (Leising et al., 2015; Robinson, 2016), although normal nearshore upwelling occurred in spring 2014 (Lilly et al., 2019). Regionwide anomalously warm conditions and near-zero nitrate and chlorophyll-*a* levels persisted from summer 2014-late winter 2015. Moderate upwelling reappeared off California in spring 2015, before renewed persistence of the Warm Anomaly and the subsequent El Niño arrival (Jacox et al., 2016; Lilly et al., 2019).

REFERENCES

Barber, R. T. & Chavez, F. P. (1986). Ocean Variability in Relation to Living Resources during the 1982-83 El-Nino. *Nature, 319*(6051), 279-285. doi:DOI 10.1038/319279a0

Bograd, S. J. & Lynn, R. J. (2001). Physical-biological coupling in the California Current during the 1997-99 El Niño-La Niña cycle. *Geophysical Research Letters, 28*(2), 275-278.

Bograd, S. J. & Lynn, R. J. (2003). Anomalous subarctic influence in the southern California Current during 2002. *Geophysical Research Letters, 30*(15). doi:10.1029/2003gl017446

Brinton, E. (1981). Euphausiid distributions in the California Current during the warm winter-spring of 1977–78, in the context of a 1949–1966 time series. *California Cooperative Oceanic Fisheries Investigations Reports, 22*, 135-154.

Chavez, F. P. (1996). Forcing and biological impact of onset of the 1992 El Niño in central California. *Geophysical Research Letters, 23*(3), 265-268.

Gentemann, C. L., Fewings, M. R. & Garcia-Reyes, M. (2017). Satellite sea surface temperatures along the West Coast of the United States during the 2014-2016 northeast Pacific marine heat wave. *Geophysical Research Letters, 44*(1), 312-319. doi:10.1002/2016gl071039

Harrison, D. E. & Chiodi, A. M. (2009). Pre-and post-1997/98 westerly wind events and equatorial Pacific cold tongue warming. *Journal of Climate, 22*(3), 568-581.

Hayward, T. L. (1993). Preliminary observations of the 1991–1992 El Niño in the California Current. *California Cooperative Oceanic Fisheries Investigations Reports, 34*(21-29).

Hu, S. N. & Fedorov, A. V. (2016). Exceptionally strong easterly wind burst stalling El Nino of 2014. *Proceedings of the National Academy of Sciences of the United States of America, 113*(8), 2005-2010. doi:10.1073/pnas.1514182113

Huyer, A. (1983). Coastal upwelling in the California Current System. *Progress in Oceanography, 12*, 259-284.

Jacox, M. G., Hazen, E. L., Zaba, K. D., Rudnick, D. L., Edwards, C. A., Moore, A. M. & Bograd, S. J. (2016). Impacts of the 2015-2016 El Nino on the California Current System: Early assessment and comparison to past events. *Geophysical Research Letters, 43*(13), 7072-7080. doi:10.1002/2016gl069716

Kim, W., Yeh, S. W., Kim, J. H., Kug, J. S. & Kwon, M. (2011). The unique 2009–2010 El Niño event: A fast phase transition of warm pool El Niño to La Niña. *Geophysical Research Letters, 38*(15).

L'Heureux, M. L., Takahashi, K., Watkins, A. B., Barnston, A. G., Becker, E. J., Di Liberto, T. E., et al. (2017). Observing and Predicting the 2015/16 El Nino. *Bulletin of the American Meteorological Society, 98*(7), 1363-1382. doi:10.1175/Bams-D-16-0009.1

Lavaniegos, B. E. (2009). Influence of a multiyear event of low salinity on the zooplankton from Mexican eco-regions of the California Current. *Progress in Oceanography, 83*(1-4), 369-375.

Lavaniegos, B. E. & Ambriz-Arreola, I. (2012). Interannual variability in krill off Baja California in the period 1997-2005. *Progress in Oceanography, 97*, 164-173. doi:10.1016/j.pocean.2011.11.008

Lee, T. & McPhaden, M. J. (2010). Increasing intensity of El Nino in the central-equatorial Pacific. *Geophysical Research Letters, 37*. doi:Artn L14603

10.1029/2010gl044007

Leising, A. W., Schroeder, I. D., Bograd, S. J., Abell, J., Durazo, R., & & Warybok, P. (2015). State of the California Current 2014-15: Impacts of the Warm-Water" Blob". *California Cooperative Oceanic Fisheries Investigations Reports, 56*, 31-68.

Li, J. Y., Liu, B. Q., Li, J. D. & Mao, J. Y. (2015). A Comparative Study on the Dominant Factors Responsible for the Weaker-than-expected El Nino Event in 2014. *Advances in Atmospheric Sciences, 32*(10), 1381-1390. doi:10.1007/s00376-015-4269-6

Lilly, L. E., Send, U., Lankhorst, M., Martz, T. R., Feely, R. A., Sutton, A. J. & Ohman, M. D. (2019). Biogeochemical anomalies at two southern California Current System moorings during the 2014-16 Warm Anomaly-El Niño sequence. *Journal of Geophysical Research: Oceans*.

Lynn, R. J. (1983). The 1982-83 warm episode in the California Current. *Geophysical Research Letters, 10*(11), 1093-1095.

Lynn, R. J. & Bograd, S. J. (2002). Dynamic evolution of the 1997-1999 El Nino-La Nina cycle in the southern California Current System. *Progress in Oceanography, 54*(1-4), 59-75. doi:Pii S0079-6611(02)00043-5

McGowan, J. A. (1998). Climate-ocean variability and ecosystem response in the northeast Pacific (vol 281, pg 210, 1998). *Science, 282*(5388), 417-417.

McPhaden, M. J. (1999a). El Nino - The child prodigy of 1997-98. *Nature, 398*(6728), 559-+. doi:Doi 10.1038/19193

McPhaden, M. J. (1999b). Genesis and evolution of the 1997-98 El Nino. *Science, 283*(5404), 950-954. doi:DOI 10.1126/science.283.5404.950

McPhaden, M. J. (2004). Evolution of the 2002/03 El Nino. *Bulletin of the American Meteorological Society, 85*(5), 677-695. doi:10.1175/Bams-85-5-677

Newman, M., Wittenberg, A. T., Cheng, L. Y., Compo, G. P. & Smith, C. A. (2018). The Extreme 2015/16 El Nino, in the Context of Historical Climate Variability and Change. *Bulletin of the American Meteorological Society, 99*(1), S16-S20. doi:10.1175/Bams-D-17-0116.1

Philander, S. G. H. (1983). Meteorology - Anomalous El-Nino of 1982-83. *Nature, 305*(5929), 16-16. doi:DOI 10.1038/305016a0

Ramp, S. R., McClean, J. L., Collins, C. A., Semtner, A. J. & Hays, K. A. S. (1997). Observations and modeling of the 1991-1992 El Nino signal off central California. *Journal of Geophysical Research-Oceans, 102*(C3), 5553-5582. doi:Doi 10.1029/96jc03050

Reid, J. L. (1960). *Oceanography of the eastern North Pacific in the last 10 years*. Retrieved from

Robinson, C. J. (2016). Evolution of the 2014–2015 sea surface temperature warming in the central west coast of Baja California, Mexico, recorded by remote sensing. *Geophysical Research Letters, 43*(13), 7066-7071.

Schwing, F. B., Murphree, T. & Green, P. M. (2002). The evolution of oceanic and atmospheric anomalies in the northeast Pacific during the El Niño and La Niña events of 1995–2001. *Progress in Oceanography, 54*(1), 459-491.

Schwing, F. B., Palacios, D. M. & Bograd, S. J. (2005). El Nino impacts of the California current ecosystem. *US CLIVAR Newsletter, 3*(2), 5-8.

Simpson, J. J. (1983). Large-Scale Thermal Anomalies in the California Current during the 1982-1983 El-Nino. *Geophysical Research Letters, 10*(10), 937-940. doi:DOI 10.1029/GL010i010p00937

Simpson, J. J. (1984). El-Nino-Induced Onshore Transport in the California Current during 1982-1983. *Geophysical Research Letters, 11*(3), 241-242.

Strub, P. T. & James, C. (2002). The 1997-1998 oceanic El Niño signal along the southeast and northeast Pacific boundaries - an altimetric view. *Progress in Oceanography, 54*(1-4), 439-458.

Takahashi, K., Montecinos, A., Goubanova, K. & Dewitte, B. (2011). ENSO regimes: Reinterpreting the canonical and Modoki El Nino. *Geophysical Research Letters, 38*. doi:10.1029/2011gl047364

Timmermann, A., An, S.-I., Kug, J. S., Jin, F. F., Cai, W., Capotondi, A., et al. (2019). El Niño-Southern Oscillation complexity. *Nature, 559*, 535-545.

Todd, R. E., Rudnick, D. L., Davis, R. E. & Ohman, M. D. (2011). Underwater gliders reveal rapid arrival of El Nino effects off California's coast. *Geophysical Research Letters, 38*. doi:10.1029/2010gl046376

Wheeler, P. A., Huyer, A. & Fleischbein, J. (2003). Cold halocline, increased nutrients and higher chlorophyll off Oregon in 2002. *Geophysical Research Letters, 30*(14). doi:10.1029/2003gl017395

Wyllie, J. G. (1966). Geostrophic flow of the California Current at the surface and at 200 m. In *CalCOFI Atlas* (Vol. 4). University of California, San Diego.

Zaba, K. D. & Rudnick, D. L. (2016). The 2014-2015 warming anomaly in the Southern California Current System observed by underwater gliders. *Geophysical Research Letters, 43*(3), 1241-1248. doi:10.1002/2015gl067550